APPLICATIONS OF ARTIFICIAL NEURAL NETWORKS IN THE IDENTIFICATION OF FLOW UNITS, HAPPY SPRABERRY FIELD, GARZA COUNTY, TEXAS

A Thesis

by

MATTHEW DAVID GENTRY

Submitted to the Office of Graduate Studies of
Texas A&M University
in partial fulfillment of the requirements for the degree of

MASTER OF SCIENCE

December 2003

Major Subject: Geology

APPLICATIONS OF ARTIFICIAL NEURAL NETWORKS IN THE IDENTIFICATION OF FLOW UNITS, HAPPY SPRABERRY FIELD, GARZA COUNTY, TEXAS

A Thesis

by

MATTHEW DAVID GENTRY

Submitted to the Office of Graduate Studies of
Texas A&M University
in partial fulfillment of the requirements for the degree of

MASTER OF SCIENCE

Approved as to style and content by:

Wayne M. Ahr (Chair of Committee)	Mark E. Everett (Member)
Richard A. Startzman (Member)	Andrew Hajash, Jr. (Head of Department)

December 2003

Major Subject: Geology

ABSTRACT

Applications of Artificial Neural Networks in the Identification of Flow Units, Happy Spraberry Field, Garza County, Texas. (December 2003)

Matthew David Gentry, B.S., Mississippi State University

Chair of Advisory Committee: Dr. Wayne M. Ahr

The use of neural networks in the field of development geology is in its infancy. In this study, a neural network will be used to identify flow units in Happy Spraberry Field, Garza County, Texas. A flow unit is the mappable portion of the total reservoir within which geological and petrophysical properties that affect the flow of fluids are consistent and predictably different from the properties of other reservoir rock volumes (Ebanks, 1987). Ahr and Hammel (1999) further state a highly "ranked" flow unit (i.e. a good flow unit) would have the highest combined values of porosity and permeability with the least resistance to fluid flow. A flow unit may also include nonreservoir features such as shales and cemented layers where combined porosity-permeability values are lower and resistance to fluid flow much higher (i.e. a poor flow unit) (Ebanks, 1987).

Production from Happy Spraberry Field primarily comes from a 100 foot interval of grainstones and packstones, Leonardian in age, at an average depth of 4,900 feet. Happy Spraberry Field is unlike most fields in that the majority of

the wells have been cored in the zone of interest. This fact more easily lends the Happy Spraberry Field to a study involving neural networks.

A neural network model was developed using a data set of 409 points where X and Y location, depth, gamma ray, deep resistivity, density porosity, neutron porosity, lab porosity, lab permeability and electrofacies were known throughout Happy Spraberry Field. The model contained a training data set of 205 cases, a verification data set of 102 cases and a testing data set of 102 cases. Ultimately two neural network models were created to identify electrofacies and reservoir quality (i.e. flow units). The neural networks were able to outperform linear methods and have a correct classification rate of 0.87 for electrofacies identification and 0.75 for reservoir quality identification.

ACKNOWLEDGEMENTS

I would like to thank Texas A&M University for providing funding for this project, without which, the science and presentation of this study would not have been a success.

I wish to thank my advisors, Dr. Wayne Ahr, Dr. Richard Startzman and Dr. Mark Everett. With encouragement, Dr. Ahr realized the usefulness in applying neural networks to reservoir characterization problems. When questions of the geology of Happy Spraberry Field arose Dr. Ahr's door was always open; plus he can cook a mean burger. Dr. Richard Startzman was the neural network guru. I thank him for his patience and delightful personality. We could use a few more Startzman's in this world. Dr. Mark Everett encouraged me to go the "petroleum" route when I first arrived at A&M. You will not meet a nicer man or find a better email address; colt45@beerfrdg.tamu.edu.

I would also like to thank my once considered fellow graduate students now considered lifelong friends. Dylan Morgan was able to provide needed relief from the rigors of academics with discussions of sports, women and a shared love of the South. Mychal Murray turned me on to Texas country music, the taste of a cold Shiner Bock from the kegerator and the women of the Outback.

Moreover, I would like to thank Bob Schneeflock and the folks at Paramount Petroleum in Jackson, Mississippi. Bob gave me my first job in the

oil industry and I can only wish I have a career as successful, rewarding and exciting as Bob's.

Jerry Greer with Citation Oil and Gas was invaluable with his knowledge of the Spraberry Field and was able to fill in the gaps when field data was absent.

I would also like to thank Lindsey. I am a better person for having you in my life. Your love and support have sustained me throughout my years at A&M.

Of course none of this would have been possible without the love of my family. I am lucky to have been born to two wonderful parents, Dave and Sheila. My luck continued with the best brother a guy could wish for, Luke. Without your love, patience and understanding I would not be where I am today. Thank you.

TABLE OF CONTENTS

Page

LIST OF FIGURES

FIGURE Page

FIGURE Page

LIST OF TABLES

INTRODUCTION

Carbonate reservoirs have long issued a set of problems uncommon to those found in siliciclastic reservoirs. Carbonate reservoirs are commonly compartmentalized and associated with subtle traps. A grounded understanding of rock and pore characteristics is paramount to the successful development of carbonate reservoirs. Due to the complexity and heterogeneity of carbonate reservoirs, innovative methods and emerging technologies should be tested and applied to obtain better analytical results than were previously available.

One such innovative technology is neural networks. There is a need for research in the field of development geology utilizing neural networks. Data commonly used in petroleum research contain unnecessary and distracting information that introduces some degree of uncertainty, which neural networks cope with quite well. In addition, neural networks are able to make generalizations and discern relationships from large amounts of data. In this study a neural network will be employed to identify and rank carbonate flow units and make inferences about pore characteristics of each flow unit from measured porosity and permeability values.

A flow unit as defined by Ebanks (1987) is the mappable portion of the total reservoir within which geological and petrophysical properties that affect the flow of fluids are consistent and predictably different from the properties of

---

This thesis follows the style and format of the American Association of Petroleum Geologists Bulletin.

other reservoir rock volumes. Ahr and Hammel (1999) further state a highly "ranked" flow unit (i.e. a good flow unit) would have the highest combined values of porosity and permeability with the least resistance to fluid flow. A flow unit may also include nonreservoir rocks such as shales and cemented carbonates where combined porosity-permeability values are lower and resistance to fluid flow much higher (i.e. a poor flow unit) (Ebanks 1987).

Flow units are zones within reservoirs that have high connectivity. High connectivity means high porosity and permeability and low resistance to fluid flow. Baffles are zones with low connectivity but they are limited in lateral and vertical extent so that fluids can flow at reasonable rates around, over, or under them. Baffles can be compared to islands in a stream. Barriers are zones that do not allow fluids to flow at reasonable rates and that may be laterally or vertically extensive, or both. Barriers can be compared to dams on a stream. They can also be seals that prevent fluid escape from reservoirs (Ahr, 2003 personal communication.).

Flow units in carbonate rocks do not always coincide with facies boundaries. Dependence on wireline log data alone does not provide correct information of such reservoir quality characteristics as permeability, pore type and diagenesis. That is why wireline log data must be integrated with analytical laboratory measurements for meaningful insights into pore characteristics and identification of flow units.

The Spraberry trend was once regarded as the world's largest uneconomic oil field (Handford, 1981). Because of this, successful production from the Spraberry is predicated on enhanced recovery methods and inventive, pioneering methods. Production from Happy Spraberry Field primarily comes from a 100 foot (30.5 m) interval of grainstones and packstones, Early Permian (lower Leonardian) in age, at an average depth of 4,900 feet (1493.5 m).

Happy Spraberry Field is unusual in most of the wells in the field have been cored. This makes the Happy Spraberry Field more amenable to a study involving neural networks.

Objectives

The objective of this study will be to answer the following question. Can a neural network identify different flow units in Happy Spraberry Field, Garza County, Texas? In addition, can information be obtained about pore characteristics of the different flow units from the identification of flow units utilizing a neural network?

Furthermore, neural networks have not been widely used in the petroleum industry. One of the goals of this study is to gain a better understanding of neural networks in order to demonstrate their value.

Field History

Happy Spraberry Field (see Figure 1) was discovered during a recompletion of the Lott 19-1 well (a previously abandoned Ellenburger well) in 1988 by Bennett Petroleum. In 1989, Bennett Petroleum along with Torch

Energy began field development and shot a 3-D seismic survey and drilled six additional wells. Initial production from the Spraberry Lime was over 1,000 barrels of oil a day from Lott 19-1. In 1991, Torch Operating Company bought all existing production and further developed the field by drilling of 9 additional wells. Between 1990 and 1992, Patterson Petroleum drilled the Lott Trust #1, the Lott Trust #2, and the Slaughter #6 in the field. The Slaughter #3, the Slaughter #4, and the Thomlinson 18-1 were wildcat wells drilled by Bradcorp between 1982 and 1984. They produce from the Ellenburger Formation and are not considered part of Happy Spraberry Field.

The field was unitized in early 1992 and a waterflood followed shortly thereafter. Initially, producing wells 19-7, 19-8 and 19-9A were converted to water injection wells to commence the 40-acre 5-spot injection program. Shortly thereafter, three additional wells were converted to water injectors. They were the 19-11, 19-12 and 19-13. Waterflooding is a process used to inject water into oil-bearing strata for pressure maintenance as well as for displacing and producing incremental oil after the economic production limit has been reached (Sam Sarem, 1992). Increased knowledge of spatial reservoir continuity is helpful when designing a waterflood project.

In October 2000, Citation Oil and Gas acquired the Happy Spraberry Field from Torch. There are currently 20 wells in the field; nine producers, six water injection wells and five dry holes. As of January 2003, cumulative production from the Happy Spraberry Field has been 5,554,308 stock tank

barrels (STB) of oil; 1,130,560 thousand cubic feet (MCF) of gas; and 2,774,554 STB of water.

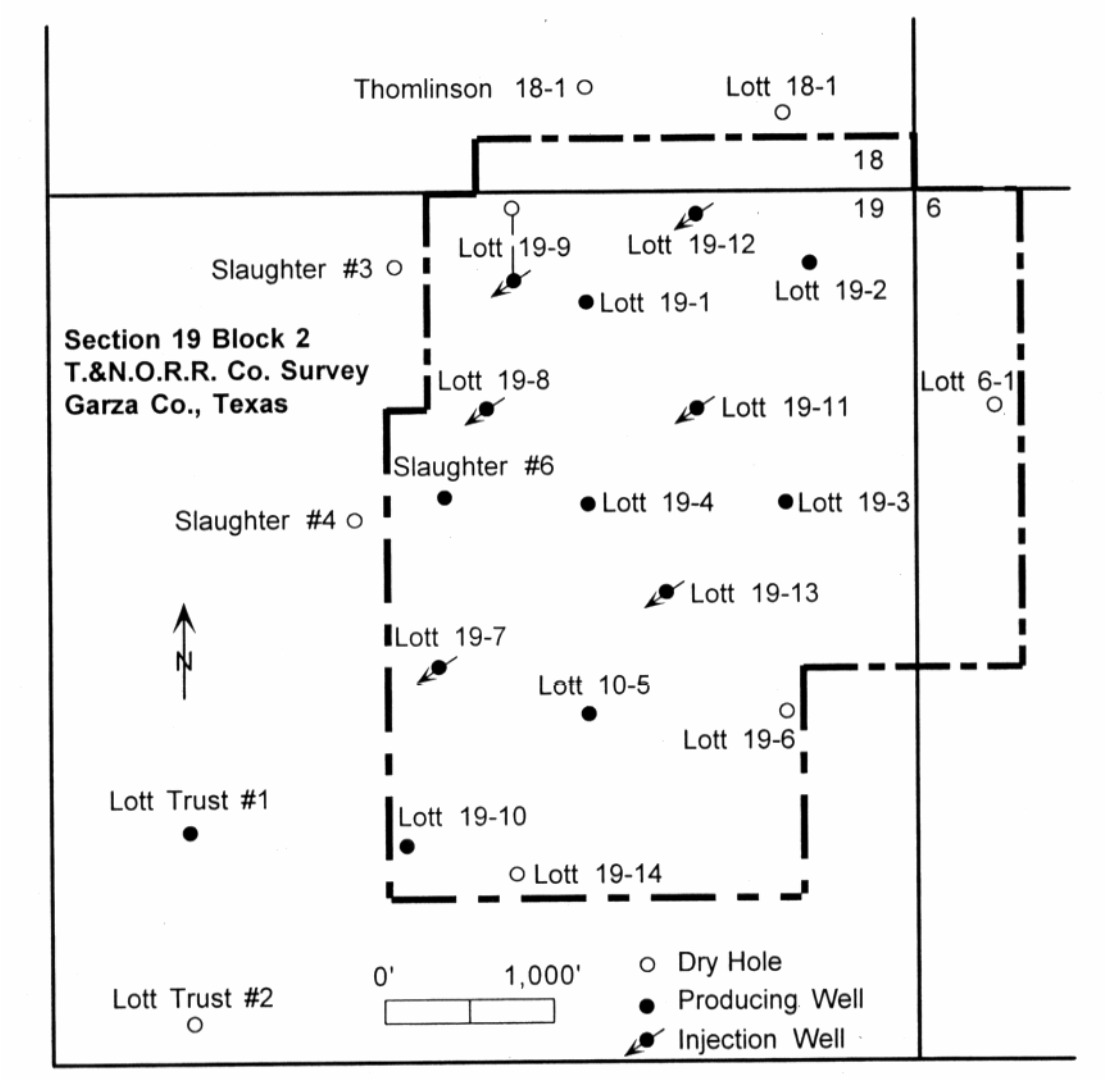

Figure 1. Base map of the Happy Spraberry Field showing the locations of dry holes, producing wells and injection wells

REGIONAL GEOLOGY

Structure

The Permian Basin (Figure 2) of West Texas and Eastern New Mexico is a major hydrocarbon producing region covering 155,000 sq. mi. (298,000 km ^{2}). The basin is an intra-cratonic basin located in the foreland of the Ouachita-Marathon orogenic belt. The basin formed during the Gondwana-Laurasia collision. Subsequent reactivation of existing zones of weakness caused the partitioning of the basin into several topographic highs and sub-basins (Ross 1986). This is highlighted by the Central Basin Platform, which separates the Delaware Basin to the west and the Midland Basin to the east. The Chadbourne Fault zone, which bounds the Midland Basin to the east, delineates the transition of marine platform facies of the Eastern Shelf to the basinal facies of the Midland Basin (Yang and Dorobek, 1994). This region has been tectonically stable and with the exception of tilting along the Permian Basin's flanks during the Triassic (Ward et al., 1986, Frenzle et al., 1988; Ewing, 1993; Mazzullo, 1995) little deformation has occurred since the Early Permian. Subsequently, Happy Spraberry carbonates are interpreted to reflect depositional relief, not fault and fold geometry. Likewise, anticlinal structures found in the Permian Basin reflect sedimentary drape over pre-Permian anticlinal features. A tectonic history of the Permian Basin is shown in Figure 3. A structure map of the Spraberry carbonates can be found in Figure 4.

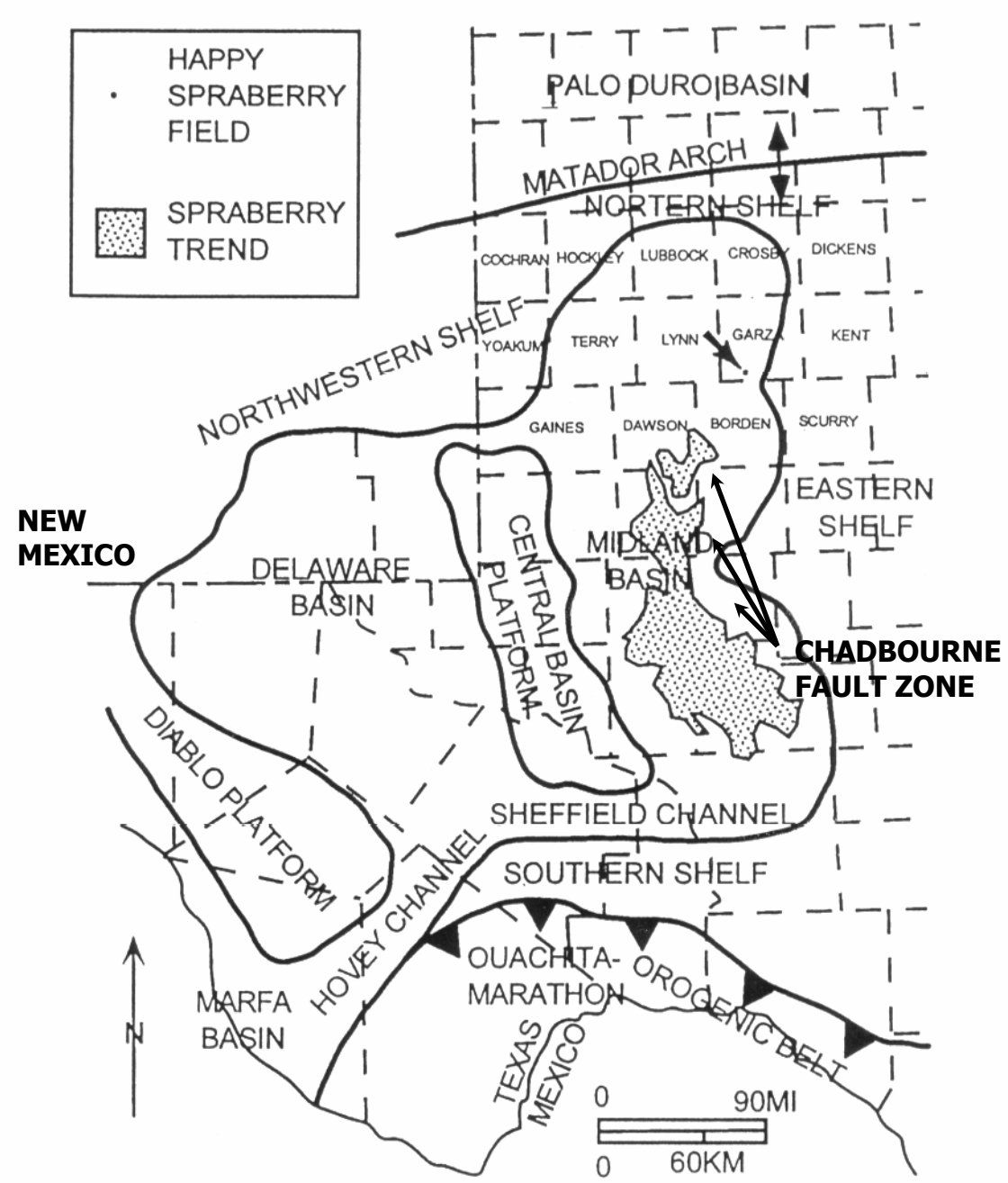

Figure 2. Tectonic Map of West Texas Permian Basin (modified from Handford 1981).

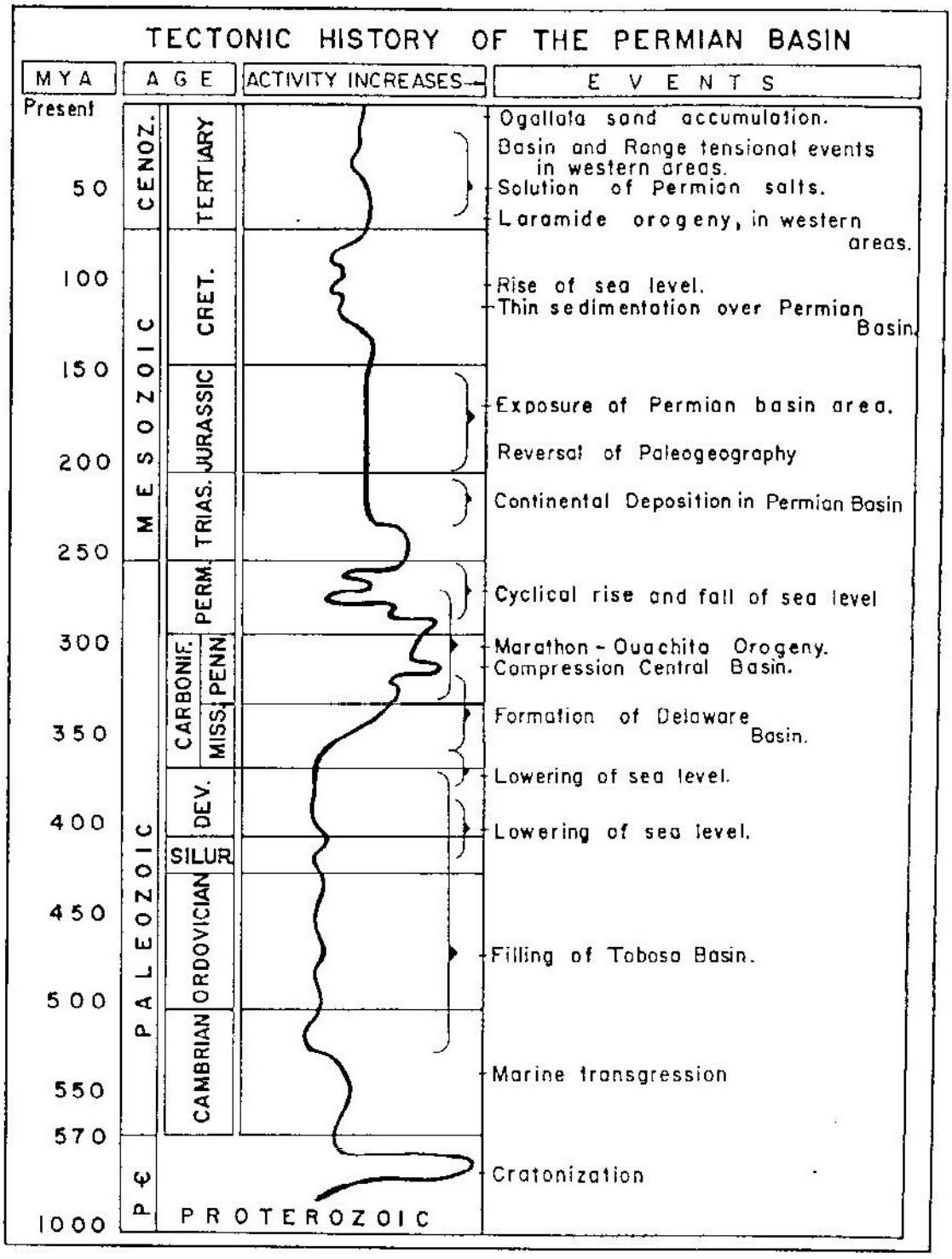

Figure 3. A tectonic history of the Permian Basin (Frenzel et al., 1988).

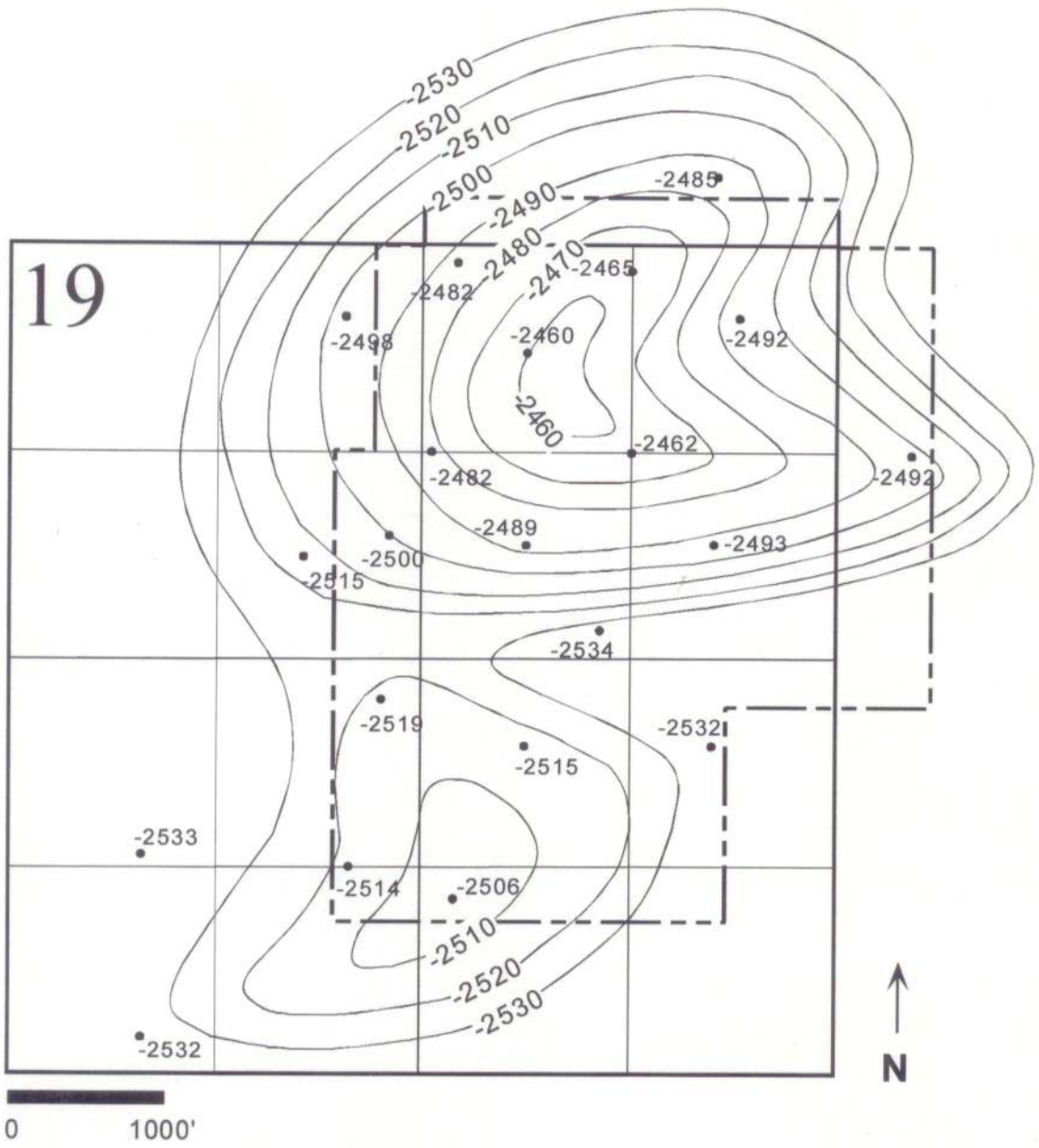

Figure 4. Structure map of the top of Spraberry carbonates (from Roy, 1998). Contour lines are feet below sea level and are contoured on a 10 foot interval.

Stratigraphy

Production from Happy Spraberry Field primarily comes from a 100 foot (30.5 m) interval of Lower Clearfork grainstones and packstones, Leonardian in age, at an average depth of 4,900 feet (1493.5 m). A detailed stratigraphic column for the Delaware and Midland Basins can be found on Figure 5. Figure 6 shows a generalized stratigraphic cross section across Garza County with the projected location of the Happy Spraberry lime and the transition from Leonardian shelf to Guadalupian ramp. Furthermore, Figure 7 shows an isopach of Spraberry carbonate.

Happy Spraberry Field is located on the upper slope of the Northern Midland Basin 4 miles basinward of the Eastern Shelf. At the time of Spraberry deposition the field was located near the Permian equator (Van Hilton, 1962; Habitch, 1979; Guevera, 1988) and inundated with shallow, warm, tropical waters. Alternating episodes of carbonate and siliclastic deposition occurred during this time.

During Early Permian (lower Leonardian), the Midland and Delaware Basins were predominantly sites of siliclastic deposition while carbonate platform development was being established along the western edge of the Eastern Shelf (Ward et al., 1986). Platform progradation of up to 24 km into the Midland Basin has been interpreted (Mazzullo and Reid, 1989). Siliclastic deposition has been interpreted as submarine fans and associated turbidites deposited during two relative sea level low stands (Silver and Todd, 1969).

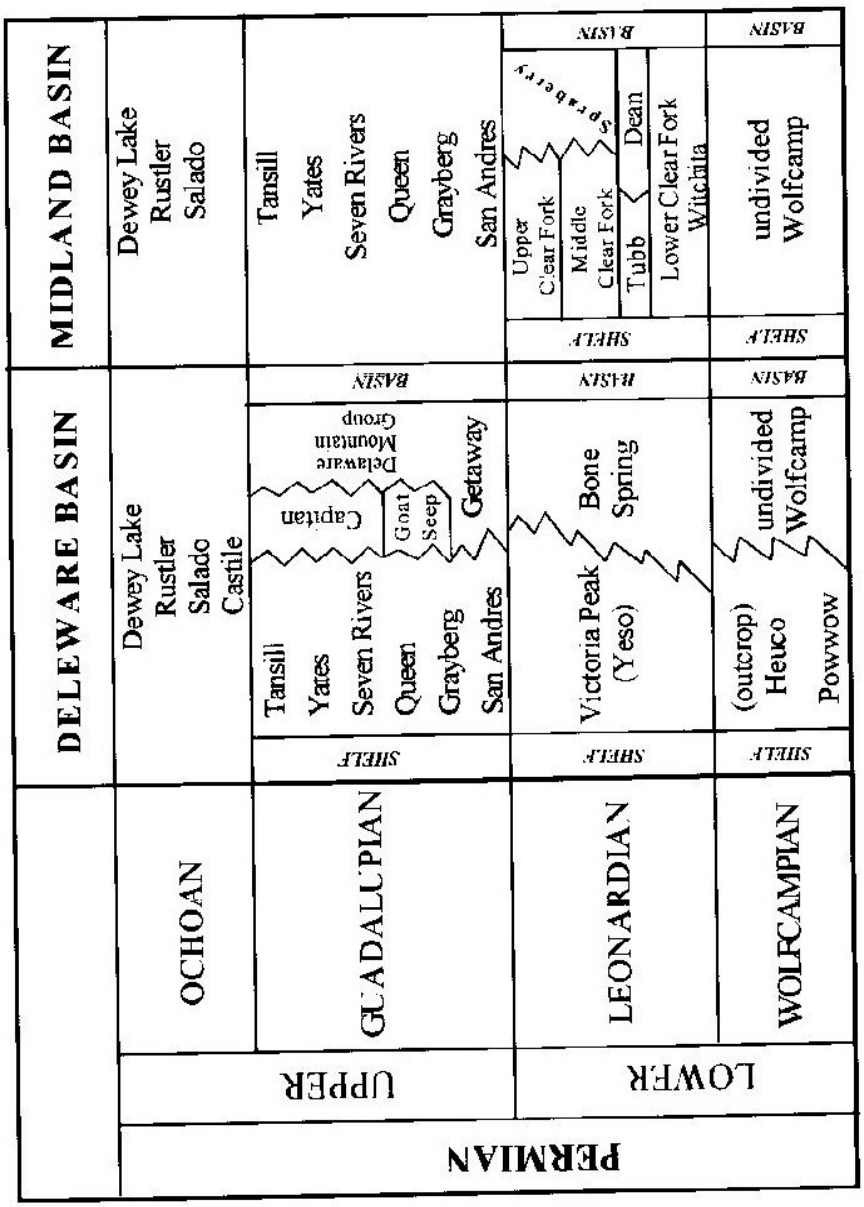

Figure 5. Stratigraphic column for the Delaware and Midland Basins (after Mazzullo, 1995).

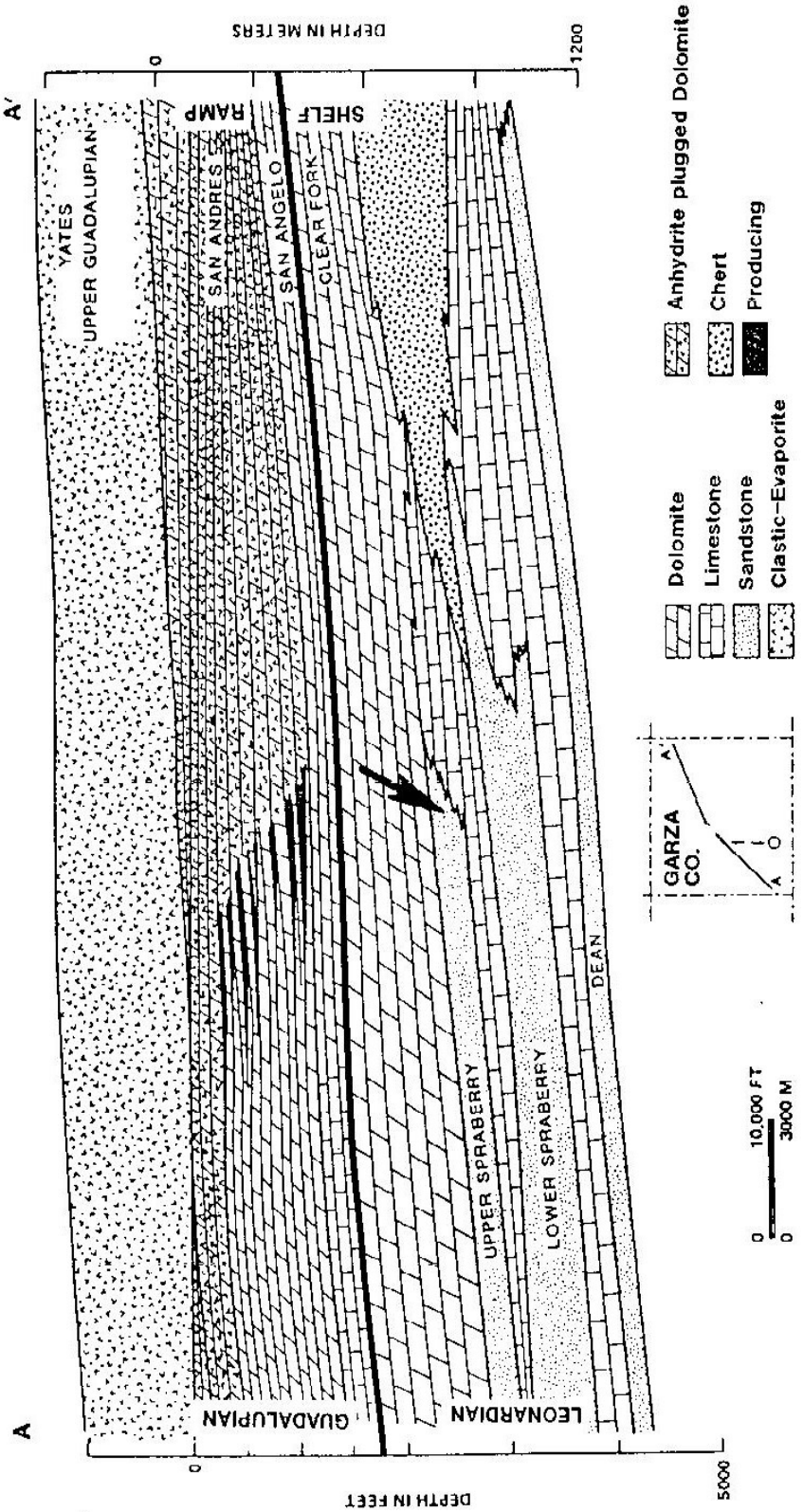

Figure 6. Stratigraphic cross section showing the projected location of the Happy Spraberry lime and the transition from Leonardian shelf to Guadalupian ramp (after Ward et al., 1986).

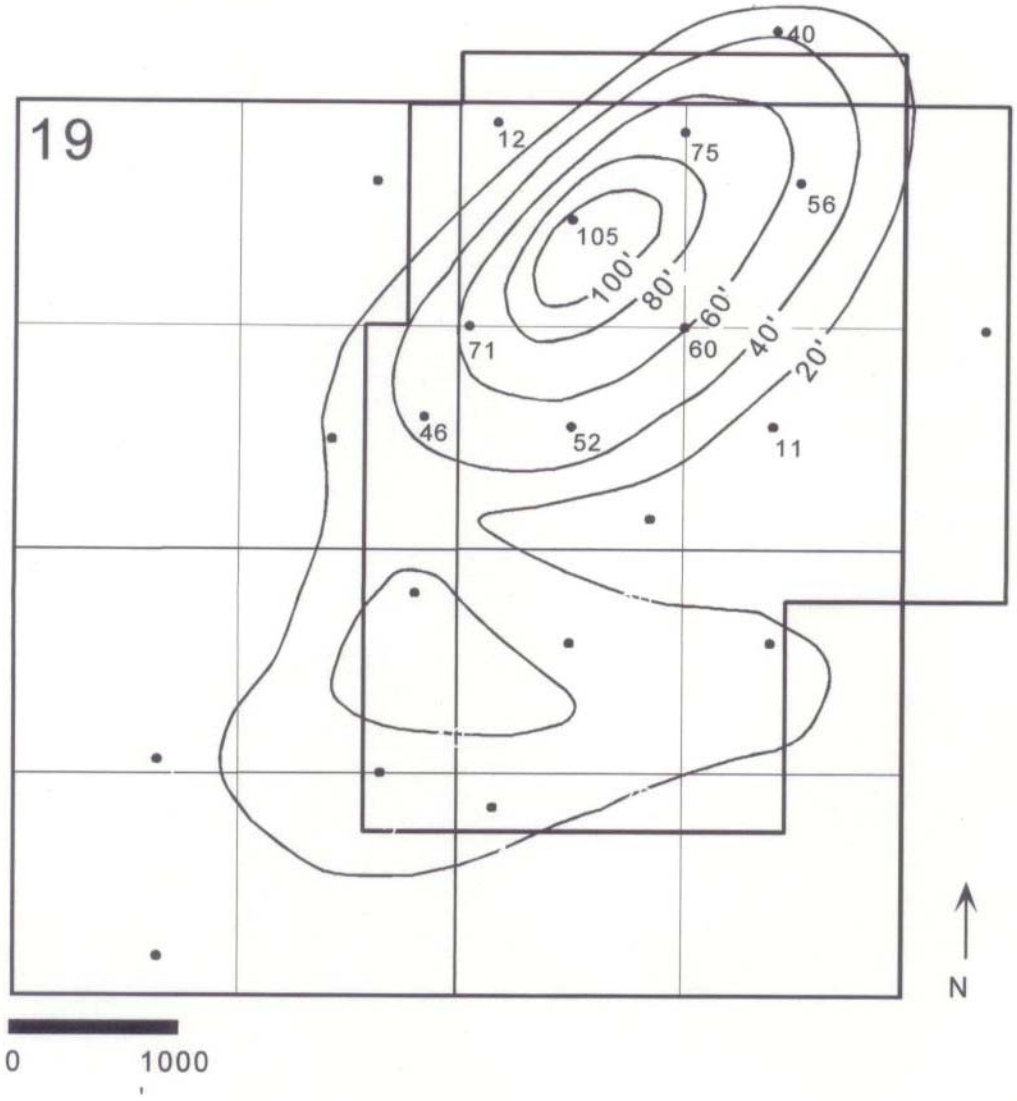

Figure 7. An isopach map showing Spraberry carbonate thickness (from Roy, 1998). The contour interval is 20 feet.

PREVIOUS WORK

Three research projects at Texas A&M have been devoted to the study of Happy Spraberry Field (Hammel 1996, Roy 1998 and Layman 2002). Hammel and Roy defined and mapped flow units based on pore geometries, origin, porosity and values. Layman based his identification of flow units on porosity characterization using petrographic image analysis.

This study differs from previous ones by making use of a neural network to identify flow units. The goal of this study is to create a neural network capable of identifying reservoir quality rocks (flow units) in Happy Spraberry Field making use of all available data. Inputs into the network include porosity data, permeability data and wireline log data. Not only will flow units be identified, but a qualitative description of reservoir quality (i.e. poor, intermediate, good) will be output using relationships obtained from wireline log data. The network will also identify inputs which have the greatest impact on reservoir rock quality thus aiding future investigators.

Neural network studies are limited in the field of petroleum geology and are more prevalent in the field of petroleum engineering. Past studies in the petroleum geosciences include the modeling of rock properties based on well log information (Nikravesh 1998), prediction of petroleum production (Boomer 1995), predicting permeability from porosity (Rogers et. al. 1995), lithology estimation (Saggaf and Nebrija 2000) and fluid property estimation (Alcocer and

Rodrigues 2001). A study involving the classification of reservoir quality in a carbonate field has yet to be undertaken.

NEURAL NETWORKS

History

A neural network attempts to emulate the parallel architecture of the mammalian brain. It is composed of a large number of highly interconnected processing elements that are analogous to neurons that are linked together with weighted connections that are analogous to synapses. Neural networks, in mathematical terms, can be thought of as multivariable, nonlinear regression analysis systems (Boomer 1995). Figure 8 shows a schematic of a typical neural network.

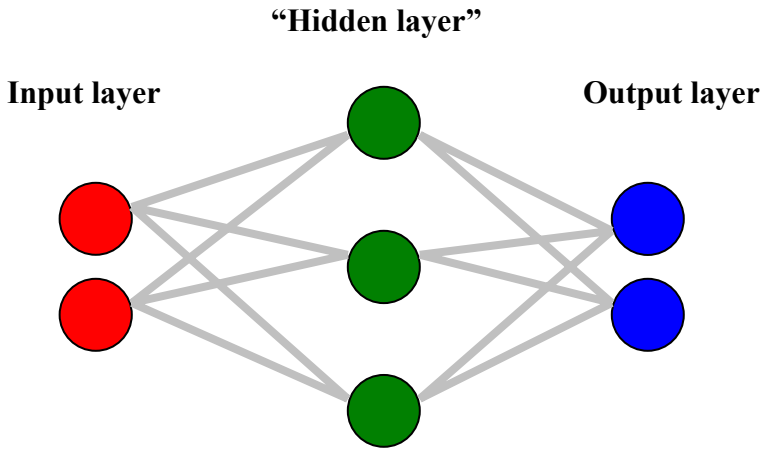

Figure 8. A schematic of a neural network. The flow of computation is from left to right.

Neural networks were first modeled with electrical circuits in 1943 by neurophysiologist Warren McCulloch and mathematician Walter Pitts. In the 1950's Nathaniel Rochester of IBM research laboratories led the first efforts to simulate neural networks. Rochester was eventually successful; however, traditional computing began to flourish and this newfound emphasis left neural computing in the background. Advocates of "thinking machines" remained however. In 1956 the Dartmouth Summer Research Project on Artificial Intelligence pioneered work on both artificial intelligence and neural networks. Shortly after the Dartmouth Project, Frank Rosenblatt, a Cornell neuro-biologist, was intrigued with the operations that tell a fly when to flee. The result of his research was the Perceptron, the oldest neural network in use today. The Perceptron computes a weighted sum of the inputs, subtracts a threshold, and passes one of two possible values out as the result. The Perceptron was limited and was proven so in the 1969 book *Perceptrons* by Marvin Minsky and Seymour Papert.

In 1959, MADALINE (Multiple ADAptive LINear Elements) became the first neural network to be used commercially. MADALINE, developed by Bernard Widrow and Marcian Hoff of Stanford, is an adaptive filter that reduces echoes in phone lines; it is still in use today. Due to these early successes in neural computing there was an exaggerated potential associated with them. Reality was that there was a limitation on the necessary computing power and the excessive hype was not realized. The excitement around neural networks

did not return until 1982. In was in 1982 that John Hopfield of Caltech eloquently presented a paper to the National Academy of Sciences that showed the role of neural networks role in creating useful devices. Shortly thereafter, research dollars began to flow and meetings and conferences were well attended. In the 1990's and into the new millennium, many of the hardware limitations had been lifted and the scope of neural networks became boundless.

Use

A neural network attempts to mimic biological learning processes. The human brain contains upwards of 100 billion neurons; each neuron can subsequently be connected with up to 10,000 other neurons through synapses (Anderson and McNeil 1992). A neural network works much the same way. A neural network is made up of highly interconnected processing elements (i.e. nodes) that are analogous to neurons that are linked with weighted connections (i.e. hidden nodes) that are analogous to synapses (Anderson and McNeil 1992). However, even highly complex neural networks are far smaller and less complicated than their inspiration, the human brain.

At the outset, a neural network makes a first attempt to answer the assigned problem assuming random relationships between the inputs and the outputs. The network will then self-modify to find the best relationship between the inputs and outputs.

A node represents the each input and output channel. The connections between the inputs and the outputs are called hidden nodes. All input nodes are

connected to hidden nodes and likewise, all output nodes are connected to hidden nodes. Neither input nodes nor output nodes are directly connected (this case would represent a linear model). All connections have an independent weighting factor associated with them. Initially the inputs are multiplied by their respective weighting factor. Next, the modified inputs are feed into a summation function. The summation function can perform various operations; however, the usual product is a sum. The output of the summation function is then sent to a transform function. The transform function contains an algorithm which transforms the input into a zero (0) or positive one (1); or a negative one (-1) or a positive one (1), or some other number. Transform functions commonly supported include sigmoid, sine, hyperbolic tangent and logistic. It is the transform function that provides non-linearity and constrains the node's signal within a fixed range. That is, no matter how "excited" a node may be, it has a fixed maximum signal that can be fired, much like a biological neuron. The result of the transform function is generally the output of the hidden node layer.

Typically, the network will attempt an initial pass through the data and produce a result that is unlikely to be correct. This is because the weighting factors initially assume a random relationship between the inputs and the outputs (i.e. the network has not learned anything). This answer is then compared to the correct answer and the weighting factors are adjusted in the hopes of minimizing error. This type of network algorithm is called back propagation; the error is back propagated through the network until the error is

minimized. It may take several million passes before the network reaches an acceptable solution (Boomer 1995).

Advantages

A neural networks primary advantage over traditional computing algorithms and statistical methods has been its ability to impersonate human characteristics such as generalization and interpretation (Hertz et al., 1991). Neural networks are capable of recognizing patterns, retrieving data associatively, filtering noise from experimental data, completing missing information and estimating sampled functions when the mathematical form of the function is unknown (Rogers et al., 1995). Because of the above qualities, neural networks are ideal at functional prediction and system modeling where physical processes are poorly understood or too complex. Neural networks also show resilience against distortions in input data and they filter noise from data admiringly. Neural networks, in short, have the ability to implicitly detect complex nonlinear relationships between dependent and independent variables.

Disadvantages

Without a complete understanding of the way neural networks function, they are often thought of as a “black box” approach instead of a useful method to generate reproducible geological models. Ignorance is the primary culprit for this belief, and with a better knowledge of neural network underpinnings and architecture the “black box” label should disappear.

Another problem with neural networks is that they are prone to “over fitting”. Like neural networks, polynomial curve fitting has much the same problem and will be used to demonstrate this concept. Polynomial shape is determined by the order, that is, the larger the number of orders the more oscillatory the shape. Given a set of data, a polynomial curve may be used to fit the data (i.e. model).

Assuming that data are replete with extraneous information, the best fit curve or surface may not necessarily pass through all data points. A low-order polynomial may not fit; whereas a high-order polynomial may fit the data exactly by adopting a highly oscillatory shape that is unrelated to the underlying function (see Figure 9, below).

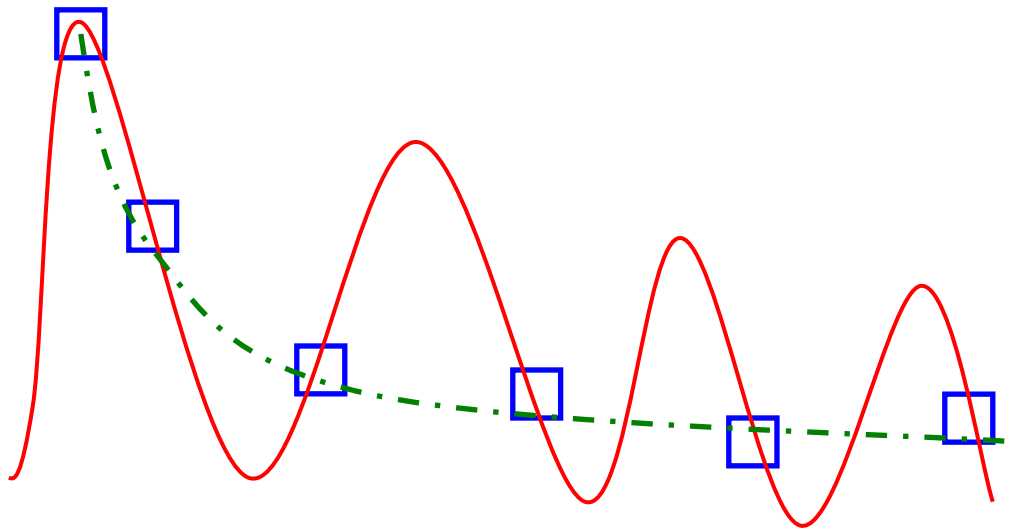

Figure 9. High order polynomial (red-line) fitting the data (blue squares) exactly but not modeling the underlying function (dotted green-line).

FLOW UNITS

In about 1990, Texas A&M University began research into the identification of carbonate reservoir flow units. A flow unit as defined by Ebanks (1987) is the mappable portion of the total reservoir within which geological and petrophysical properties that affect the flow of fluids are consistent and predictably different from the properties of other reservoir rock volumes. Ahr and Hammel (1999) define a “ranked” flow unit (i.e. a good flow unit) as one with the highest combined values of porosity and permeability with the least resistance to fluid flow. A flow unit may also include nonreservoir features such as shales and cemented layers where combined porosity-permeability values are lower and resistance to fluid flow much higher (i.e. a poor flow unit) (Ebanks 1987). Ebanks et al. (1992) stated that flow units have the following characteristics in common:

1. A flow unit is a specific volume of a reservoir, which is composed of one or more reservoir quality lithologies and any nonreservoir quality rock types within that same volume, as well as the fluids they contain.
2. A flow unit is correlative and mappable at the interwell scale.
3. A flow unit zonation is recognizable on wireline logs.
4. A flow unit may be in communication with other flow units.

Figure 10 (from Ebanks et. al. 1992) shows a progression of geological and petrophysical data used in identifying flow units. Where this study differs from previous studies is that a neural network will be employed in the identification of flow units in a carbonate reservoir.

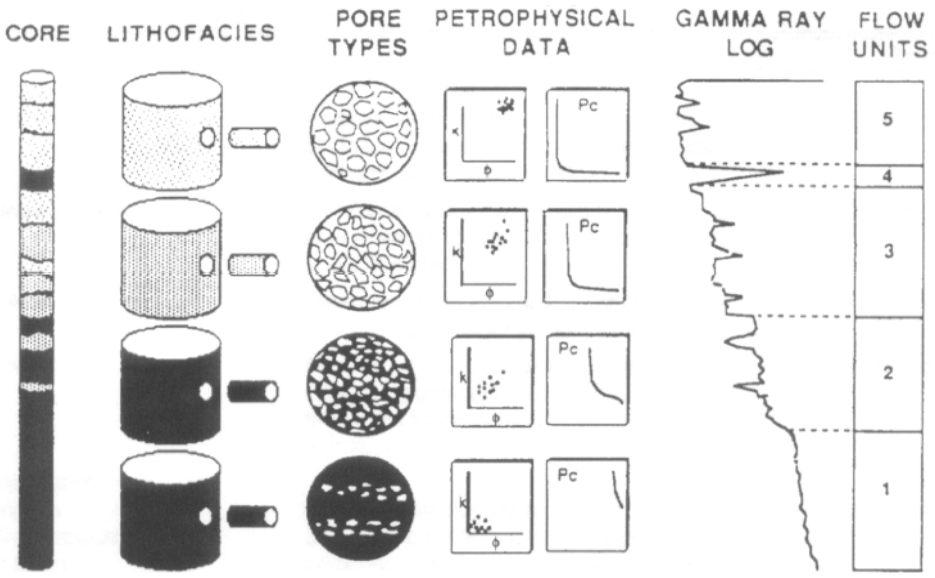

Figure 10 (from Ebanks et. al. 1992). Flow unit identification and the interdependence of lithologic and petrophysical data.

An important note is that Ebanks' notion of flow units is limited to the study of siliciclastic reservoirs. Flow unit identification in carbonate reservoirs is somewhat more difficult. For example, carbonate flow units can not be identified by wireline log data alone as Ebanks has shown. This is because carbonate

pore systems have different pore categories than do siliciclastics. That is, porosity and permeability values greatly differ among the various lithofacies. It is necessary to use cores and pore characteristics in the identification of carbonate flow units.

LITHOLOGY

Four distinctive lithofacies were identified in Happy Spraberry Field based on constituent composition, depositional texture and sedimentary structures (Appendix A from Hammel, 1996; Roy, 1998; Layman, 2002). Reservoir facies include oolitic skeletal grainstones/packstones and skeletal rudstones. Non-reservoir facies contain floatstones and shaly siltstones. Most of Happy Spraberry production is from the oolitic grainstone facies. A type log showing typical wireline log signature of each facies is shown in Figures 11 and 12. The oolitic grainstone/packstone interval is distinguishable by its comparatively low gamma ray value that reaches a minimum of 15 API units. This is coupled with increased resistivity values reaching as high as 200 ohm-m and density-neutron porosity between 13 and >30%. Rudstone sections typically show somewhat higher gamma ray values (~ 30-40 API units) coupled with lower resistivity values (~5 ohm-m). Density-neutron porosity through the rudstone interval averages 10-15 %. Floatstones display a gamma ray reading between 40 and 70 API units with resistivity values only slightly lower than that of the rudstones. Density-neutron values for floatstones average approximately 14%. Shaly siltstones typically incase the carbonate interval and exhibit much higher gamma ray values (>70 API units). Resistivity values for the shaly siltstones averages 2-5 ohm-m and density-neutron porosity characteristically runs 10-15%.

The oolitic grainstones and packstones are typically found near the top of the Happy Spraberry sequence. This facies represents deposition in a shallow

marine setting. In fact, carbonate facies were interpreted by previous investigators (Hammel, 1996; Roy, 1998) to be deposited on a distally steepened ramp as an oolitic sand and skeletal buildup shoal complex. Siliciclastics were also interpreted as being deposited in an open marine setting.

Reservoir Facies

Oolitic Skeletal Grainstone and Packstone Facies

This facies forms the largest reservoir unit and is present in all wells ranging in thickness from 15 to 50 feet. The rock is typically pale gray to white in color; however, oil staining is common and may alter the color to dark tan or brown. Figure 13 shows core photos representative of this facies. Ooids and peloids make up more than 75% of this rock type while the remainder is comprised of skeletal fragments of crinoids, bryozoans, brachiopods, mollusks, ostracods and foraminifera. Lime mud is also present but rare (Hammel, 1996).

The ooids, peloids and skeletal fragments are well rounded and well sorted with average ooid grain diameter between 200 and 300 microns (Layman 2002). The presence of coated grains and the lack of matrix are indicative of deposition in shallow agitated waters. Because of its presence in all field cores at approximately the same depth, the facies is interpreted to be laterally continuous within the Happy Spraberry field limits.

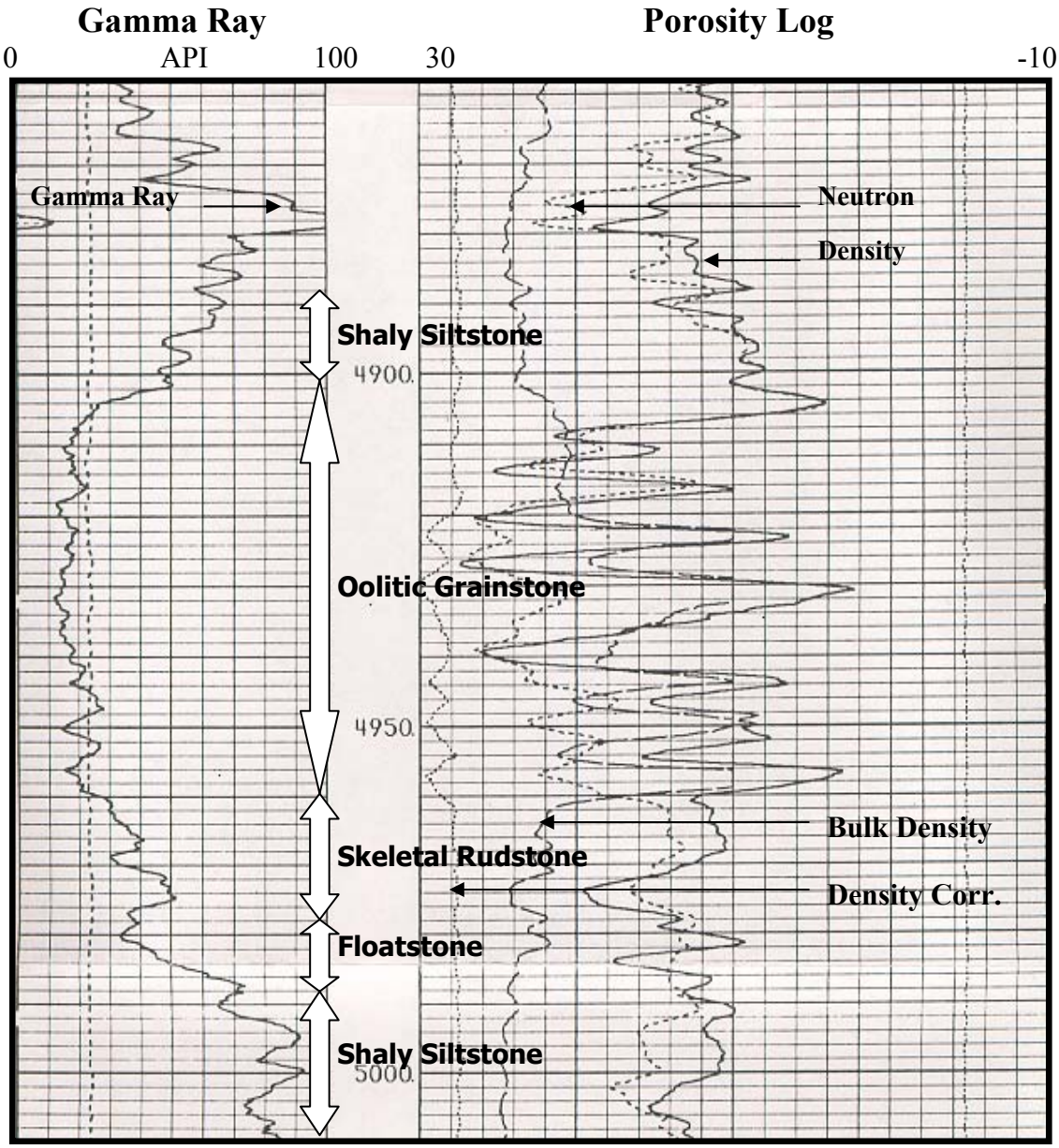

Figure 11. Type log showing Happy Spraberry well Lott #19-4 (porosity).

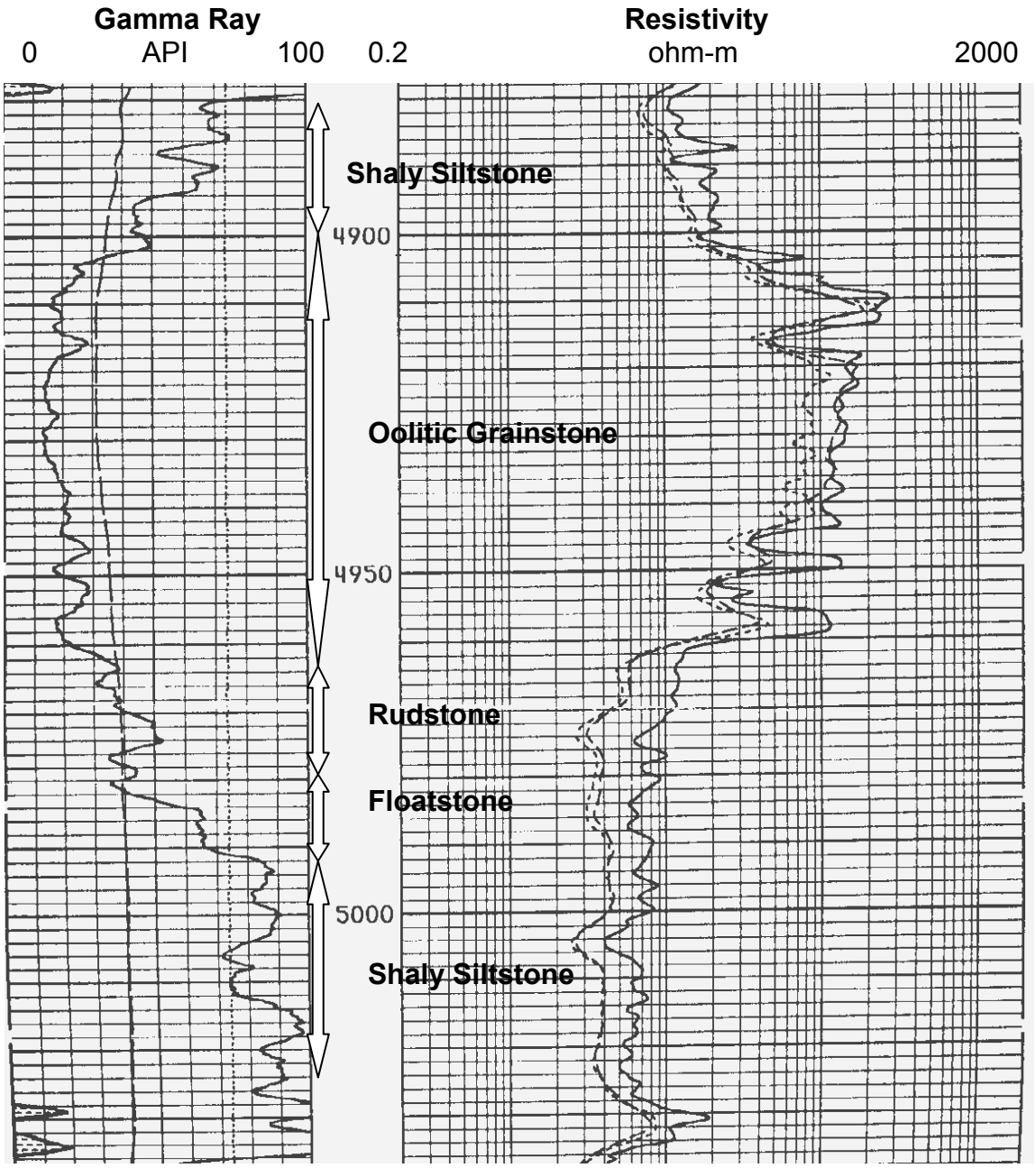

Figure 12. Type log showing Happy Spraberry well Lott#19-4 (resistivity).

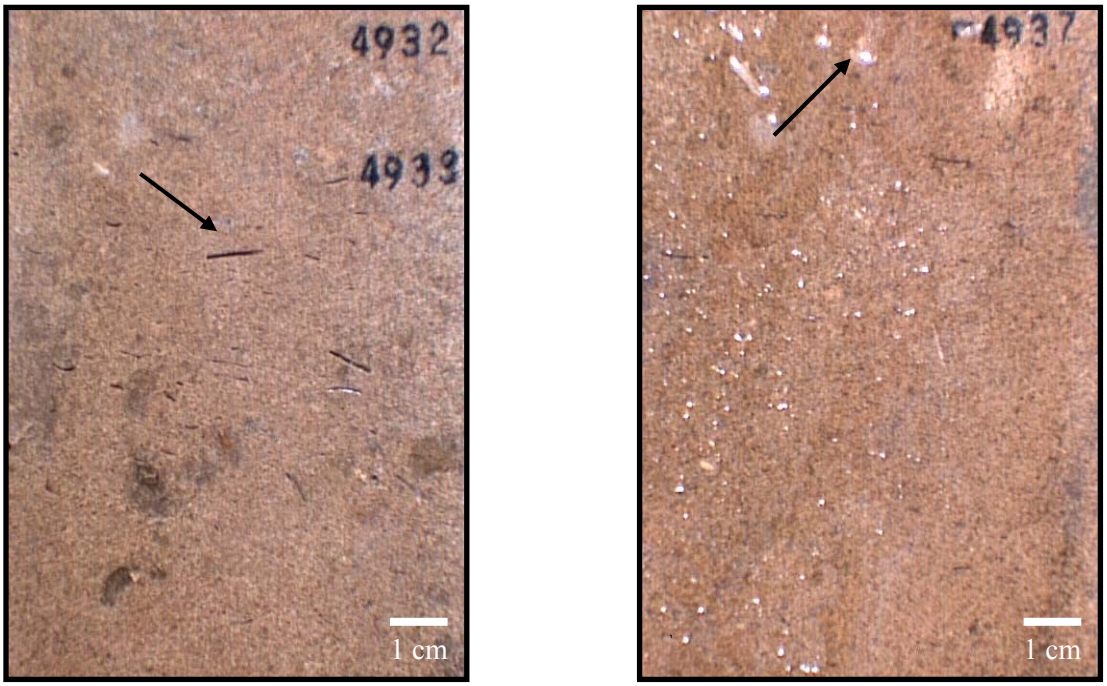

Figure 13. Core photos showing typical oolitic skeletal grainstone/packstone facies. Core photos (Layman, 2002) taken from Lott #19-4 at depths of 4933'and 4937' respectively. The arrow in *A* shows well developed skel-moldic porosity. The arrow in *B* is beaded water due to residual oil saturation.

Figures 14, 15 and 16 show the relationship between lab porosity and lab permeability, lab porosity and neutron porosity, and lab porosity and density porosity respectively.

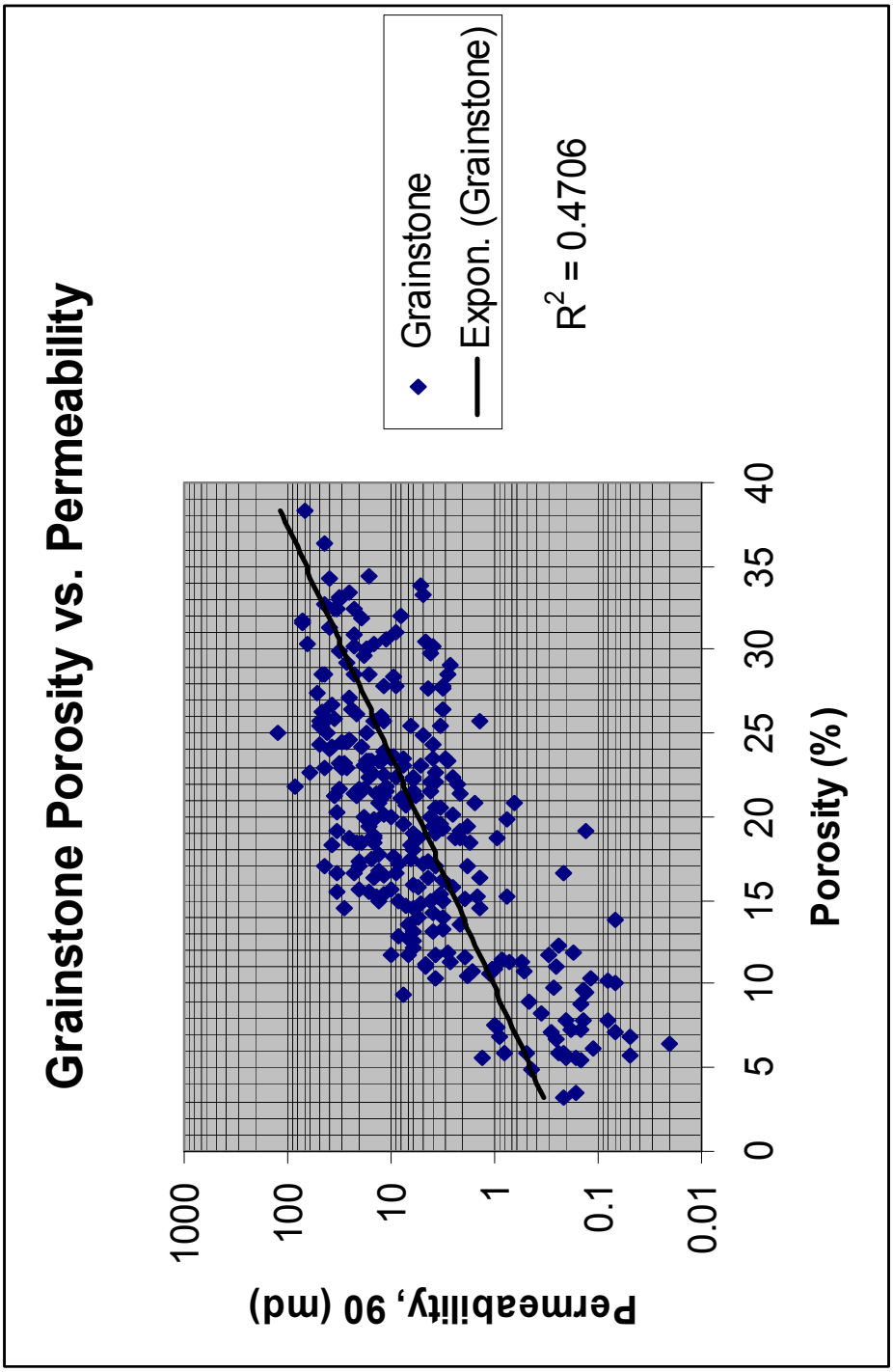

Figure 14. Grainstone porosity versus permeability.

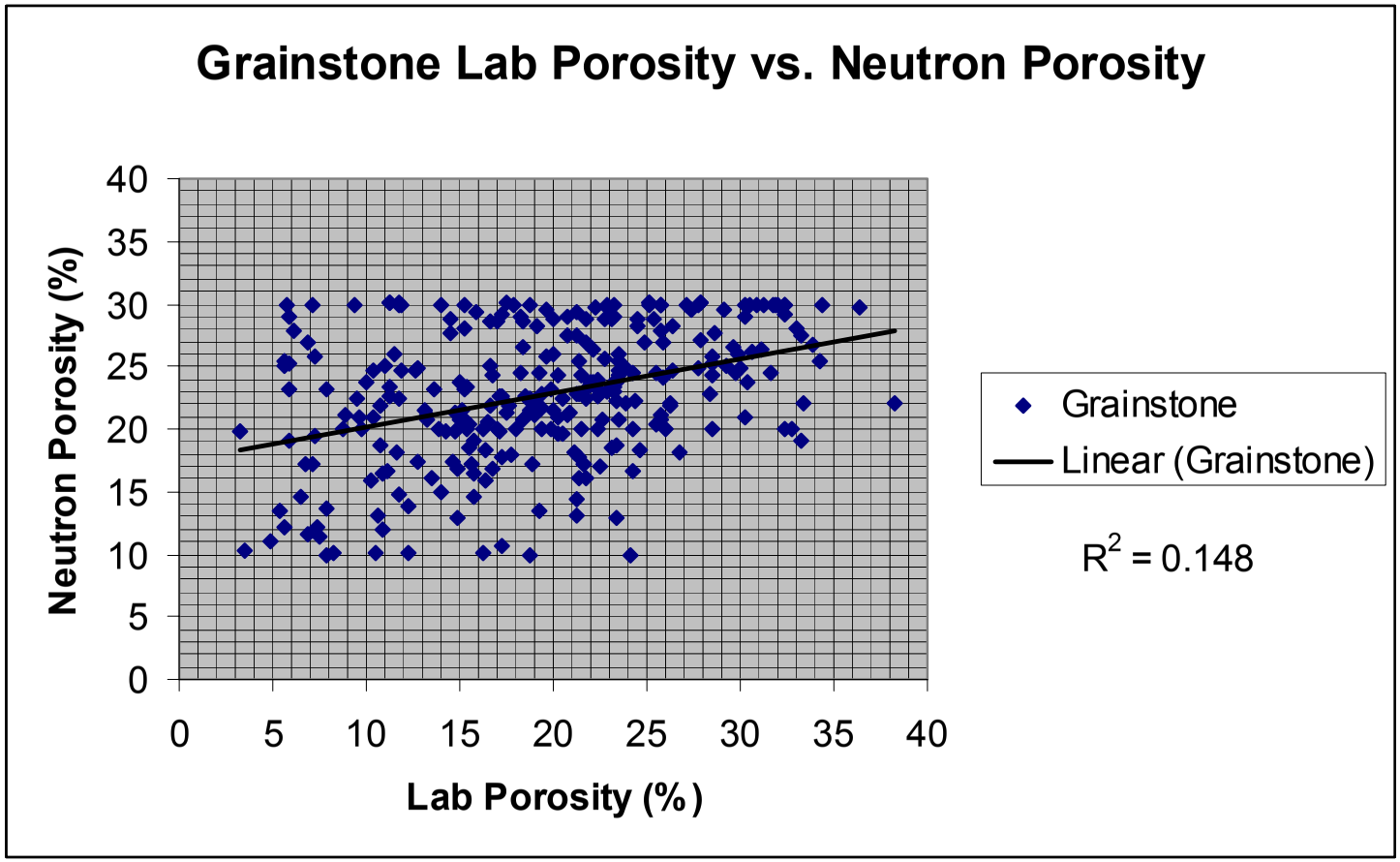

Figure 15. Grainstone lab porosity versus neutron porosity.

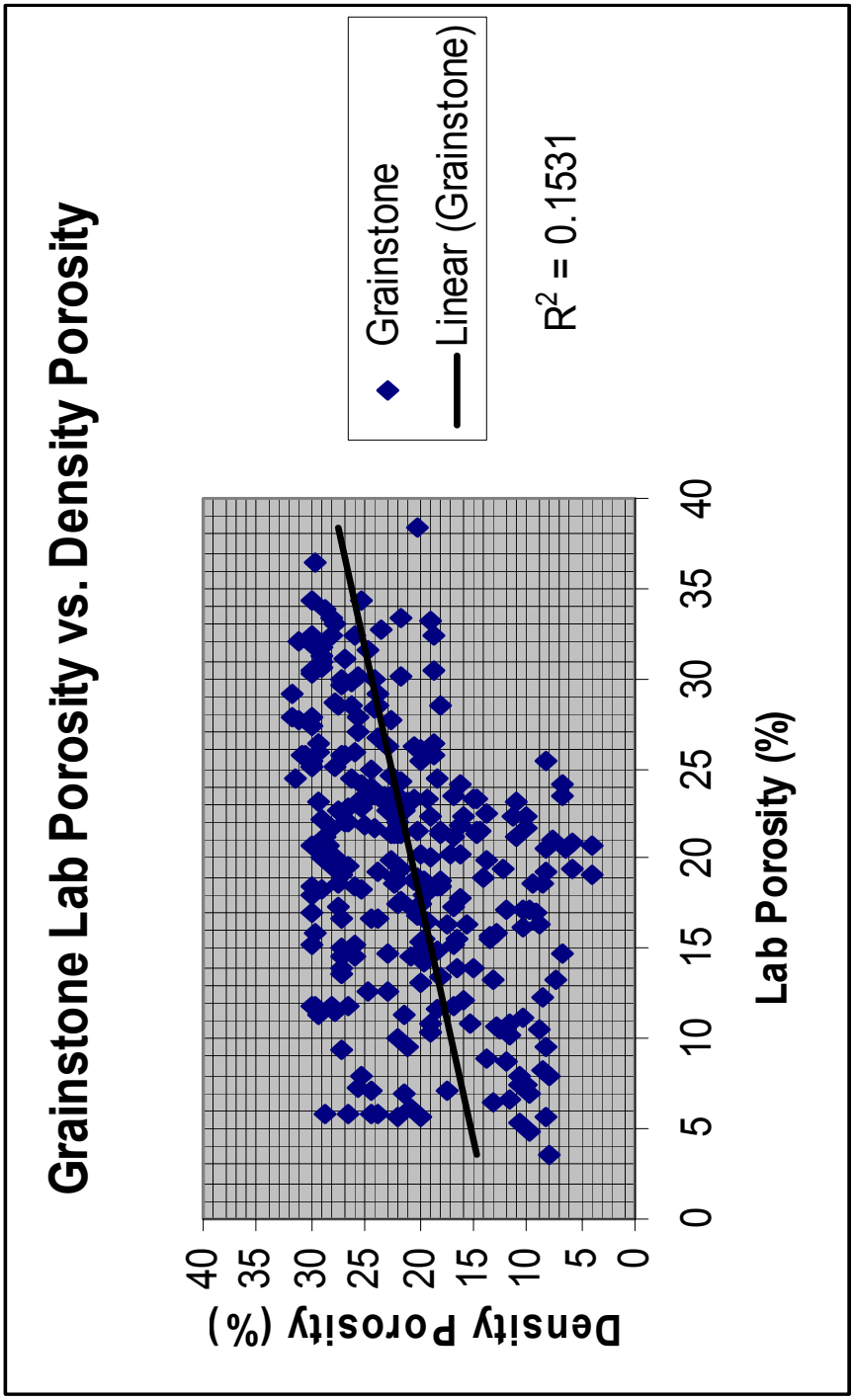

Figure 16. Grainstone lab porosity versus density porosity.

Skeletal Rudstone Facies

The skeletal rudstone facies is light gray to brown in color. Skeletal fragments of crinoids, bryozoans, brachiopods, mollusks, ostracods and foraminifera constitute approximately 75% of this facies type while the remaining 25% is divided among *Tubiphytes*, lime mud and siliciclastics. This rock type is poorly sorted and the skeletal grains are subrounded to subangular with an average grain size of 0.7 mm (Hammel, 1996).

Because of their large clasts and absence of fine matrix, the rudstones are interpreted to have been deposited close to an organic buildup (i.e. reef). Clasts are typically composed of the oolitic grainstone facies and represent shedding off the reef (Layman, 2002). Figure 17 shows a core photo of the rudstone facies.

Figures 18, 19 and 20 show the relationship between core porosity and permeability, core porosity and neutron porosity, and core porosity and density porosity respectively.

Figure 17. Core photo (Layman, 2002) of rudstone facies from Lott #19-4 at a depth of 4963'.

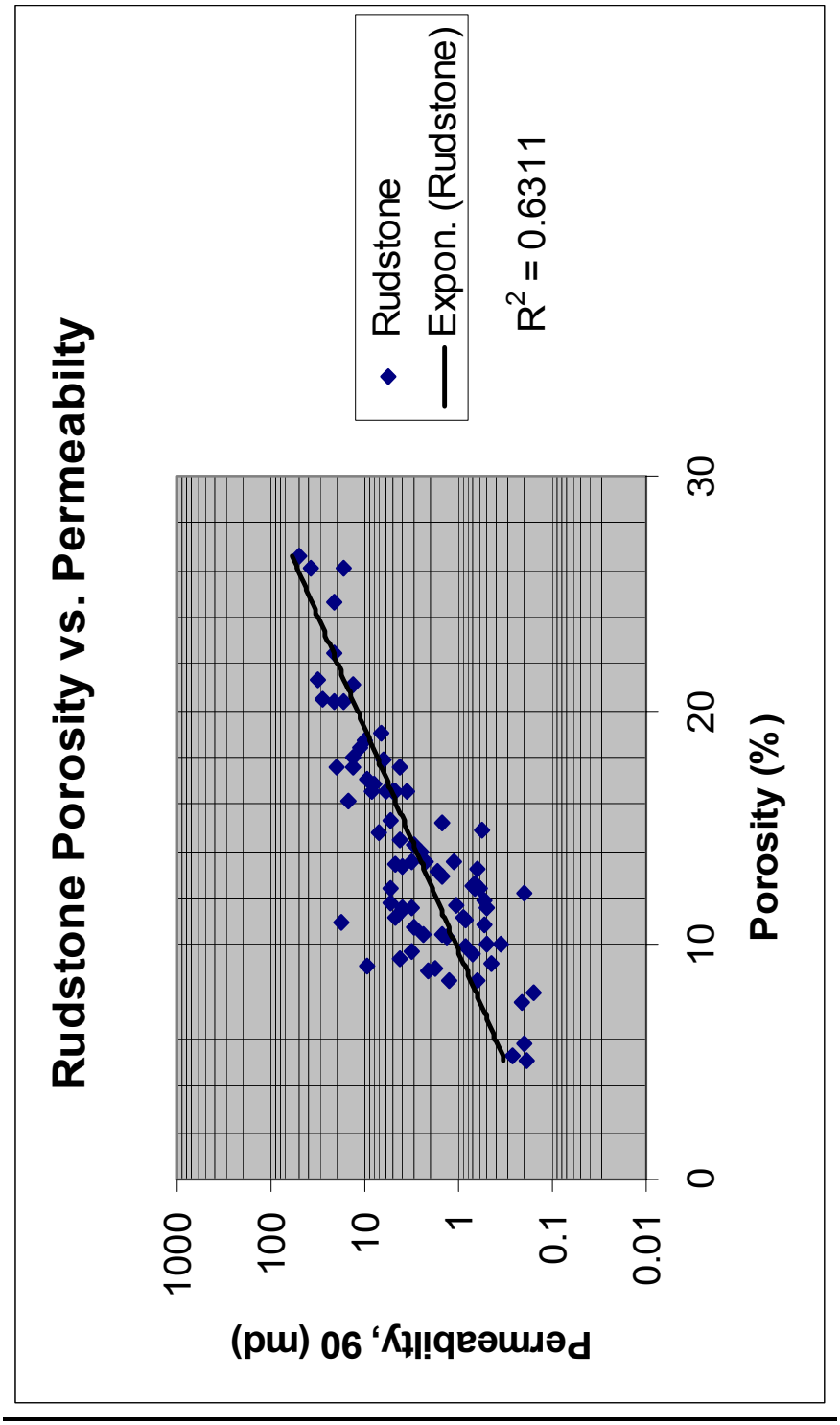

Figure 18. Rudstone porosity versus permeability.

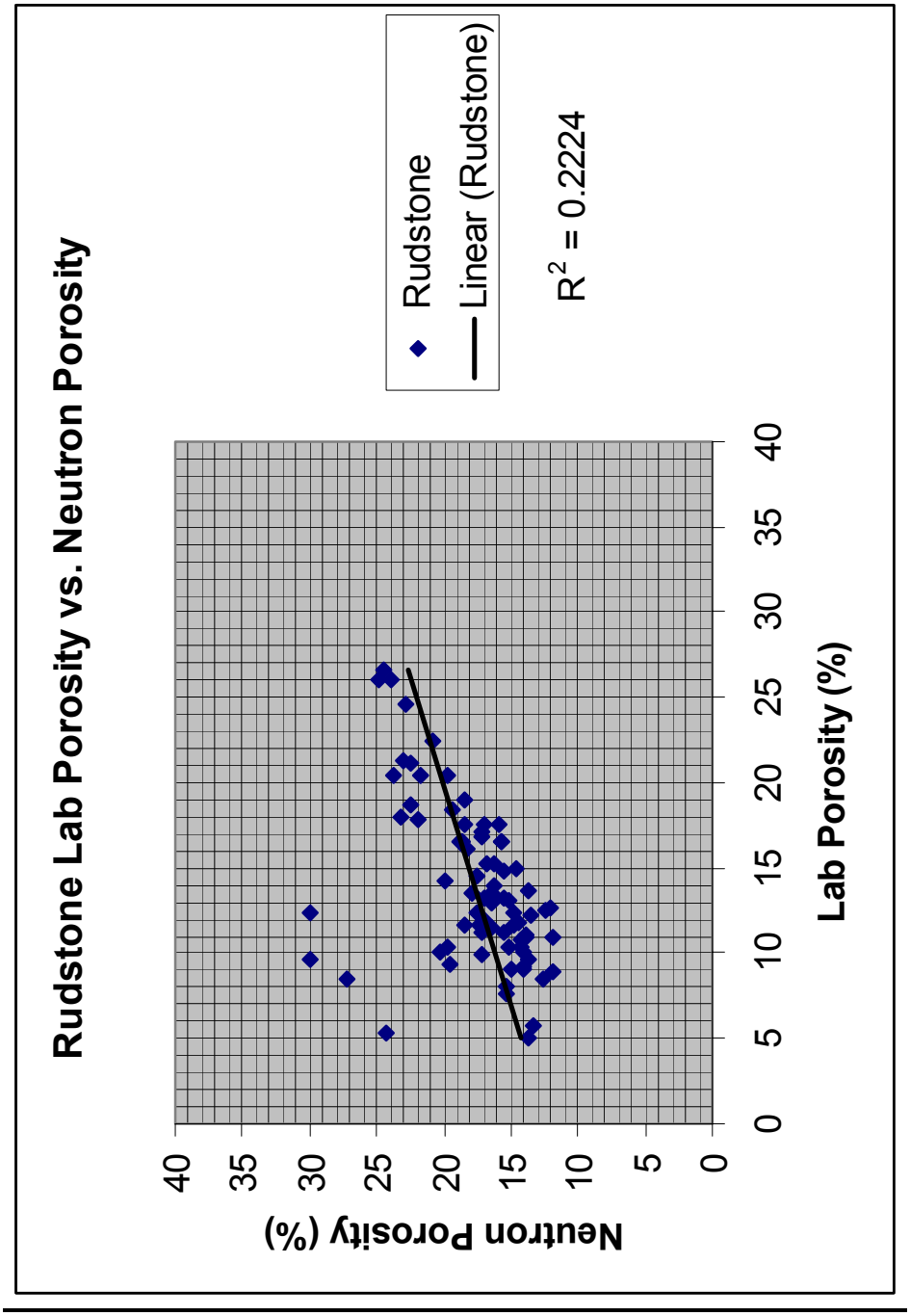

Figure 19. Rudstone lab porosity versus neutron porosity.

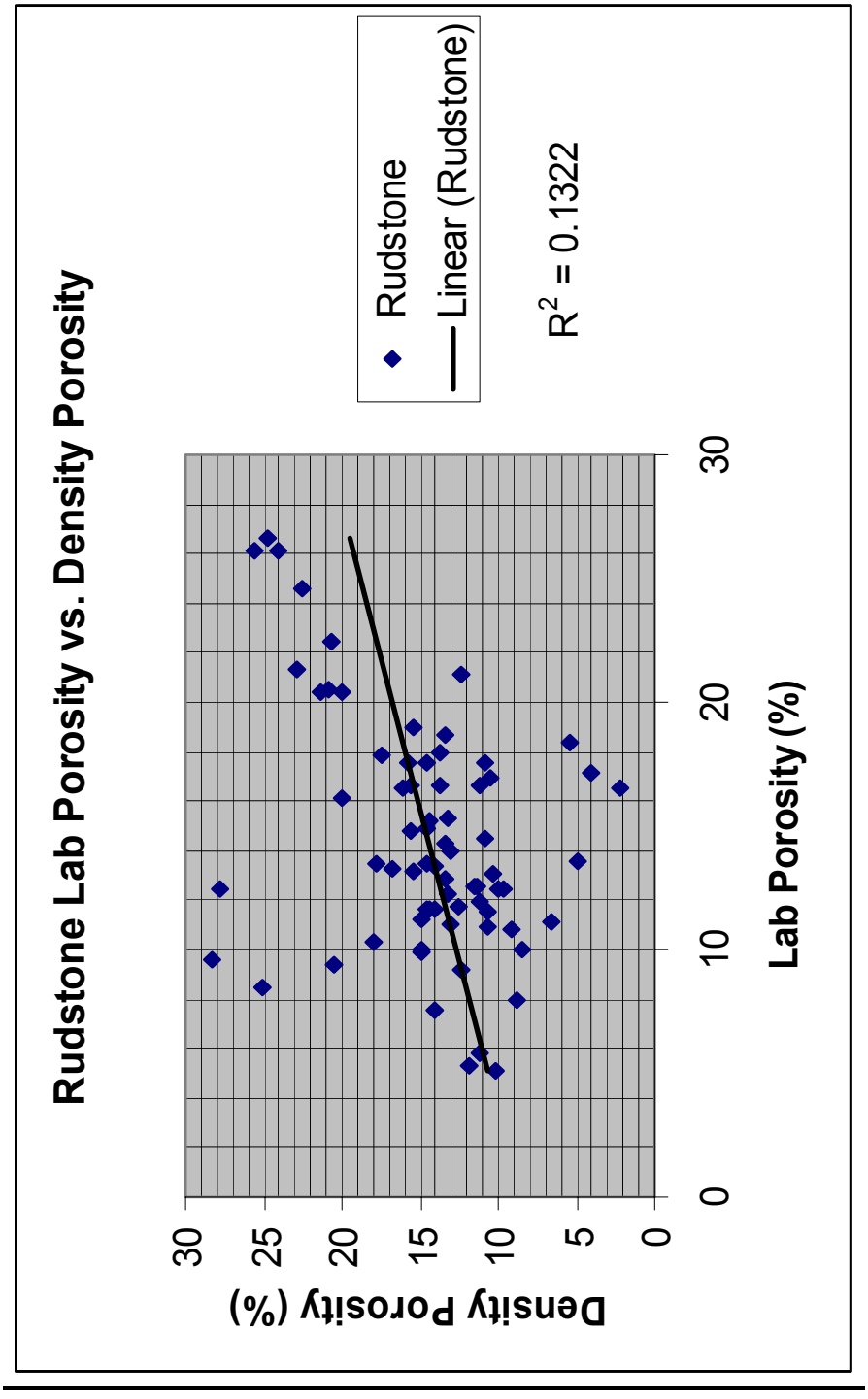

Figure 20. Rudstone lab porosity versus density porosity.

Non-reservoir Facies

Floatstone

Floatstones in Happy Spraberry characteristically have light gray to white clasts surrounded by a dark gray to black matrix. Clasts of the oolitic grainstone and skeletal rudstone facies constitute 50% of this rock type. The clasts are angular to subangular and range in size from 1 mm to 12 mm (Hammel, 1996). Floatstones are interpreted to have been deposited as reworked material next to the oolitic source. Figure 21 shows a core photo of the floatstone facies.

Figures 22, 23 and 24 show the relationship between core porosity and permeability, core porosity and neutron porosity, and core porosity and density porosity respectively.

Figure 21. Core photo (Layman, 2002) of floatstone facies from the Lott #19-4 well at a depth of 4981'.

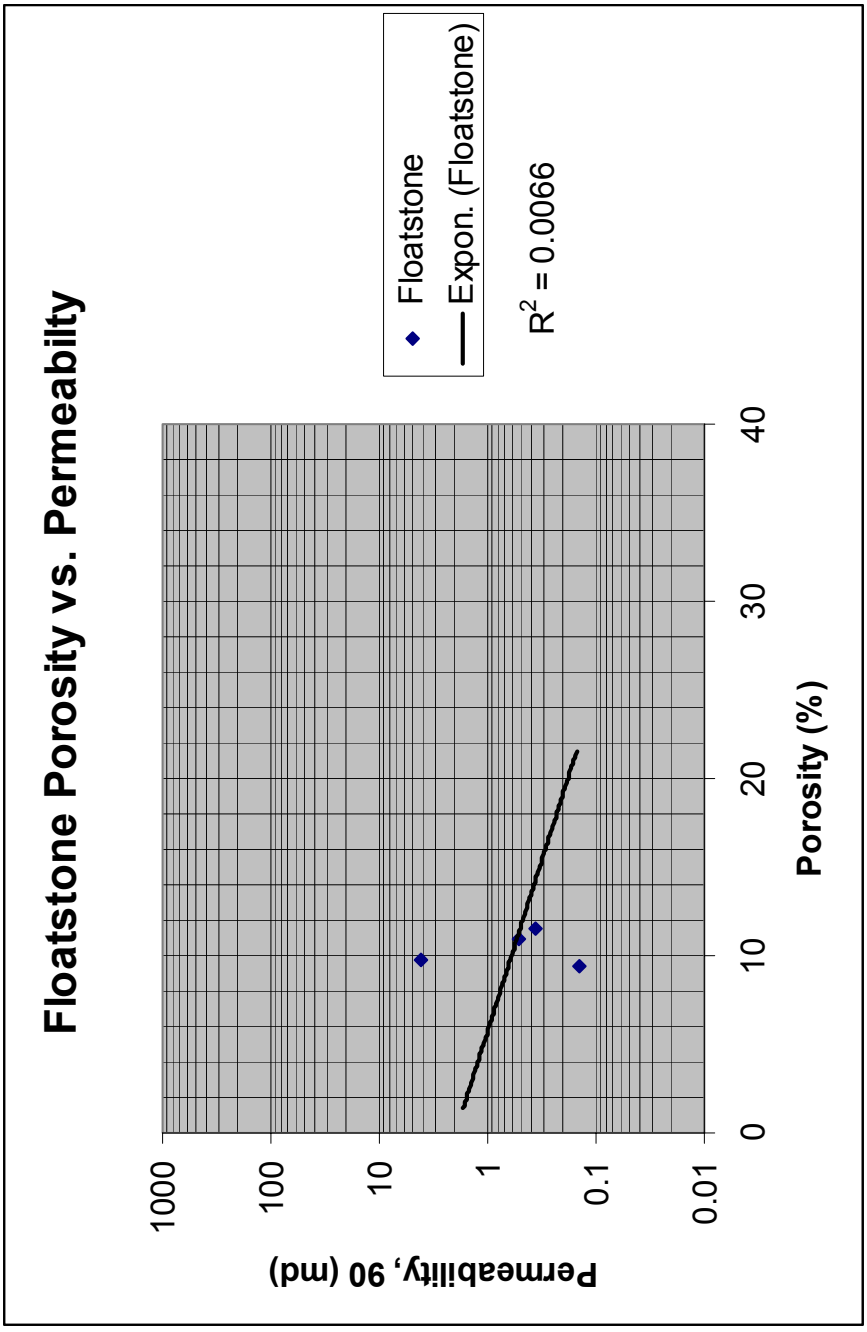

Figure 22. Floatstone porosity versus permeability.

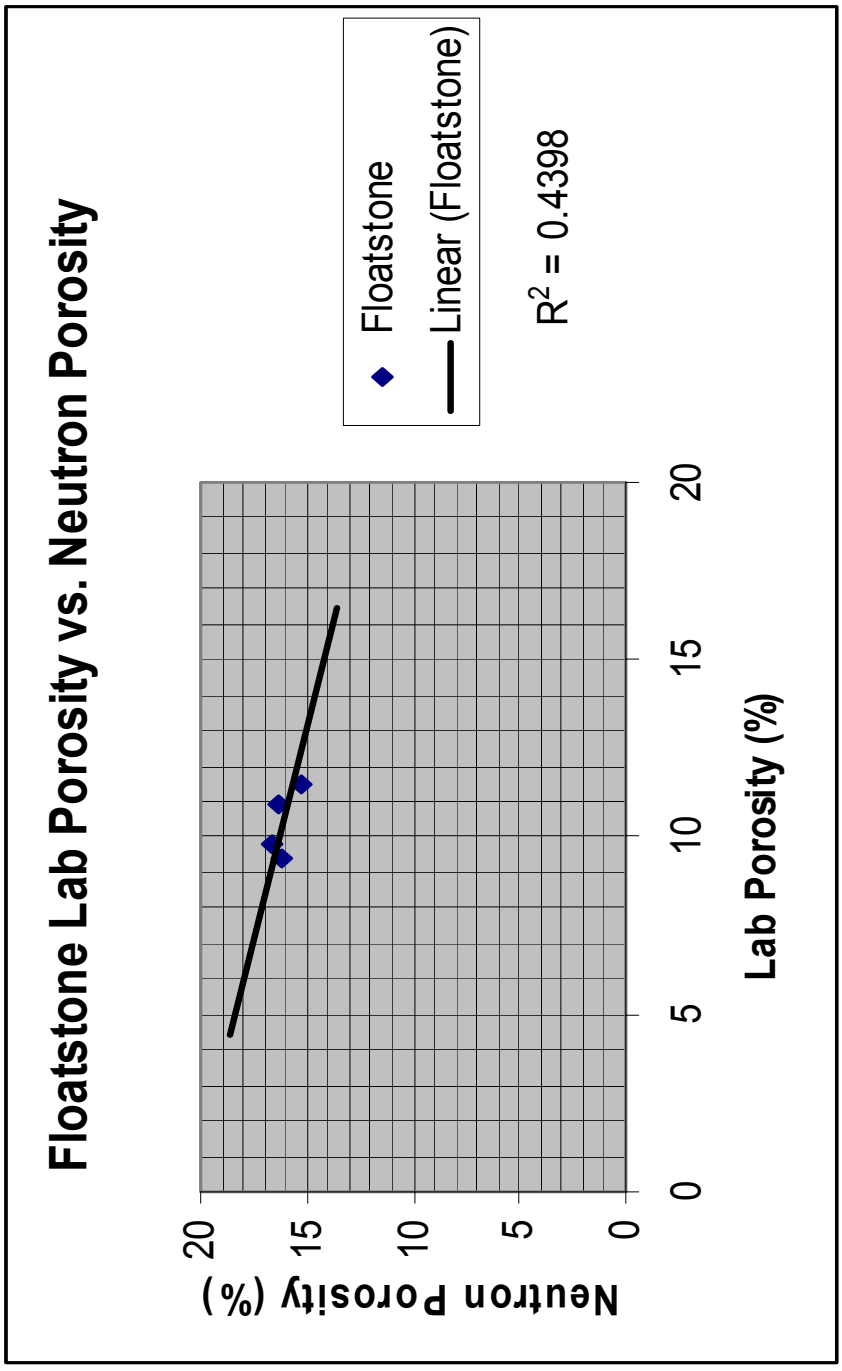

Figure 23. Floatstone lab porosity versus neutron porosity.

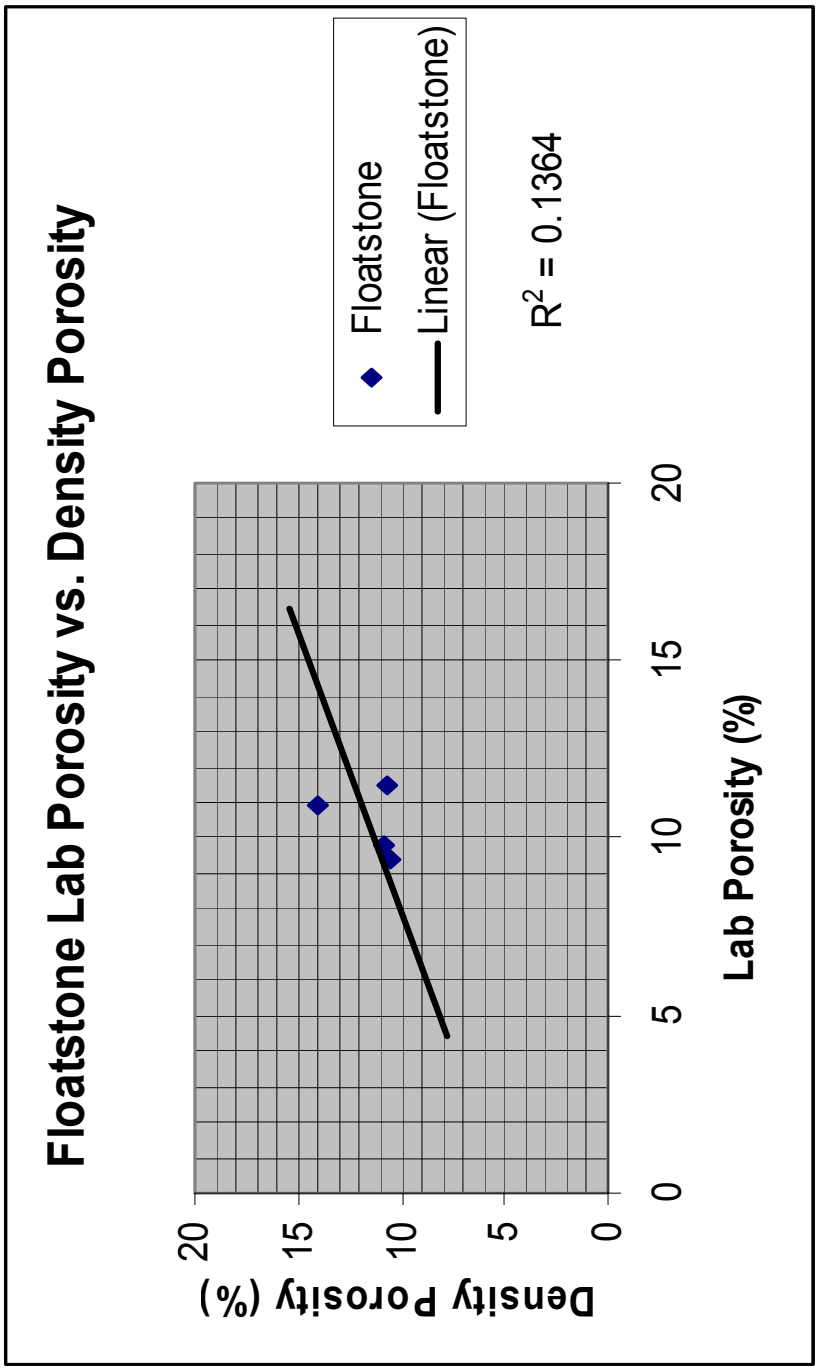

Figure 24. Floatstone lab porosity versus density porosity.

Shaly Siltstone

This light gray to tan facies is commonly found above and beneath the carbonate interval. Quartz silt makes up between 50% and 95% of this facies. Skeletal fragments are subrounded to subangular and make up less than 1% of this rock type. Packstone stringers are scattered throughout and there is typically a slightly fining upward trend in grain size (Layman, 2002 and Hammel, 1996). A core photo of this facies is found in figure 25.

Figures 26, 27 and 28 show the relationship between core porosity and permeability, core porosity and neutron porosity, and core porosity and density porosity respectively.

Figure 25. A core photo (Layman, 2002) of the shaly siltstone facies from Lott #19-4 at a depth of 4975'.

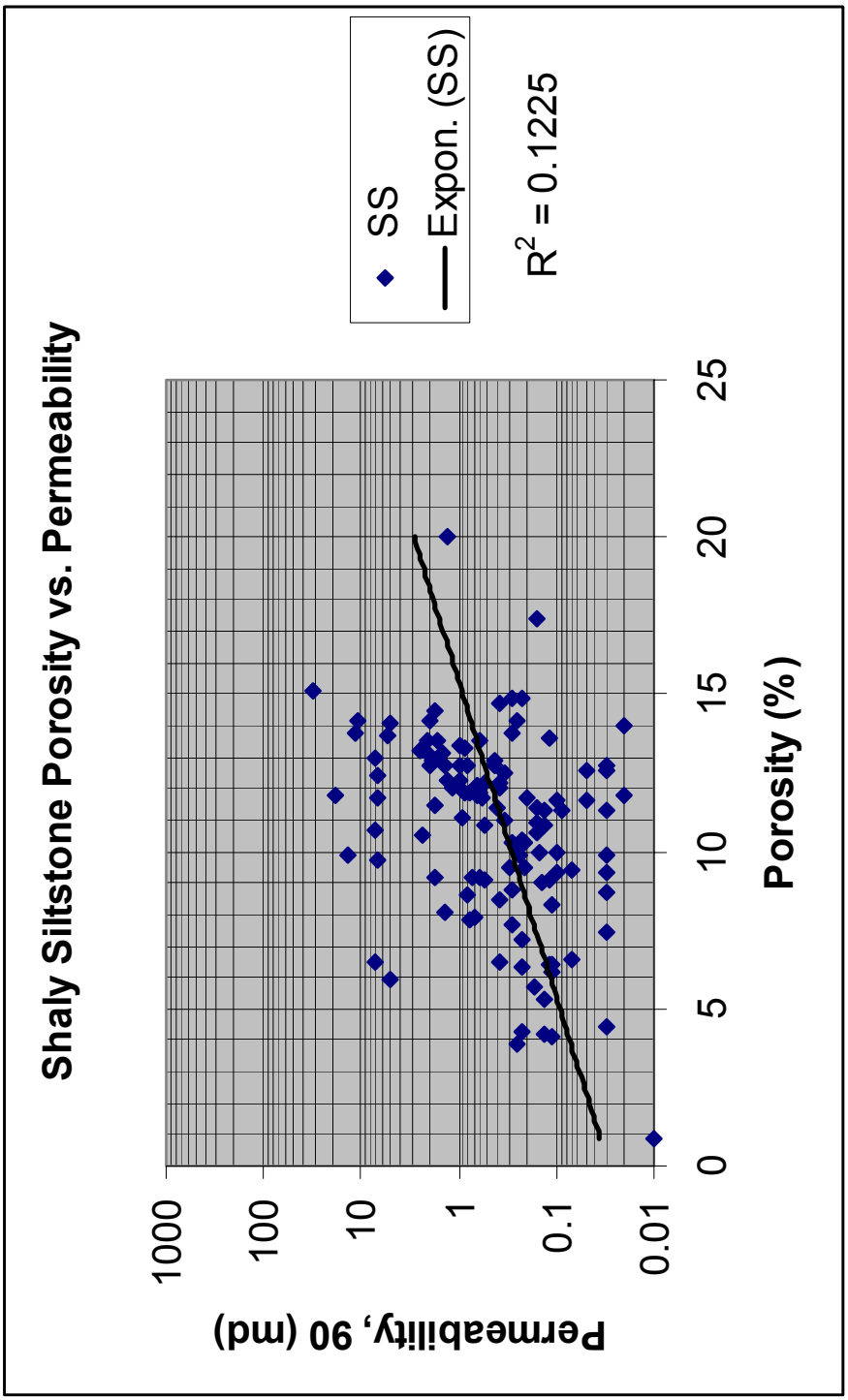

Figure 26. Shaly siltstone porosity versus permeability.

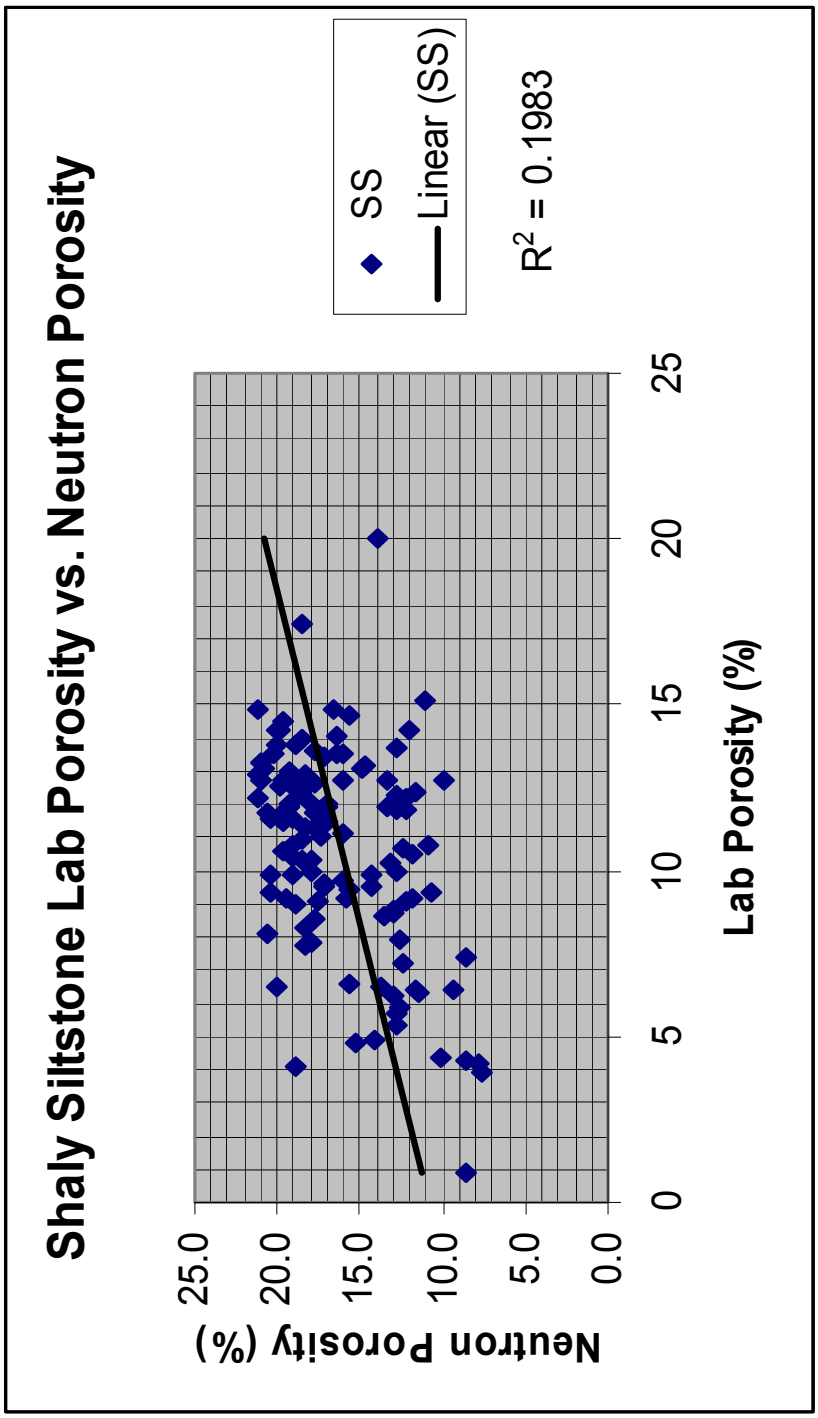

Figure 27. Shaly siltstone lab porosity versus neutron porosity.

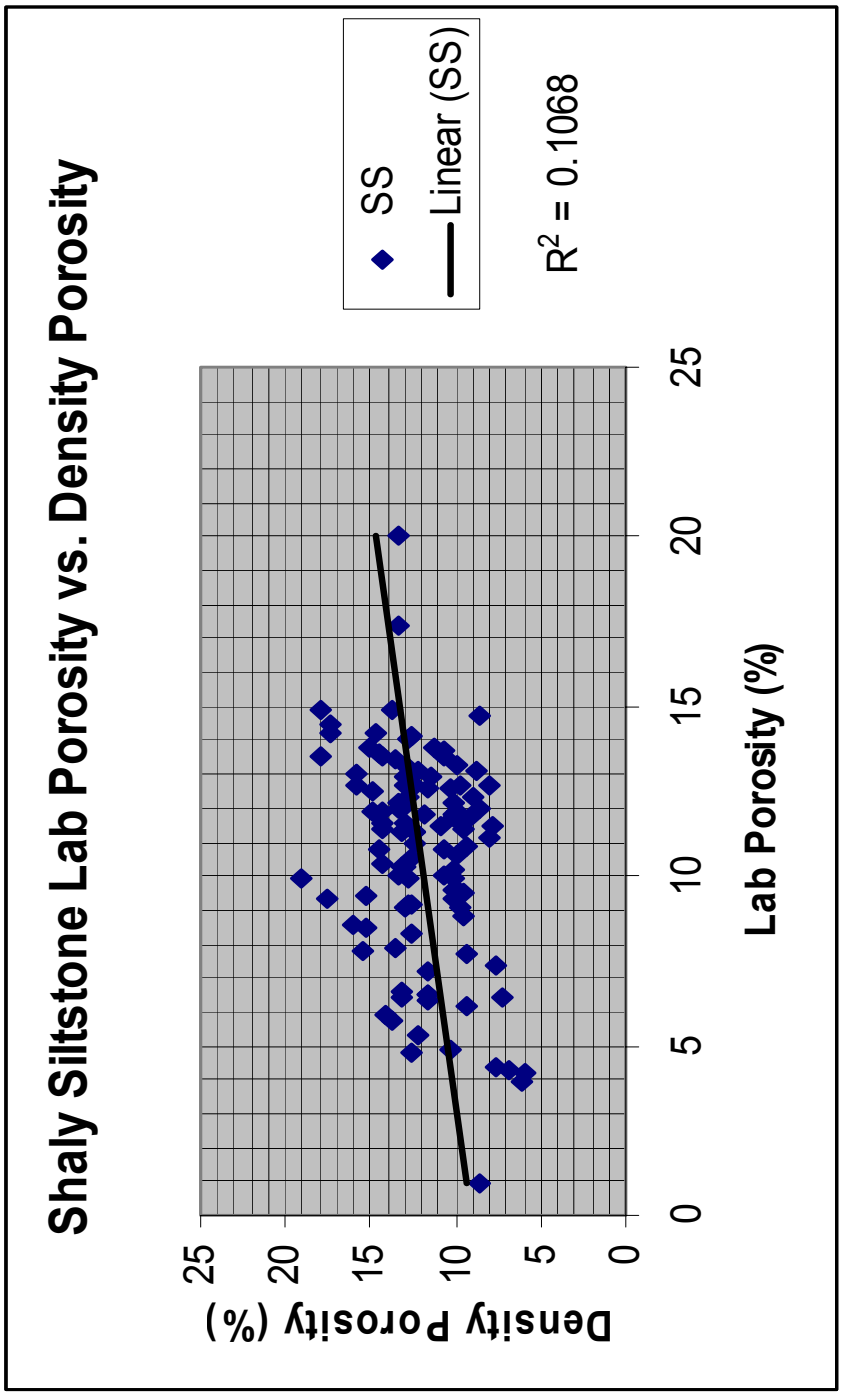

Figure 28. Shaly siltstone lab porosity versus density porosity.

PORE TYPES

There are many classification systems for describing carbonate porosity. In 1952 Gus Archie developed a classification system based on rock matrix texture, visible pore structure and associated petrophysical behavior. Choquette and Pray (1970) developed a scheme where pores were classified based on their being fabric selective or not. In addition, pore size modifiers and diagenetic alteration descriptors were supplemented. Lucia (1983) classified porosity as interparticle or vuggy; this was to take into account the different petrophysical properties associated with each. Furthermore, vugs were subdivided into touching and non-touching.

The goal of any carbonate classification system is to relate the essential pore characteristics to the petrophysical properties of carbonates. For this reason, a genetic classification system (Figure 28) in which carbonate pores are the result of three processes - depositional, diagenetic and fracture – will be used (Ahr and Hammel, 1999). Where this scheme differs from previous classification systems is its attempt to link geologic process with pore generation. By making a connection between geologic process and pore characteristics, predictions of porosity and permeability at the field scale becomes a much more manageable task.

Pores in Happy Spraberry are principally the result of diagenetic and depositional end-members as shown in Figure 29. Hence, facies selective diagenesis greatly contributes to Happy Spraberry porosity.

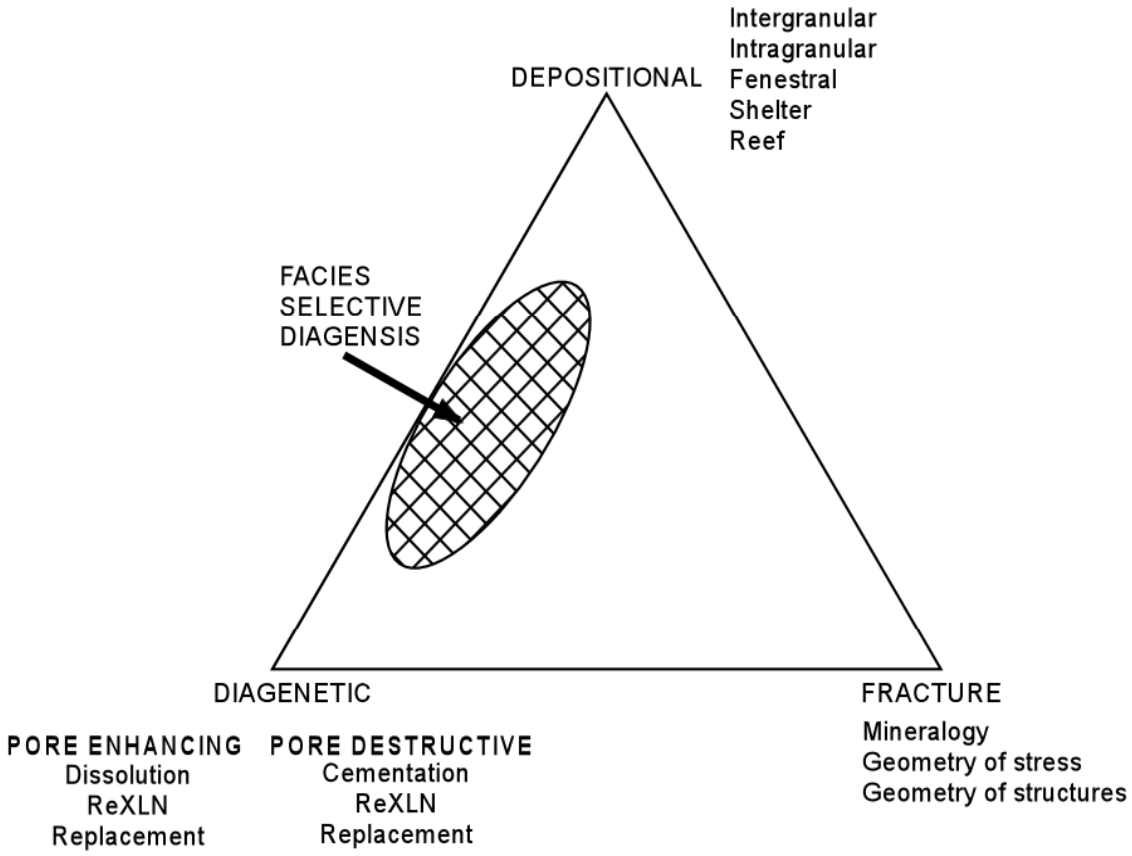

Figure 29. Genetic classification of carbonate pores. Three end member processes (deposition, diagenesis and fracture) are responsible for carbonate porosity. Pores at Happy Spraberry formed from the combined effects of deposition and diagenesis and are shown in the stripped oval region (after Ahr and Hammel, 1999).

Grain Moldic and Incomplete Moldic

These diagenetic pore types are created by the complete or partial dissolution of constituent grains respectively. Figure 30 shows a photomicrograph of these pore types. Moldic pores are easily identifiable by the sharp, regular outline of their leached grains, while incomplete moldic pores have less distinctive boundaries. These pore types are the most abundant across the field and dominate the oolitic skeletal grainstone packstone facies.

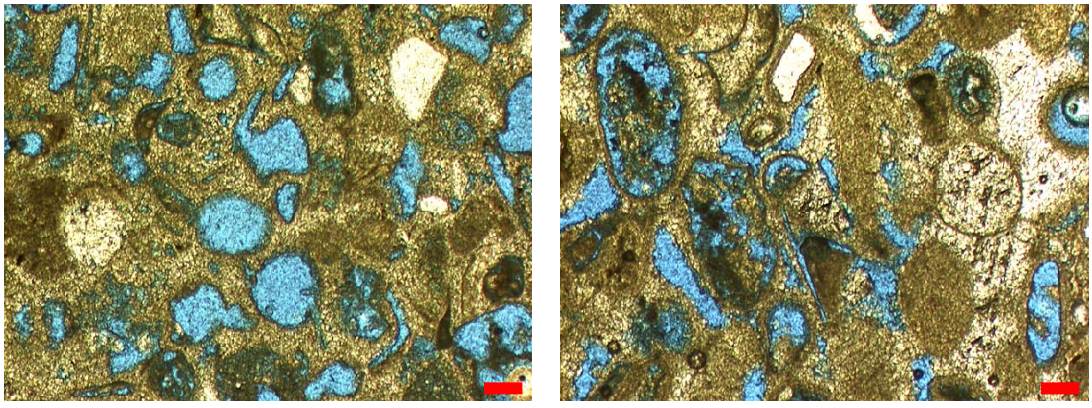

A **B**

Figure 30. Photomicrograph of A) grain moldic and B) incomplete moldic pore types from Lott #19-4 at a depth of 4949.3' and Lott #19-7 at a depth of 4954.7' respectively. The red scalebar is 100 microns. The blue outlines represent porosity and are the result of epoxy being injected into the pore space.

Solution Enhanced Intergranular

Solution enhanced intergranular pores formed from the dissolution of cement or matrix between carbonate grains. Figure 31 shows a photomicrograph of this pore type. It is commonly found in the oolitc skeletal grainstone packstone facies.

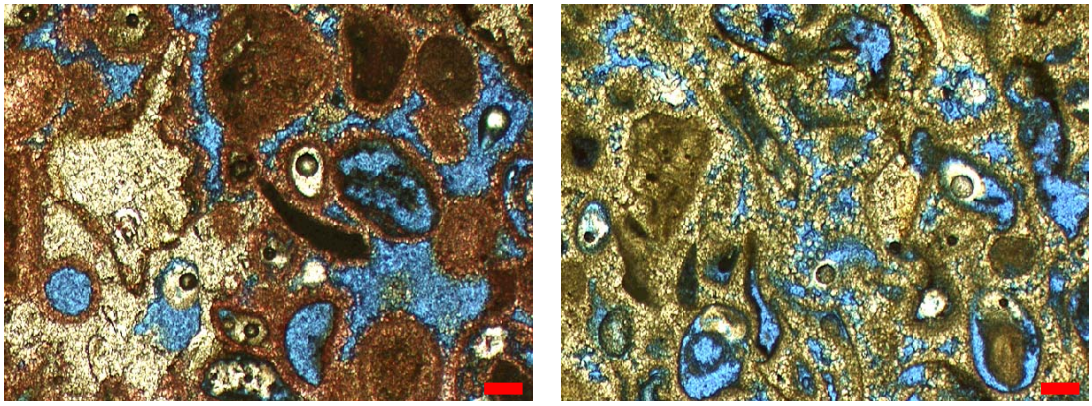

Figure 31. A photomicrograph of solution enhanced intergranular pores from A) Lott #19-4 at a depth of 4930.1' and B) Lott #19-4 at a depth of 4940.8'. The red scalebar is 100 microns

Solution Enhanced Intramatrix

Solution enhanced intramatrix pores formed from the dissolution of peloidal, carbonate mud matrix and is common in muddier, non-grain dominated facies. This precursor stage to vuggy porosity contributes little to effective porosity and represents the small pore types found in Happy Spraberry Field. A photomicrography of this pore type is shown below (Figure 32).

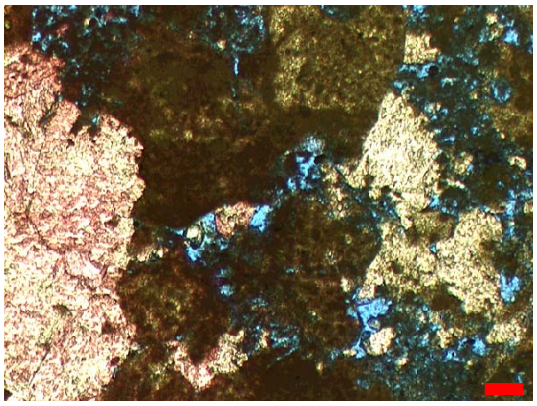

Figure 32. A photomicrograph of solution enhanced intramatrix pores from Lott #19-4 at a depth of 4972.6'. The white areas are anhydrite cement. The red scalebar is 100 microns.

Vuggy

Vugs are formed by the dissolution of a preexisting pore. The outline maybe sharp or non-distinct and is not indicative of a particular grain type. Vugs are limited to the muddier lithofacies and only contribute to effective porosity when they are sufficiently connected by intramatrix porosity. A photomicrography (Figure 33) showing vuggy porosity is featured below.

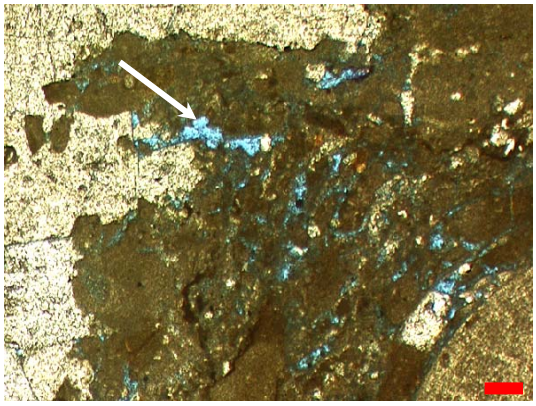

Figure 33. A photomicrograph of a skeletal rudstone showing vuggy porosity in Lott #19-4 at a depth of 4980.7'. A large bryozoan fragment is also located in the lower right portion of the photograph. The red scalebar is 100 microns.

Intraparticle

This depositional pore type exists in the form of intraskeletal pores. Occurrence of this pore type is limited to bryozoan mesopores and gastropods; it contributes little in the way of effective porosity to the field. A photomicrograph of this pore type is shown below (Figure 33).

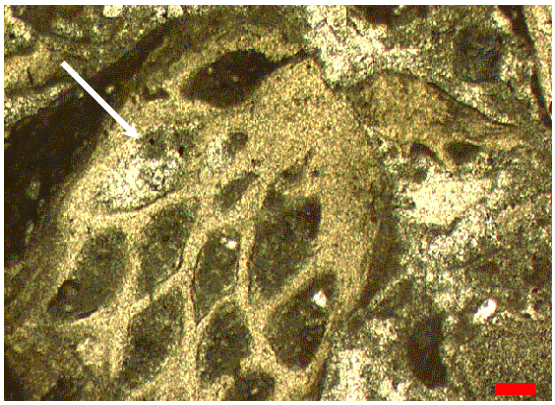

Figure 34. A photomicrograph of intraparticle pores from Lott #19-4 at a depth of 4967.2'. The red scalebar is 100 microns.

Primary Intergranular

Primary intergranular pores represent preserved depositional porosity of winnowed clay sized particles. This pore type contributes little to effective porosity and is a minor constituent to total field pore volume. A photomicrograph is shown below (Figure 34).

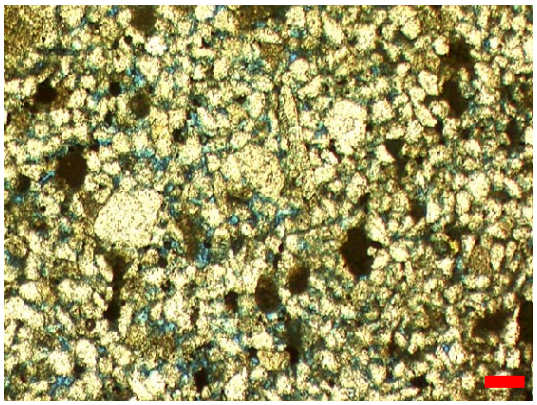

Figure 35. A photomicrograph showing primary intergranular pores from Lott #19-7 at a depth of 4991.6'. This is a siltstone showing preserved depositional porosity. The red scalebar is 100 microns.

METHODS

Step 1

Initially, all data in Happy Spraberry Field were in paper form and not easy to manipulate. Data includes paper logs, core analysis (porosity and permeability data over the cored interval), pore analysis, mercury injection capillary pressure data and thin sections.

A large electronic database was created. Paper logs over those areas of interest were scanned into a personal computer. Scanned images were saved as tagged image files (.tif). The tif images were then loaded in PETRA GeoPlus™. Once in PETRA, images were depth registered. Depth registration allows the program to associate a depth at any point within the scanned wireline log tif file. After completion of depth registration, log track boundaries (i.e. edges of the logs) were defined and values associated with each track boundary edge given. At this point, one is able to trace wireline log signatures and store the values in an electronic database. Gamma ray, deep resistivity, neutron porosity and density porosity curves were digitized. Figure 36 shows a screen capture for the process.

Paper core analysis data were also entered into an electronic database. Helium porosity, maximum permeability, 90 degree permeability (i.e. permeability perpendicular to the core axis), vertical permeability, oil saturation, water saturation and grain density values were all digitized.

Additionally, core descriptions previously compiled in studies

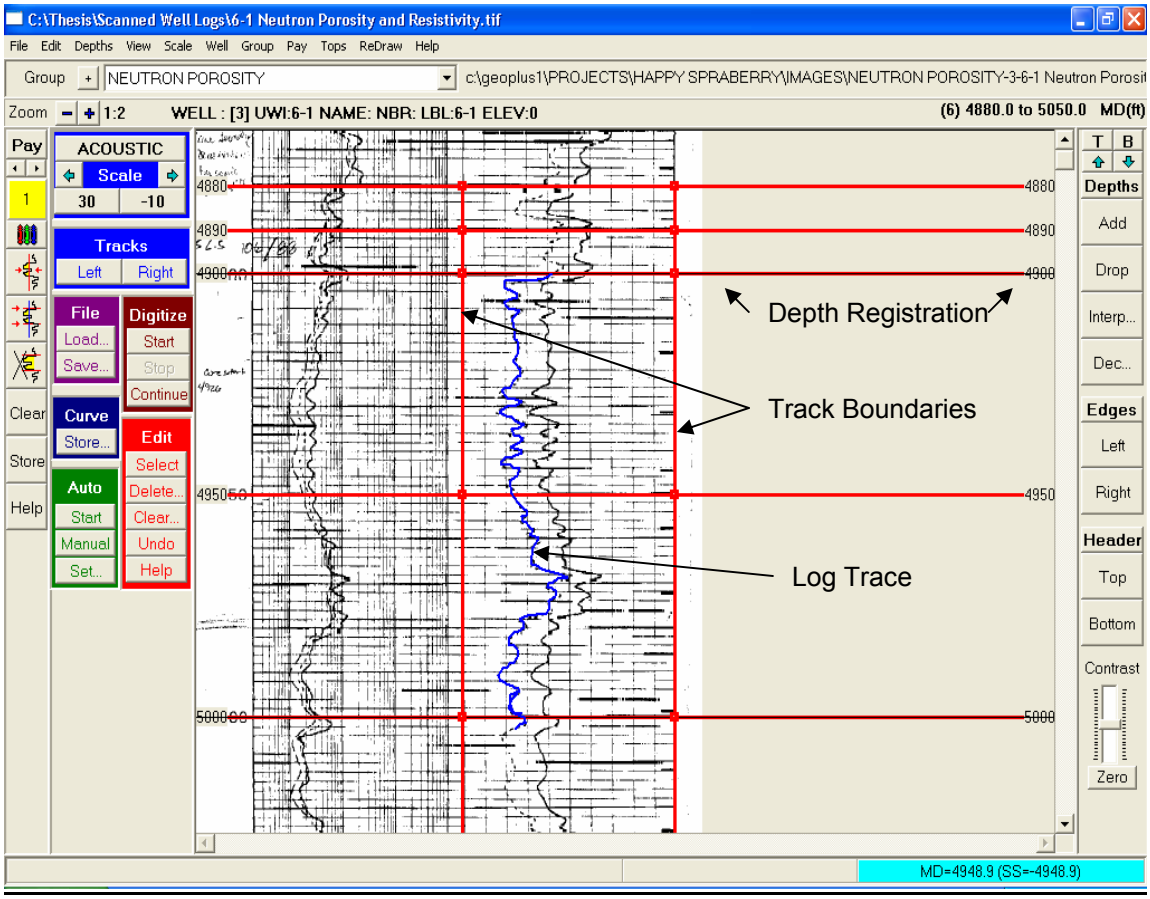

Figure 36. A screen capture from PETRA GeoPlus™ showing depth registration, track boundary definition and the tracing of a neutron porosity curve from a once paper log. All curve values were stored in an electronic database for easy manipulation.

(Hammel, 1996; Roy, 1998; Layman, 2002) were digitized to render geological lithofacies. Figure 37 shows the availability of core and core analysis data throughout Happy Spraberry Field. Geological lithofacies were also identified by Citation Oil and Gas Company and entered into the emerging geological database. Electrofacies were identified by the author and subsequently entered (Appendix B). Comparison of the wireline log signatures and the geological lithofacies descriptions were made to correct for any depth shift that may have occurred during logging operations. A depth shift is required when core depth and lithofacies description does not correspond to wireline log depth and electrofacies. This was done to the following field wells due to availability of data: Lott #19-2, Lott #19-3, Lott #19-4, Lott #19-5, Lott #19-6, Lott #19-8, Lott #19-9ST, Lott #19-10, Lott #19-11 and Lott Trust # 1. Pore types were also entered into the database at their respective depths and wells.

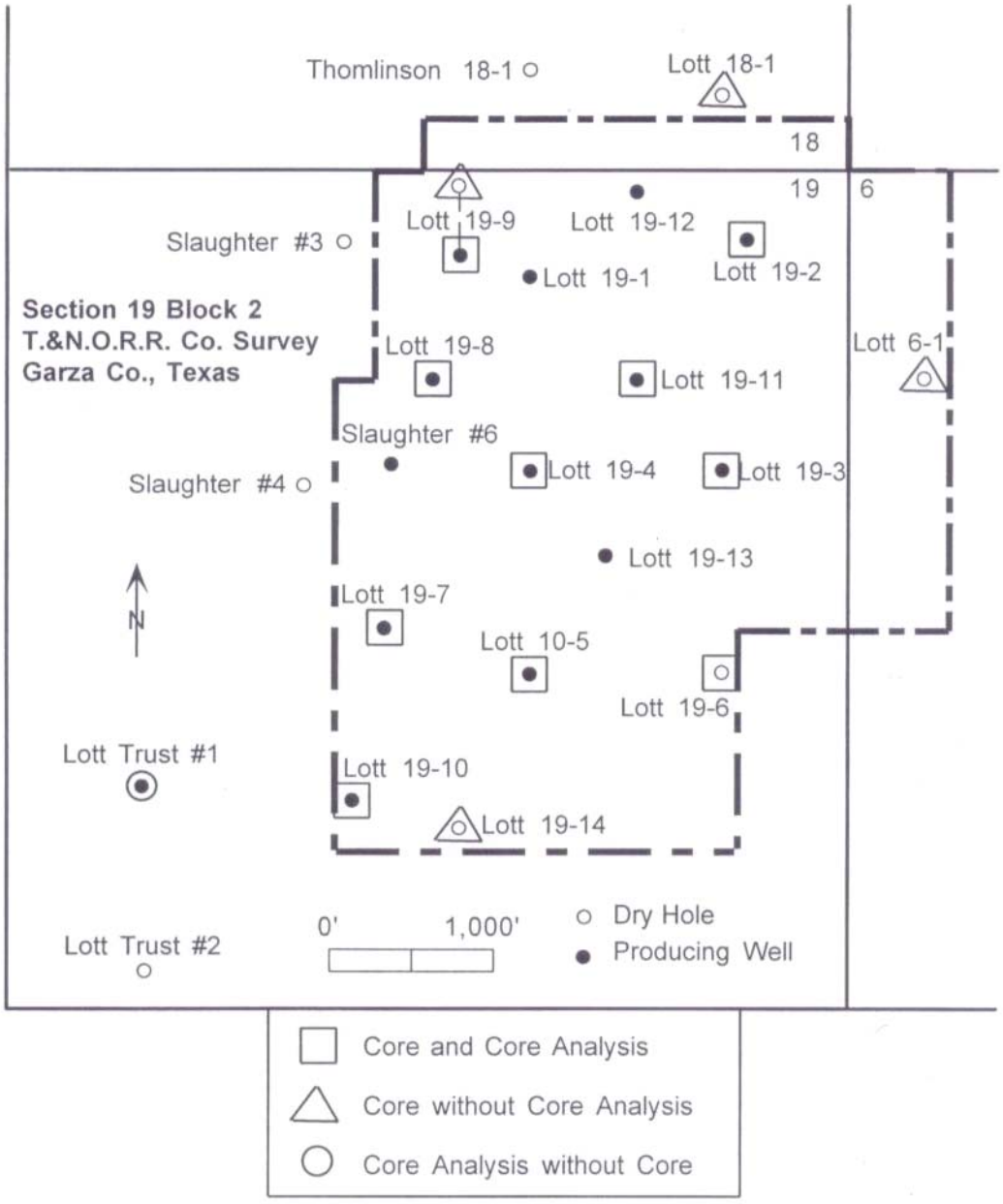

Figure 37. Base map of Happy Spraberry Field showing the availability of core and core analysis data (from Hammel, 1996).

Step 2

Reservoir quality classes will then be defined. In this study, reservoir quality will be defined as a range of porosity values and corresponding permeability values. That is, a single reservoir quality class will have representative ranges of both porosity and permeability values.

Hammel (1996) created a reservoir quality classification scheme by dividing the range of average porosity and permeability into three sets of equal sub-ranges. The sub-ranges were identified as high, medium and low. Figure 38 shows Hammel's reservoir quality classification scheme.

In this study, the author will make use of a modified Hammel reservoir quality classification scheme (Figure 38). Reservoir quality classes (RQC) 1 and 2 will be characterized as having "good" reservoir quality (green boxes of Figure 38). RQC 3 and 4 will be expressed as having "intermediate" reservoir quality (yellow boxes of Figure 38). And RQC 5 and 6 will be denoted as having "poor" reservoir quality (red boxes of Figure 38). This is done to constrain the neural network to 3 nominal output variables (good, intermediate and poor) in an effort to build a more robust model.

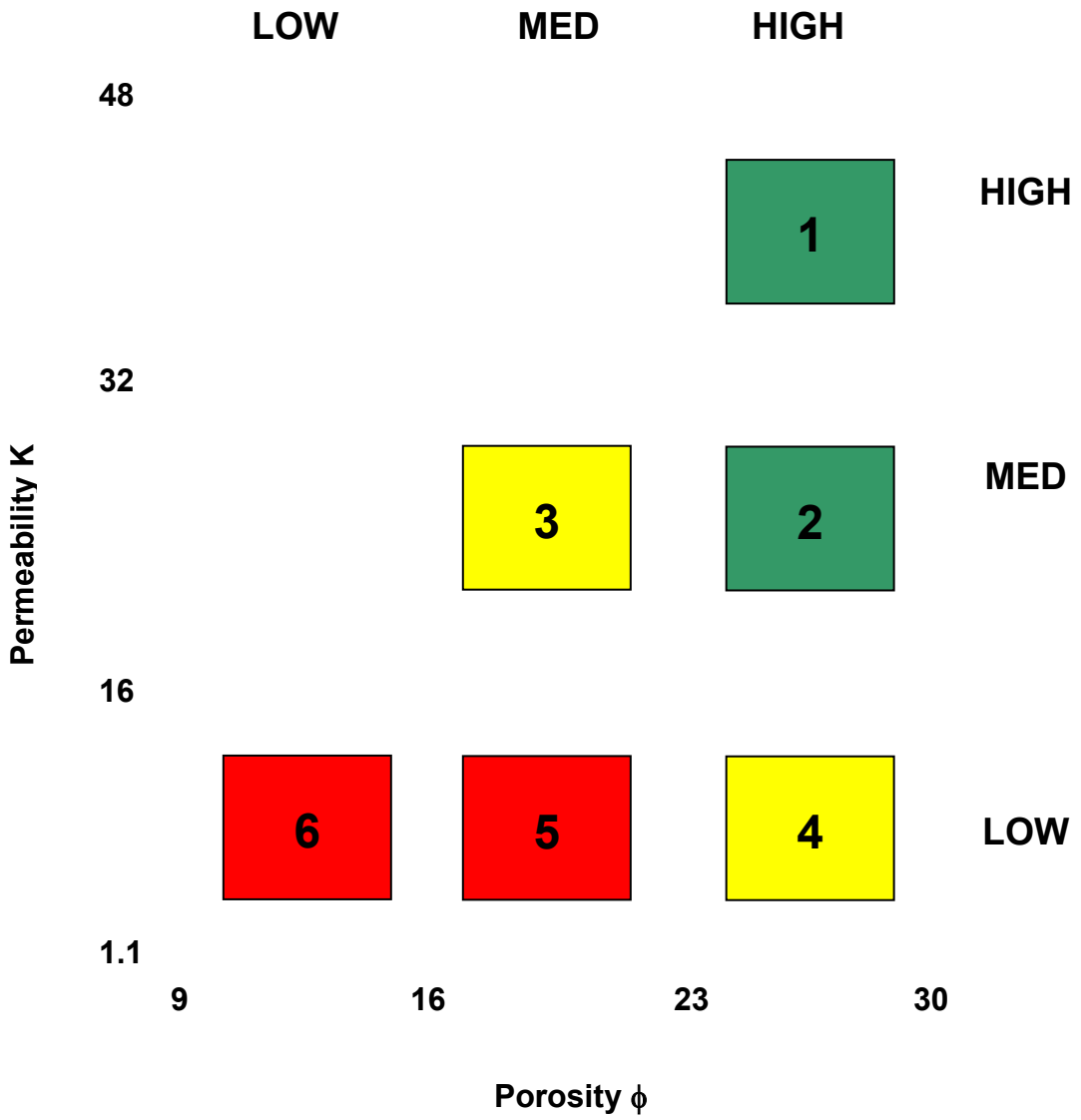

Figure 38. Modified Hammel reservoir quality classification scheme. Hammel reservoir quality classes are numbered 1-6 with 1 representing the highest RQC and 6 the lowest. In the modified scheme RQC classes 1 and 2 represent good reservoir quality (green boxes), RQC classes 3 and 4 represent intermediate reservoir quality (yellow boxes) and RQC classes 5 and 6 represent poor reservoir quality (red boxes).

Step 3

For many years linear modeling has been the most commonly used modeling technique due to their well known optimization strategies. Where linear optimization was not valid the models suffered accordingly. Neural networks curb the dimensionality problem which hinders attempts to model non-linear functions with large numbers of variables. While regression analysis is popular due to availability of commercial software packages, regression analysis predicts mean values and accordingly overestimates lower values and underestimates higher values. Neural networks do not force predicted values to lie near the mean values, thus preserving actually variability (Rogers et. al, 1995) similar to nonparametric regression.

A goal of neural network design is to create a robust model. This will be achieved by striking a balance between the numbers of input parameters with network performance. Initially, six input parameters will be used: porosity, permeability, gamma ray value, deep resistivity value, neutron porosity value and density porosity value. An important requirement for neural network use is there be a known relationship between the proposed known inputs and the unknown output. Measurements of all parameters were made within one-foot intervals over the cored zone of interest in all wells used in this study. There is approximately 500 feet of core in Happy Spraberry field representing 500 data points. Seventy-five percent (75%) of these data points are chosen at random to serve as a certified training data set. It is imperative that the training data set be

indicative of the entire field. This is ensured by making sure the training data set contains examples of all electrofacies and reservoir quality rankings. The remaining twenty-five percent (25%) is used for network validation.

Step 4

Build a neural network from the certified training data set that will identify electrofacies and give a reservoir quality ranking (i.e. good, intermediate, poor). The key here is the neural network architecture. All neural networks are composed of several basic elements: an input layer, a summation function, a transfer function and an output layer. This is why the author will not attempt to "build" a neural network program from scratch. What is far more productive is tuning the network architecture of an existing program. The number of hidden layers, the number of nodes, selection of a summation function, selection of a transfer function, selection of input variables, and the number of epochs control network architecture.

Step 5

Test the neural network and verify the initial results with the remaining field wells. These remaining wells were initially withheld from the training stage. After the neural network built in Step 4 is allowed to identify flow units field wide, verify the accuracy of the network from the withheld wells.

Step 6

Compare the results to those obtained by more "conventional" linear methods.

RESULTS & DISCUSSION

A neural network was first designed to identify electrofacies throughout the field. A comma separated values (.csv) file was loaded into Statistica Neural Networks ™ (SNN), a commercial neural network package that supports a number of training algorithms and network architectures. Potential inputs were identified and included: X location, Y location, depth, gamma ray value, deep resistivity value, density porosity value and neutron porosity value. All inputs were identified in one foot intervals in cored sections of wells Lott #19-2, Lott #19-3, Lott #19-4, Lott #19-5, Lott #19-6, Lott #19-8, Lott #19-9ST, Lott #19-10, Lott #19-11 and Lott Trust # 1. The only requisite for identifying potential input parameters in a neural network is a suspicion that a relationship exists between the known inputs and the unknown output.

Two types of training can be used in the fabrication of a neural network: supervised and unsupervised. Unsupervised learning, sometimes called self-supervised learning, use no external influences to adjust weights. Instead, they monitor their performance internally. Supervised learning is most commonly used and is employed here. In supervised learning, the user compiles a set of training data. The training data consists of examples of inputs together with corresponding outputs. It is imperative that the training data be certified true. The network then infers a relationship between the two. In this case, training data is taken from known location, wireline log data and the corresponding

electrofacies. The result is a neural network that can identify electrofacies from location and wireline log data values.

The most well known supervised training algorithm is back propagation (Rumelhart et al., 1986). Back propagation adjusts the networks weights and thresholds in order to minimize the error in its prediction on the training data set. A properly trained network will then have learned to model the unknown function which relates the input variables to the output variables and can subsequently be used to make predictions where the output is not known. Neural networks also handle non-numeric data well.

The most common type of non-numeric data is nominal-value variables. In this case such values are *Electrofacies = {Grainstone, Shaly Siltstone, Rudstone, Floatstone}*. However, neural networks in general do not cope with large numbers of nominal (named) variables very well.

There are two main types of prediction problems using neural networks: classification and regression (i.e. curve-fitting). The objective of a classification problem (of which type this network belongs) is to determine which of a number of discrete classes a given input case belongs. In regression, the desire is to predict the value of a continuous variable. An example of regression would be the prediction of tomorrow's NASDAQ closing value. The problem in this thesis is to classify input data as discrete electrofacies

All neural networks should be compared against other models including linear models. Linear models are often preferred over neural networks when

training data is sparse and not enough information is available to properly train a network. All neural networks produced in this project will be compared to linear models. SNN supports logistic regression for classification problems. Logistic regression is based on the assumption that the classes are normally distributed with equal covariance matrices. Where this assumption is untrue (as it may commonly be), a neural solution may be the more valid alternative.

After potential inputs were identified in the electrofacies network, the dataset was randomly subdivided into three sets: training, testing and verification. The neural network is trained only using the training data sunset. The verification subset keeps an independent check of the networks performance during training, with worsening verification errors an indication of over-learning. When this occurs, network training is halted and restored to a state with minimum verification errors. If a network has good verification error but poor generalization capabilities, a third data subset (testing) is used to visually inspect performance after training. There were 205 training cases, 102 testing cases and 102 verification cases.

Neural network training algorithms are iterative, training over a period of time, and need to be repeated over a number of times until a satisfactory solution is reached. In this case the training time was over two hours on an 850 MHz machine. During which time decisions are made on network type, network complexity, network architecture and optimal input variables to use. Eventually, 699 networks were tested with the 20 best networks retained and reviewed.

The optimal neural solution is shown in Figure 39 (Electrofacies model 1). Inputs into the network include X location, Y location, gamma ray value and deep resistivity value. Density porosity values and neutron porosity values were not used in this network. The output of the network is electrofacies. The correct classification rate for this network is 0.93. A correct classification rate of 1.0 indicates a perfect solution.

This network is a multilayer perceptron (MLP), perhaps the most popular neural network architecture in use today (Bishop, 1995). MLP's perform a biased weighted sum of their inputs and pass this activation level through a transfer function to produce their output, and the units are arranged in a layered, feedfoward topology. The most common transfer function, the sigmoid function, is utilized in this study. Networks such as the ones in this study can model very complex functions, with the number of layers and the number of units in each layer determining the function complexity.

An MLP uses the training dataset along with different training algorithms to automatically adjust the weights and thresholds to minimize the error. This is equivalent to fitting the model represented by the network to the training data available. The error is determined by running all training cases through the network and comparing the actual output generated with the desired output.

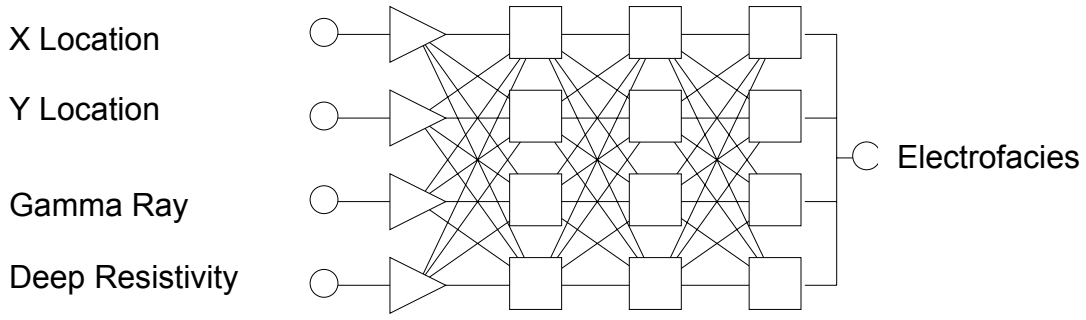

Figure 39. Electrofacies model 1. Multilayer perceptron neural network with X and Y location, gamma ray value, and deep resistivity value as inputs. The output is electrofacies.

Network error is given by an error function. Sum-squared error, where individual errors of output units on each case are squared and summed, is a common error function. However, SNN reports the RMS which is the sum-squared error

normalized for the number of cases and variables. This way, we get an error for the entire training set and set of output units.

MLP's also make use of an error surface. Each of the *N* weights and thresholds of the network is taken to be a dimension in space. The network error is the *N+1th* dimension. For any possible configuration of weights the error can be plotted in the *N+1th* dimension, forming an error surface. In linear methods, the error surface is a parabola which has a smooth bowl shape and a single local minimum (i.e. it is easy to locate the minimum). Neural network error surfaces are much more complex and are sometimes characterized by many local minima. Local minimas are lower than the surrounding topography but may not represent the global minimum. Local minimas could be flat spots, plateaus, saddles or ravines in the error surface. It is impossible to analytically determine the location of the global minimum on a general error surface. Therefore, neural network training can be thought of as the search for the global minimum by making use of different training algorithms. This search is conducted by computing the slope of the error surface at a point and then moving downhill. Eventually the training algorithm will locate a minimum, which could be a local or global minimum. In back propagation, the gradient vector of the error surface is calculated. The vector points in the steepest downhill direction. Moving a short step in that direction will reduce the error and eventually locate a minimum.

The RMS error for the first network, electrofacies model 1(Figure 39), was 0.077 for the 205 training data points, 0.15 for the 102 verification data points and 0.065 for the 102 testing data points. The only cause for concern is the difference in RMS error between the training data and the verification error (Figure 40). When there are large differences in RMS error between training data sets and verification training sets, this is often indicative that network may have suffered over-learning as discussed earlier and shown in Figure 9. Upon closer inspection however, this does not appear to be the case. Table 1, Table 2 and Table 3 show classification statistics for training, testing and verification respectively. Inspection of these tables reveals little difference in results between the three data sets. However, heuristic guidelines suggest that the number of weighted connections be 10% of the number of training data points. Examination of Figure 39 shows 48 weighted connections. With a training data set of 205 training data points, the optimal number of weighted connections would be less than 20. To have an optimal number of weighted connections, it may be necessary to sacrifice network quality (i.e. reduction in correct classification rate) for a more robust neural model. Such a model is found in figure 41 (Electrofacies Model 2).

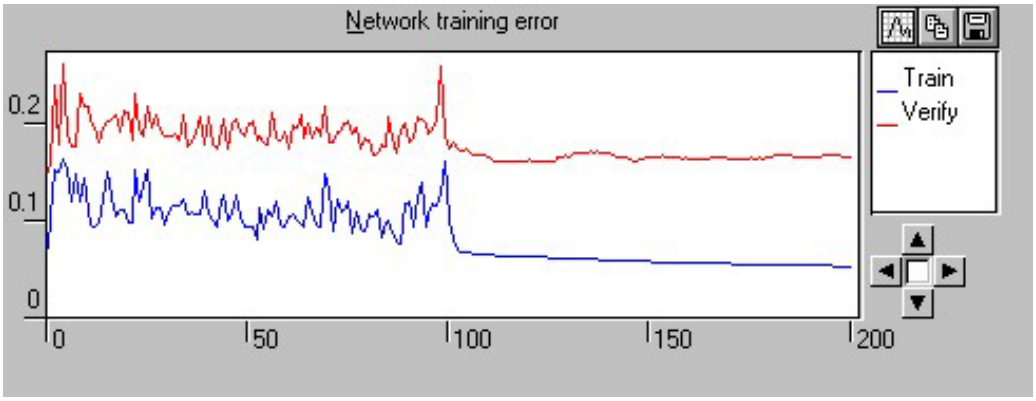

Figure 40. Difference in training data set and verification training data set network error.

Table 1. Classification statistics for training data set for neural network model 1.

	Grainstone	Rudstone	Shaly Siltstone	Floatstone
Total	117	34	52	2
Correct	117	34	51	0
Wrong	0	0	1	2
Unknown	0	0	0	0
Grainstone	117	0	0	0
Shaly Siltstone	0	0	51	2
Rudstone	0	34	1	0
Floatstone	0	0	0	0

Table 2. Classification statistics for verification data set for neural network model 1.

	Grainstone	Rudstone	Shaly Siltstone	Floatstone
Total	59	15	26	2
Correct	58	14	23	0
Wrong	1	1	3	2
Unknown	0	0	0	0
Grainstone	58	0	2	0
Shaly Siltstone	1	1	23	2
Rudstone	0	14	1	0
Floatstone	0	0	0	0

Table 3. Classification statistics for testing data set for neural network model 1.

	Grainstone	Rudstone	Shaly Siltstone	Floatstone
Total	59	18	25	0
Correct	59	18	25	0
Wrong	0	0	0	0
Unknown	0	0	0	0
Grainstone	59	0	0	0
Shaly Siltstone	0	0	25	0
Rudstone	0	18	0	0
Floatstone	0	0	0	0

Again, the model shown in figure 41 is an MLP. The correct classification rate for this model is 0.87. Moreover, there is little variation between the RMS error for the training data set and the verification data set. RMS error for the training data set was 0.20 while the error for the verification data set was 0.22. RMS error for the testing data set was 0.22 as well. Inspection of tables 4, 5 and 6 show very good predictive powers of this more robust network. Where this model suffers as compared to the previous model is in the classification of rudstones. Where the previous model was able to successfully classify all rudstones, the current model only classified rudstones successfully 44% of the time. This is most likely due to little differentiation between deep resistivity responses between rudstones and shaly siltstones. Also, neither model was able to successfully identify floatstones. It is possible that there was simply not enough representative training data.

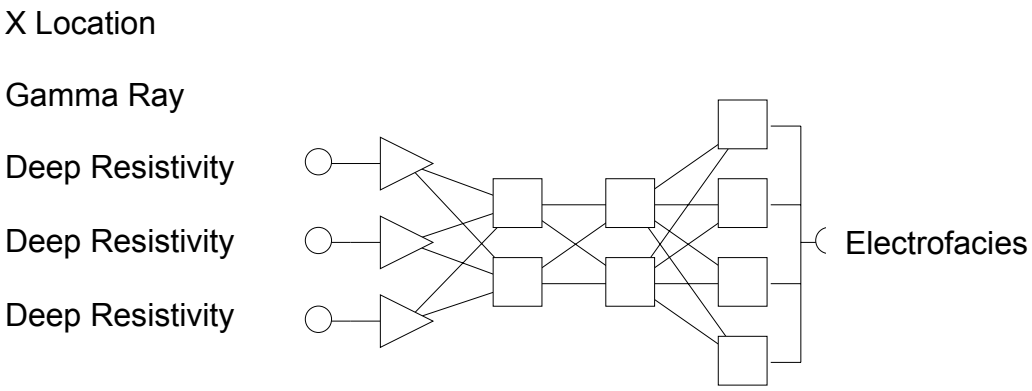

Figure 41. Electrofacies model 2. Multilayer perceptron neural network with X location, gamma ray value, and deep resistivity value as inputs. The output is electrofacies.

Table 4. Classification statistics for training data set for neural network model 2.

	Grainstone	Rudstone	Shaly Siltstone	Floatstone
Total	117	34	52	2
Correct	116	17	52	0
Wrong	1	17	0	2
Unknown	0	0	0	0
Grainstone	116	0	0	0
Shaly Siltstone	1	17	52	2
Rudstone	0	17	0	0
Floatstone	0	0	0	0

Table 5. Classification statistics for verification data set for neural network model 2.

	Grainstone	Rudstone	Shaly Siltstone	Floatstone
Total	59	15	26	2
Correct	55	9	25	0
Wrong	4	6	1	2
Unknown	0	0	0	0
Grainstone	55	0	1	0
Shaly Siltstone	4	6	25	2
Rudstone	0	9	0	0
Floatstone	0	0	0	0

Table 6. Classification statistics for testing data set for neural network model 2.

	Grainstone	Rudstone	Shaly Siltstone	Floatstone
Total	59	18	25	0
Correct	56	8	25	0
Wrong	3	10	0	0
Unknown	0	0	0	0
Grainstone	56	0	0	0
Shaly Siltstone	3	10	25	0
Rudstone	0	8	0	0
Floatstone	0	0	0	0

The above neural solutions are now compared to a linear solution. The best linear solution found by SNN had a correct classification rate of 0.75. Figure 42 shows a schematic of the optimum linear solution. RMS error was 0.26, 0.31, and 0.30 for the training, verification and testing data sets respectively. In addition, the linear solution requires six input parameters while both neural solutions mandated fewer input parameters. Tables 7, 8 and 9 show the shortcomings of the linear solution when compared to the above neural solutions. Classification errors are present for all electrofacies outputs. It is clear that a neural solution would be preferred to a linear solution when attempting to classify electrofacies.

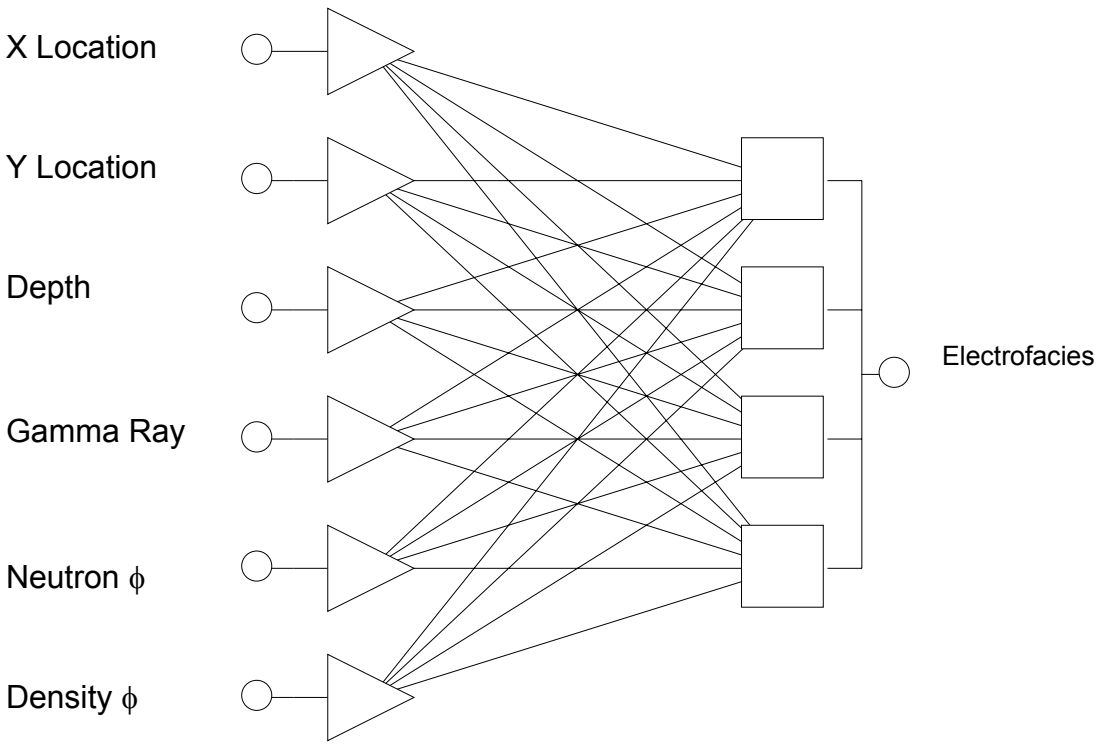

Figure 42. Linear solution for the electrofacies problem.

Table 7. Classification statistics for training data set for linear solution.

	Grainstone	Rudstone	Shaly Siltstone	Floatstone
Total	117	34	52	2
Correct	106	28	37	0
Wrong	11	6	15	2
Unknown	0	0	0	0
Grainstone	106	5	12	0
Shaly Siltstone	6	1	37	2
Rudstone	5	28	3	0
Floatstone	0	0	0	0

Table 8. Classification statistics for verification data set for linear solution.

	Grainstone	Rudstone	Shaly Siltstone	Floatstone
Total	59	15	26	2
Correct	50	10	16	0
Wrong	9	5	10	2
Unknown	0	0	0	0
Grainstone	50	3	8	0
Shaly Siltstone	4	2	16	2
Rudstone	5	10	2	0
Floatstone	0	0	0	0

Table 9. Classification statistics for testing data set for linear solution.

	Grainstone	Rudstone	Shaly Siltstone	Floatstone
Total	59	18	25	0
Correct	48	10	16	0
Wrong	11	8	9	0
Unknown	0	0	0	0
Grainstone	48	6	6	0
Shaly Siltstone	4	2	16	0
Rudstone	7	10	3	0
Floatstone	0	0	0	0

The next problem was to design a neural network capable of giving a qualitative description (good, intermediate, poor) of reservoir quality. These reservoir quality classes were described in a previous section. This coupled with electrofacies would give a flow unit designation. Potential inputs into the network included X location, Y location, depth, gamma ray value, density porosity value, neutron porosity value, deep resistivity value and electrofacies. Over 550 networks were tested in an eight hour period with the best 30 networks retained for review.

Again, the top network was an MLP (RQC Model 1). This model (Figure 43) had a correct classification rate of 0.80. There was minimal variation between training RMS error, 0.30, and verification RMS error, 0.29. While this shows that the likelihood of over fitting is small, there is cause for concern with the number of weighted connections. Ideally, the number of weighed connections should be 10% of the number of training cases, in this case 20. Here there are over 60 weighted connections in RQC model 1.

To trim the number of weighted connections, neural network performance must be compromised. A more robust model is presented in Figure 44 (RQC Model 2). The correct classification rate for RQC model 2 is 0.75. There is little difference in RMS error from training, 0.33, to verification, 0.31. Additionally, fewer inputs are required to determine the appropriate reservoir quality class (good, intermediate, poor). Tables 10, 11 and 12 show classification statistics for training, verification and testing data sets respectively.

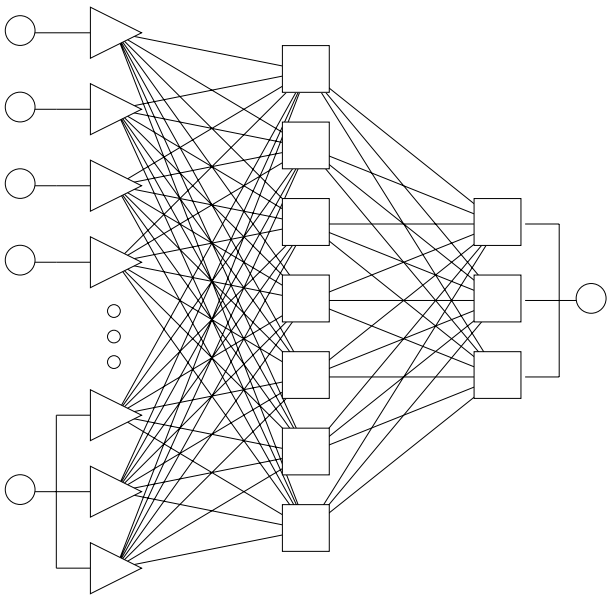

Figure 43. RQC model 1. Input parameters into the model include X location, Y location, depth, deep resistivity value, density porosity value and electrofacies.

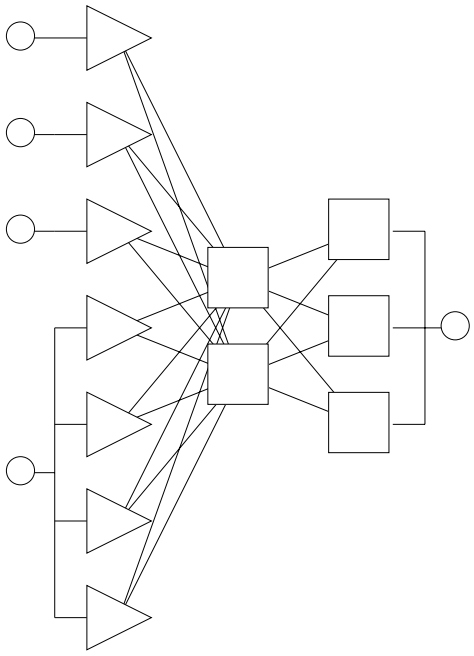

Figure 44. RQC Model 2. Inputs into the model include X location, deep resistivity value, density porosity value and electrofacies.

Table 10. Classification statistics for training data set for RQC model 2.

	Good	Intermediate	Poor
Total	30	34	141
Correct	20	9	127
Wrong	10	25	14
Unknown	0	0	0
Good	20	8	8
Intermediate	4	9	6
Poor	6	17	127

Table 11. Classification statistics for verification data set for RQC model 2.

	Good	Intermediate	Poor
Total	10	17	75
Correct	6	4	66
Wrong	4	13	9
Unknown	0	0	0
Good	6	6	4
Intermediate	3	4	5
Poor	1	7	66

Table 12. Classification statistics for testing data set for RQC Model 2.

	Good	Intermediate	Poor
Total	14	15	73
Correct	7	3	69
Wrong	7	12	4
Unknown	0	0	0
Good	7	6	3
Intermediate	4	3	1
Poor	3	6	69

Inspection of the above tables shows that RQC model 2 has great difficulty in distinguishing between the intermediate reservoir quality classes. Viewing a cluster diagram, a scatter diagram plotting cases belong to various classes (supplied by the nominal variable) in two dimensions (Figure 45), shows the intermediate quality reservoirs are pervasive in good and poor reservoir quality rankings, affecting the ability of the neural network to accurately predict intermediate reservoir quality rankings. The network does however differentiate between good and poor reservoir quality classes.

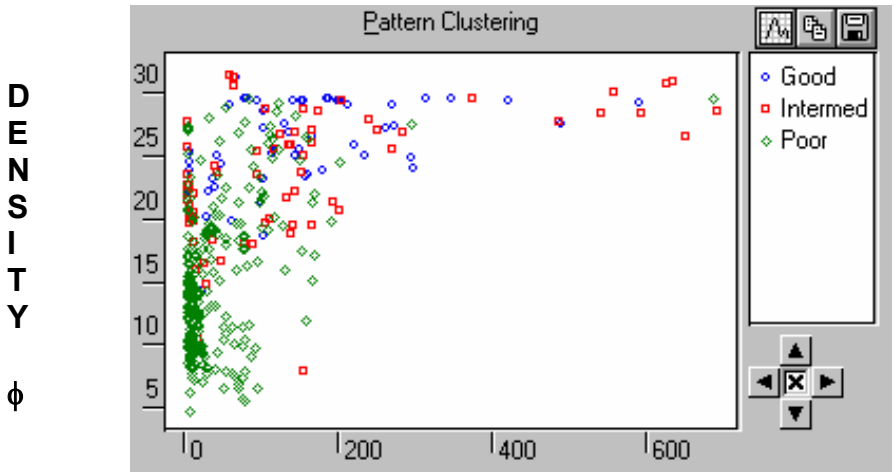

Figure 45. Cluster diagram for determining reservoir quality classes.

RQC models 1 and 2 were then compared to a linear model, RQC model 3 (Figure 46). The linear model had a correct classification rate 0.69 with little difference between training RMS error, 0.34, and verification RMS error, 0.32. Surprisingly, the linear model only required one input parameter, neutron porosity value; RQC models 1 and 2 did not require neutron porosity to output a solution. Like RQC models 1 and 2, the linear model was unable to distinguish intermediate quality reservoir classes from good and poor reservoir quality classes.

Again, the robust neural solution is preferred to the optimal linear solution. Nevertheless, unlike the electrofacies problem, the neural solution for the reservoir quality problem is much closer to the linear solution (0.75 correct classification rate versus 0.69 correct classification rate). Also, there is much less confidence in models used to predict reservoir quality rankings than there are in the models used to predict electrofacies.

Reservoir quality rankings are controlled by two parameters: porosity and permeability. As shown in figures 15, 16, 19, 20, 23, 24, 27 and 28, it is difficult to predict actual porosity from wireline logs. To complicate matters, if successful predications of porosity were obtained from wireline logs, permeability predication from porosity would be arduous if not impossible (Figures 14, 18, 22 and 26). In fact, a neural network assigned to predict solely laboratory porosity from wireline logs only had a correct classification rate of 0.59 with numerous

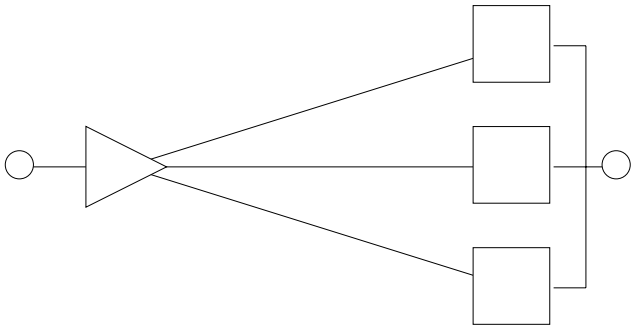

Figure 46. RQC Model 3, a linear model, with only one input parameter, neutron porosity value.

weighted connections; permeability prediction from wireline logs using a neural network are near pointless, yielding extremely high RMS errors.

Where porosity and permeability are actually known (with laboratory data), reservoir quality ranking becomes an easy task (Figure 47).

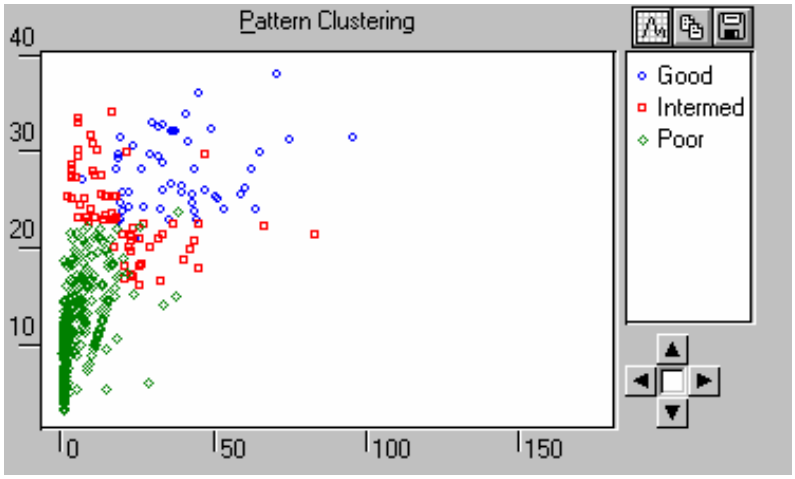

Figure 47. Reservoir quality ranking. Porosity versus permeability.

Wireline logs and their prediction of porosity in carbonates is a difficult task. Carbonate reservoirs display a degree of heterogeneity unknown to siliciclastic reservoirs. Carbonate reservoirs have differing pore systems which greatly influence the effective porosity and thus the reservoir quality. The presence of dolomite and anhydrite affects the grain density and again affecting the wireline log measurements. Diagenetic pulses flush through the reservoir

affecting permeability, pore characteristics and reservoir quality as well. Accurate prediction of porosity and permeability (i.e. reservoir quality) is complicated without the use of analytical data.

This method has limitations when employed in a carbonate reservoir. The neural networks produced in this project are site specific. This network could not be used in another carbonate field just 10's of miles away. A network must be trained on data representative of a single area. If this network were utilized in a field containing boundstones, the network would attempt to classify the boundstone as a grainstone, rudstone, floatstone or shaly siltstone. This is because the training data set contained no boundstones.

That said, an attempt must be made to attempt to predict reservoir quality in the face of little data. Most fields are unlike Happy Spraberry field with nearly all its wells cored in the interval of interest. With luck, a few wells may be cored in the zone of interest and an attempt should be made to extrapolate reservoir quality from the available data, typically wireline logs. This project has shown that neural networks outperform linear methods in correctly classifying both electrofacies and reservoir quality.

REFERENCES CITED

Ahr, W.M. and B.S. Hammel, 1999, Identification and mapping of flow units in carbonate reservoirs; An example from the Happy Spraberry (Permian) Field, Garza County, Texas USA: Energy Exploration & Exploitation, v. 17, p.311-334.

Alcocer, Y. and P. Rodrigues, 2001, Neural Networks Models for Estimation of Fluid Properties: SPE 69624.

Anderson, D. and G. McNeil, 1992, Artificial neural networks technology: Rome, NY, Data & Analysis Center for Software, 83 pp.

Bishop, C., 1995, Neural networks for pattern recognition, Oxford, Oxford University Press, 504 p.

Boomer, R.J., 1995, Predicting Production Using a Neural Network (Artificial Intelligence Beats Human Intelligence): SPE 30202.

Choquette, P.W., and L.C. Pray, 1970, Geologic nomenclature and classification of porosity in sedimentary carbonates: AAPG Bulletin, v. 2, p. 207-250.

Dunham, R. J., 1962, Classification of carbonate rocks according to depositional texture, *in* W. E. Ham, ed., Classification of Carbonate Rocks-A Symposium: AAPG Memoir 1, p. 108-121.

Ebanks, W.J., 1987, Flow Unit Concept--Integrated Approach to Reservoir Description for Engineering Projects, AAPG Meeting Abstracts, v.1, issue 5, p. 521-522.

Ebanks, W.J., Jr., M.H. Schiehing, and C.D. Atkinson, 1992, Flow units for reservoir characterization, *in* Morton-Thompson, D., and A.M. Woods, eds., Development Geology Reference Manual: AAPG Methods in Exploration Series, No. 10, p. 282-285.

Ewing, T.E., 1993, Erosional margins and patterns of subsidence in the late Paleozoic West Texas Basin and adjoining basin of West Texas and New Mexico: New Mexico Geological Society Guidebook, 44th Field Conference, Santa Fe, New Mexico, p. 155-166.

Frenzel, H.N., R.R. Bloomer, R.B. Cline, J.E. Cys, J.E. Galley, W.R. Gibson, J.M. Hills, W.E. King, W.R. Seager, F.E. Kottlowski, S. Thompson III, G.C. Luff, B.T. Pearson, and D.C. Van Sicilan, 1988, The Permian Basin region, *in* L.L. Sloss, ed., The Geology of North America, v. D-2, Sedimentary Cover-North American Craton: United States, Geological Society of America, p. 261-306.

Guevera, E.H., 1988, Geological characterization of Permian submarine fan reservoirs of the Driver Waterfloor Unit, Spraberry Trend, Midland Basin, Texas Bureau of Economic Geology, University of Texas-Austin, Report of Investigations No. 172, 44 p.

Habitch, J.K.A., 1979, Paleoclimate, paleomagnetism, and continental drift: AAPG Studies in Geology No. 9, 30 p.

Hammel, B. S., 1996, High resolution reservoir characterization of the Permian (upper Leonardian) Spraberry Formation, Happy Spraberry Field, Garza County, Texas: Unpublished Master's Thesis, Texas A&M University, 1996, 157 pp.

Handford, C. R., 1981, Sedimentology and genetic stratigraphy of Dean and Spraberry formations (Permian), Midland Basin, Texas: AAPG Bulletin, v. 65, p. 1602-1616.

Hertz, J., A. Krogh, R.D. Palmer, 1991, Introduction to the theory of neural computation. Reading: Addison-Wesley, 327 p.

Layman, J.M., 2002, Porosity characterization utilizing petrographic image analysis: Implications for identifying and ranking reservoir flow units, Happy Spraberry Field, Garza County, Texas: Unpublished Master's Thesis, Texas A&M University, 2002, 103 p.

Lucia, F.J., 1983, Petrophysical parameters estimated from visual description of carbonate rocks: a field classification of carbonate pore space: Journal of Petroleum Technology, v. 35, p. 626-637.

Mazzullo, S.J., 1995, Permian stratigraphy and facies, Permian Basin (Texas-New Mexico) and adjoining areas in the mid-continent United States, *in* P.A. Scholle, T.M. Peryt, D.S. Ulmer-Scholle, eds., The Permian of Northern Pangea: Sedimentary Basins and Economic Resources, Spring-Verlag, New York, v. 2, p. 41-60.

Mazzullo, S. J. and A. M. Reid, 1989, Lower Permian platform and basin depositional systems, northern Midland Basin, TX, *in* P.D. Crevello, J.L. Wilson, J.F. Sarg, J.F. Read, eds., Controls on Carbonate Platform and Basin Development: SEPM Special Publication No. 44, p. 305-320.

McCreesh, C. A., R. Ehrlich, and S.J. Crabtree, 1991, Petrography and reservoir petrophysics II: Relating thin section porosity to capillary pressure, the association between pore types and throat size: AAPG Bulletin, v. 75, p. 1563-1578.

Nikravesh, M., 1998, Neural Network Knowledge-Based Modeling of Rock Properties Based on Well Log Databases: SPE 46206.

Rogers, S.L., Chen, D.C., Kopaska-Merkel, D.C. and Fang, J.H., 1995, Predicting permeability from porosity using artificial neural networks: AAPG Bulletin, v.79, No. 12, p. 1786-1797.

Ross, C.A., 1986, Paleozoic evolution of southern margin of Permian basin: Geological Society of America Bulletin, v. 97, p. 536-554.

Roy, E., 1998, High resolution mapping of flow units for enhanced recovery program planning, Happy Spraberry Lime Field, Garza County, Texas: Unpublished Master's Thesis, Texas A&M University, 1998, 106 pp.

Saggaf, M.M. and Nebrija, E.L., 2000, Estimation of lithologies and depositional facies from wire-line logs: AAPG Bulletin, v. 84, no. 10, p. 1633-1646.

San Sarem, E., 1992, Waterflooding, *in* Morton-Thompson, D., and A.M. Woods, eds., Development Geology Reference Manual: AAPG Methods in Exploration Series, No. 10, p. 523-526.

Silver, B.A., and R.G. Todd, 1969, Permian cyclic strata, northern Midland and Delaware Basins, West Texas and southeastern New Mexico: AAPG Bulletin, v. 53, p. 2223-2251.

Van Hilton, D., 1962, Presentation of paleomagnetic data, polar wandering, and continental drift: American Journal of Science, v. 62, p. 401-426.

Ward, R. F., C.G Kendall, and P.M Harris, 1986, Upper Permian (Guadalupian) facies and their association with hydrocarbons-Permian basin, West Texas and New Mexico: AAPG Bulletin, v. 70, p. 239-262.

Yang, K. M., and S.L. Dorobek, 1994, The Permian Basin of west Texas and New Mexico: Tectonic history of a "composite" foreland basin and its effect on stratigraphic development, *in* S.L. Dorobek and G. M. Ross, eds., Stratigraphic Evolution of Foreland Basins, SEPM Special Publication no. 52, p. 147-172.

APPENDIX A

Core Description
Bennett Petroleum
Lott 19 #2
Happy Spraberry Field
Garza County, Texas
Core Interval 4914.0'-4991.0'

Depth (ft.)	Thickness (ft.)	Description
4914.0	2.0	Limestone. Light gray to dark brown, very fine grained packstone, well sorted, mostly ooids/peloids and mollusk fragments, massive, grain moldic porosity, differential oil staining.
4916.0	4.0	Core removed for special core analysis.
4920.0	2.0	Siltstone and shale. Dark gray, very fine grained quartz silt and clay. Fossils rare. Parallel to rippled laminations.
4922.0	3.0	Limestone. Brown to medium gray, moderately sorted grainstone. Ooids, peloids, and lithoclasts. Brachiopods, crinoids, and mollusks, massive, differential oil staining.
4925.0	1.0	Siltstone. Light to medium gray, very fine grained quartz. Calcite cementation, rippled to planar laminations, microfaults.
4926.0	9.0	Limestone. Medium gray to dark brown, well sorted, fine grained grainstone. Rare fossils, massive, imbricated lithoclasts, grain moldic and vuggy porosity.
4935.0	1.0	Siltstone. Light to medium gray, fine grained quartz. No fossils. Rippled laminations, microfaults.
4936.0	8.0	Limestone. Dark brown to medium gray, fine grained grainstone. Rare fossils, massive with isolated, planar ripples. Differential oil staining, vuggy and grain moldic porosity.

Core Description
Bennett Petroleum
Lott 19 #2 (cont.)
Happy Spraberry Field
Garza County, Texas
Core Interval 4914.0'-4991.0'

Depth (ft.)	Thickness (ft.)	Description
4944.0	5.0	Core removed for special analysis.
4949.0	1.0	Limestone. Light gray, moderately sorted packstone. Composed of mostly ooids, lithoclasts, and skeletal fragments. Mollusks, crinoids, brachiopods, and ostracods common.
4950.0	5.0	Limestone. Medium gray to dark brown, well sorted, fine grained grainstone. Massive, differential oil staining, grain moldic porosity.
4955.0	1.0	Sandstone. Light gray, moderately sorted very fine grained sandstone with skeletal packstone stringers. Mollusk, crinoids common, planar, wavy laminations.
4956.0	8.0	Siltstone. Light gray to medium gray, well sorted quartz grains, fossils very rare. Discontinuous wavy laminations, microfaulted with contorted bedding.
4964.0	16.0	Siltstone. Medium gray to dark gray, moderately sorted quartz grains. Fossils rare, Continuous wavy to planar laminations, microfaulted.
4980.0	11.0	Mudstone. Dark gray to black, well sorted clay particles. Fossils rare, continuous wavy laminations.
4991.0	------	END OF CORE

Core Description
Bennett Petroleum
Lott 19 #5
Happy Spraberry Field
Garza County, Texas
Core Interval 4926.0'-5025.0'

Depth (ft.)	Thickness (ft.)	Description
4926.0	5.0	Limestone. Light gray to medium gray, fine grained moderately sorted, silty, oolitic skeletal grainstone. Mudstone lithoclasts, skeletal fragments, parallel, continuous laminations, microfaults. Spotty oil staining rare.
4931.0	6.0	Siltstone. Medium gray to black, very fine grained siltstone. Calcite cement, isolated skeletal packstone stringers, continuous, wavy laminations, shaly discontinuous laminations, microfaults.
4937.0	5.0	Limestone. Light tan to dark brown. Very fine grained oolitic skeletal grainstone. Skeletal fragments including crinoids, ostracods, and bryozoans. Massive, imbricated mud-pebble lithoclasts, grain moldic porosity, differential oil staining.
4942.0	5.0	Limestone. Light tan to light gray, fine grained oolitic grainstone. Calcite cement banding in tight spots. Continuous, wavy, non-parallel laminations, grain moldic porosity, spotty oil staining.
4947.0	1.0	Siltstone. Dark gray to black, very fine grained siltstone. Rare fossil fragments, calcite cement, continuous, wavy, parallel laminations.
4948.0	12.0	Limestone. Medium gray to light gray oolitic skeletal, fine grained grainstone. Mudstone lithoclasts, massive with isolated wavy, shaly, microfaulted laminations.

Core Description
Bennett Petroleum
Lott 19 #5 (cont.)
Happy Spraberry Field
Garza County, Texas
Core Interval 4926.0'-5025.0'

Depth (ft.)	Thickness (ft.)	Description
4960.0	5.0	Core removed for special core analysis.
4965.0	2.0	Siltstone. Dark gray to medium gray, very fine grained siltstone with interbedded skeletal packstone stringers. Wavy, continuous, parallel laminations with microfaults.
4967.0	5.0	Limestone. Light tan to medium brown, fine grained, well sorted, oolitic and skeletal grainstone. Common ostracods, crinoids, and mollusks. Spotty oil staining with well developed grain moldic porosity.
4972.0	1.0	Limestone. Medium tan, poorly sorted, oolitic grainstone. Lithoclast present include reefy fragments as well as whole fossils. Grain moldic porosity.
4973.0	4.0	Siltstone. Light gray to medium gray, very fine grained quartz. Fossil fragments, calcite cement common, discontinuous, non-parallel laminations.
4977.0	7.0	Mudstone. Dark gray to black mudstone. Wavy, discontinuous laminations, microfaults, and contorted bedding.
4984.0	3.0	Siltstone. Medium gray very fine grained quartz. Fossil fragments rare, discontinuous, non-parallel laminations, microfaults.
4987.0	38.0	Lost core.

Core Description
Bennett Petroleum
Lott 19 #5 (cont.)
Happy Spraberry Field
Garza County, Texas
Core Interval 4926.0'-5025.0'

Depth (ft.)	Thickness (ft.)	Description
5025.0	------	END OF CORE.

Core Description
Bennett Petroleum
Lott 19 #11
Happy Spraberry Field
Garza County, Texas
Core Interval 4873.0'-4986.0'

Depth (ft.)	Thickness (ft.)	Description
4873.0	8.0	Limestone. Medium tan to light gray, moderately sorted, fine grained oolitic grainstone. Anhydrite replacement cement, fossils rare. Isolated continuous, wavy, parallel laminations, with minor microfaults. Grain moldic porosity and differential oil staining.
4881.0	2.0	Limestone. Light gray to light tan, poorly sorted, oolitic grainstone with mud pebble lithoclasts. Anhydrite cement, grain moldic porosity.
4883.0	1.0	Limestone. Light tan, well sorted, fine grained oolitic grainstone. Fossils rare, grain moldic porosity, differential oil staining.
4884.0	2.0	Lost Core.
4886.0	38.0	Limestone. Light gray to medium tan, well sorted, fine grained oolitic skeletal grainstone. Anhydrite replacement cement, abundant fossil fragments, including mollusks, ostracods, and crinoids. Massive, non-bedded, grain moldic porosity of ooids and skeletal fragments, differential oil staining.
4924.0	3.0	Limestone. Light gray to medium gray, moderately sorted, fine grained, silty, oolitic skeletal packstone. Anhydrite cement, with isolated continuous, wavy, parallel laminations. Skeletal grainstone stringers with grain moldic porosity.
4927.0	14.0	Lost Core.

Core Description
Bennett Petroleum
Lott 19 #11 (cont.)
Happy Spraberry Field
Garza County, Texas
Core Interval 4873.0'-4986.0'

Depth (ft.)	Thickness (ft.)	Description
4941.0	11.0	Limestone. Light gray to medium gray, poorly sorted, skeletal rudstone. Pervasive anhydrite cement, abundant skeletal fragments, including bryozoans, mollusks, crinoids, and ostracods. Massive with stylolites and differential oil staining.
4952.0	5.0	Limestone. Light gray to light tan, well sorted, fine grained skeletal packstone grainstone. Massive, fossils include mollusks, bryozoans, and crinoids. Vuggy porosity and differential oil staining.
4957.0	19.0	Limestone. Light gray to medium tan, poorly sorted, skeletal rudstone. Pervasive anhydrite cement, fossils include mollusks and bryozoans with some intervals as in situ bindstones. Vuggy porosity with differential oil staining.
4976.0	1.0	Siltstone. Medium gray, moderately sorted, very fine grained quartz with isolated fossil fragments. Isolated packstone stringer, contorted bedding and soft sediment deformation.
4977.0	9.0	Siltstone. Medium gray to dark gray, very fine grained quartz grains with interbedded mudstone. No fossils, wavy, continuous, parallel laminations with microfaults.
4986	------	END OF CORE.

Core Description
Bennett Petroleum
Lott 19 #4
Happy Spraberry Field
Garza County, Texas
Core Interval 4910.0'-4994.0'

Depth (ft.)	Thickness (ft.)	Description
4910.0	1.5	Limestone. Brown, very fine grained packstone, massive, well sorted, composed of mostly undifferentiated foraminifera and ooids/peloids. With common ostracod fragments and rare crinoid, bryozoan, brachiopod and mollusk fragments.
4911.5	3.5	Limestone. Light gray, fine grained grainstone, massive, well sorted, mostly undifferentiated foraminifera and ooids/peloids, with rare crinoid, bryozoan, brachiopod and mollusk fragments. Grain moldic and vuggy porosity.
4915.0	1.0	Limestone. Medium gray, very fine grained packstone composed mainly of ooids and peloids. Micro-faulted, parallel, planar silt/shale laminations.
4916.0	1.0	Siltstone and shale. Tan and dark gray, very fine grained quartz silt and clay. No fossils. Micro-faulted, parallel, planar silt/shale laminations.
4917.0	0.7	Limestone. Brown, very fine grained, packstone, massive, well sorted, composed mostly of ooids and peloids, with rare undifferentiated skeletal fragments.
4917.7	0.3	Siltstone and shale. Tan and dark gray, very fine grained quartz silt and clay. No fossils. Micro-faulted, parallel, planar silt/shale laminations.

Core Description
Bennett Petroleum
Lott 19 #4 (cont.)
Happy Spraberry Field
Garza County, Texas
Core Interval 4910.0'-4994.0'

Depth (ft.)	Thickness (ft.)	Description
4918.0	1.0	Limestone. Medium gray to brown, very fine to fine grained packstone, massive, well sorted, composed mainly of ooids and peloids, with rare crinoid, bryozoan, brachiopod, mollusk, ostracod and tubiphytes fragments. Grain moldic porosity.
4919.0	23.0	Limestone. Medium gray to white, spotty oil staining, fine to medium grained grainstone, massive, moderately well sorted, composed of mostly ooids and peloids, with rare crinoid, bryozoan, brachiopod, mollusk, ostracod and tubiphytes fragments. Anhydrite pre filling cement. Graining moldic porosity.
4942.0	1.0	Limestone. Medium gray, fine grained, grainstone, massive with styolites, well sorted, composed of mostly ooids and peloids, with rare undifferentiated skeletal fragments. Grain moldic porosity.
4943.0	2.0	Limestone. Medium gray to brown, fine grained, packstone, moderately well sorted, composed of ooids/peloids and foraminifera, with rare crinoid and ostracod fragments. Parallel, wavy laminations and vertical burrows. Anhydrite poor filling cement.
4945.0	0.5	Limestone. Medium gray to white, fine grained, grainstone, massive well sorted composed of mostly ooids/peloids and foraminifera, with rare undifferentiated skeletal fragments.

Core Description
Bennett Petroleum
Lott 19 #4 (cont.)
Happy Spraberry Field
Garza County, Texas
Core Interval 4910.0'-4994.0'

Depth (ft.)	Thickness (ft.)	Description
4945.5	0.5	Limestone. Medium gray to brown, fine grained packstone, massive well sorted, composed of mostly ooids/peloids and foraminifera, with rare undifferentiated skeletal fragments.
4946.0	3.0	Limestone. Medium gray to white, spotty oil staining, fine to medium grained, grainstone, massive, moderately well sorted, composed of mostly ooids and peloids, with rare crinoid, bryozoan, brachiopod and mollusk fragments. Grain moldic porosity.
4949.0	1.0	Limestone. Medium gray to brown, fine grained, packstone, moderately well sorted, composed of mostly crinoid fragments. Parallel, wavy silt/shale laminations with abundant lithoclasts.
4950.0	1.0	Limestone. Medium gray to white, spotty oil staining, fine to medium grained, grainstone, massive, moderately well sorted, composed of mostly ooids and peloids, with rare crinoid, bryozoan, brachiopod and mollusk fragments/ Grain moldic porosity.
4951.0	5.0	No core.

Core Description
Bennett Petroleum
Lott 19 #4 (cont.)
Happy Spraberry Field
Garza County, Texas
Core Interval 4910.0'-4994.0'

Depth (ft.)	Thickness (ft.)	Description
4956.0	5.5	Limestone. Medium gray to white, spotty oil staining, fine to medium grained, grainstone, massive, moderately well sorted, composed mostly of ooids and peloids, with rare crinoid, bryozoan, brachiopod, mollusk, ostracod and tubiphytes fragments. Anhydrite pore filling cement. Grain moldic porosity.
4961.5	0.5	Limestone. Light gray, poorly sorted, very coarse grained conglomeritic grainstone containing fine to medium grained oolitic-peloidal grainstone with gravels and cobbles of skeletal rudstone. Bounded at the base by a sharp and irregular scour surface.
4962.0	0.5	Shale. Black, very fine grained, very thinly laminated. No fossils. Truncated by overlying conglomeritic grainstone.
4962.5	7.0	Limestone. Medium to light gray, poorly sorted, coarse grained skeletal rudstone to packstone composed of mainly crinoid and bryozoan fragments with rare fragments of ooids/peloids, brachiopods, mollusks, foraminifera, ostracods and tubiphytes. Coarse brecciated texture with slight contorted bedding.
4969.5	1.0	Siltstone. Light gray to tan, very well sorted, very fine grained quartz silt containing no clay and minor calcite cement. Massive texture with few pebble sized lithoclasts. Truncated by overlying skeletal rudstone.

Core Description
Bennett Petroleum
Lott 19 #4 (cont.)
Happy Spraberry Field
Garza County, Texas
Core Interval 4910.0'-4994.0'

Depth (ft.)	Thickness (ft.)	Description
4970.5	2.5	Lime Floatstone. Dark gray shaly siltstone matrix with light gray skeletal rudstone breccia containing mainly crinoid and bryozoan fragments, along with rare ooids/peloids, brachiopods, mollusks, foraminifera, ostracods and tubiphytes fragments. Poorly sorted, containing interbedded shale with parallel wavy laminations. Anhydrite cement.
4973.0	4.0	Sandstone. Light gray to tan, very well sorted, very fine grain quartz sand containing no clay and minor calcite cement and rare crinoid fragments. Massive to rippled texture at base. Truncated by overlying floatstone.
4977.0	0.5	Shaly Siltstone. Dark gray, well sorted, very fine grained quartz silt and shale, exhibiting discontinuous wavy laminations.
4977.5	2.0	Lime Floatstone. Dark gray shaly siltstone matrix with light gray skeletal rudstone breccia containing mainly crinoid and bryozoan fragments, along with rare ooids/peloids, mollusks, foraminifera, ostracods and tubiphytes fragments. Poorly sorted.
4979.5	1.0	Shaly siltstone. Dark gray, well sorted, very fine grained quartz silt and shale, exhibiting contoured bedding and lithoclasts.

Core Description
Bennett Petroleum
Lott 19 #4 (cont.)
Happy Spraberry Field
Garza County, Texas
Core Interval 4910.0'-4994.0'

Depth (ft.)	Thickness (ft.)	Description
4980.5	4.5	Lime Floatstone. Dark gray shaly siltstone matrix with light gray skeletal rudstone breccia containing mainly crinoid, bryozoan and brachiopod fragments, along with rare ooids/peloids, brachiopods, mollusks, foraminifera, ostracods and tubiphytes fragments. Poorly sorted.
4985.0	1.0	Sandstone. Light gray to tan, very well sorted, massive, very fine grained quartz sand containing minor clay and rare crinoid fragments. Truncated by overlying floatstone.
4986.0	5.0	Lime Floatstone. Dark gray shaly siltstone matrix with light gray skeletal rudstone breccia containing poorly sorted, undifferentiated, well cemented skeletal grains and rare crinoid fragments. Matrix exhibits contorted bedding and lithoclasts.
4991.0	3.0	Shaly siltstone. Dark gray, well sorted, very fine grained quartz silt and shale, exhibiting parallel, wavy laminations to parallel planar laminations at the base.
4994.0	------	END OF CORE.

Core Description
Bennett Petroleum
Lott #19-7
Happy Spraberry Field
Garza County, Texas
Core Interval 4936.0'-5057.0'

Depth (ft.)	Thickness (ft.)	Description
4936.0	0.1	Shale. Black, carbonaceous, very fine grained, very thinly laminated. No fossils.
4936.1	8.9	Silty Limestone. Light gray to brown, interbedded fine grain oolitic-peloidal packstone and very fine quartz silt containing abundant bryozoan, crinoid, undifferentiated skeletal fragments and occasional carbonaceous shale (coal?) and mudstone lithoclasts. Well to poorly sorted, massive to poorly laminated with micro faults and fractures with minor contorted bedding. Large vertical burrow at base.
4945.0	2.0	Shaly siltstone. Light gray to tan, containing no fossils. Fine grained well sorted, laminated with high angle cross beds.
4947.0	0.5	Limestone. Brown to gray, skeletal oolitic-peloidal packstone containing abundant bryozoan, crinoid and foraminifera fragments. Fine grained, massive and poorly sorted with wavy to contorted bedding.
4947.5	2.5	Limestone. Light gray, skeletal oolitic-peloidal grainstone containing bryozoan and crinoid fragments. Fine grained, moderately sorted and weakly cross bedded. Grain moldic porosity.

Core Description
Bennett Petroleum
Lott #19-7 (cont.)
Happy Spraberry Field
Garza County, Texas
Core Interval 4936.0'-5057.0'

Depth (ft.)	Thickness (ft.)	Description
4950	19.0	Limestone. Medium to light gray, poorly sorted, coarse grained skeletal rudstone to packstone composed of mainly crinoid, bryozoan and brachiopod fragments with rare to common fragments of mollusks, foraminifera, ostracods, tubiphytes and ooids/peloids with common to rare silt. Coarse brecciated texture with slight contorted bedding. Common anhydrite filling and styolites. Vuggy porosity.
4969.0	1.5	Shale. Dark gray, well sorted containing quartz silt and carbonate lithoclasts. No fossils.
4970.5	18.5	Limestone. Light gray, oolitic-peloidal grainstone containing common fragments of crinoids, bryozoan, brachiopods and mollusks with minor silt. Fine to medium grained, moderately sorted and massive, common anhydrite filling. Vuggy to grain moldic porosity.
4989.0	5.0	Sandstone. Light gray to tan, very well sorted, very fine grained quartz sand containing no clay and minor calcite cement and rare crinoid fragments. Massive to poorly laminated. Intergranular porosity.
4994.0	2.0	No core.

Core Description
Bennett Petroleum
Lott #19-7 (cont.)
Happy Spraberry Field
Garza County, Texas
Core Interval 4936.0'-5057.0'

Depth (ft.)	Thickness (ft.)	Description
4996.0	2.0	Limestone. Light gray to white, fine grained, moderately sorted, cemented oolitic-peloidal grainstone, intraclast breccia with siltstone matrix. Well cemented with no shale.
4998.0	0.5	Limestone. Dark gray to brown, very fine grained mudstone, well sorted massive. No fossils.
4998.5	6.5	Siltstone. Light to dark gray, fining upward quartz silt, with increasing shale and decreasing calcite cement. Minor undifferentiated skeletal grains and lithoclasts at the base of the unit. Discontinuous to continuous ripple laminations, contorted bedding and microfaults.
5005.0	5.0	Limestone. Light gray to white, medium to coarse grained skeletal grainstone composed primarily of bryozoan, brachiopod, crinoid and mollusk fragments along with abundant silt and common lithoclasts. Poorly sorted, massive to brecciated chaotic texture. Large anhydrite fillings.
5010.0	7.0	Siltstone. Light gray to tan, very fine grained, coarsening upward beds (1-6") alternating from laminated to massive. Increasing calcite cement near top of unit, with no fossils.

Core Description
Bennett Petroleum
Lott #19-7 (cont.)
Happy Spraberry Field
Garza County, Texas
Core Interval 4936.0'-5057.0'

Depth (ft.)	Thickness (ft.)	Description
5017.0	7.0	Shaly siltstone. Very fine grained, planar to rippled laminations. No fossils.
5024.0	4.0	Shaly siltstone. Very fine grained, planar to rippled laminations with thin interbedded lime sand composed of ooids/peloids and undifferentiated skeletal fragments. Large recumbent fold in shaliest part of unit.
5028.0	4.0	Shaly siltstone. Very fine grained, planar to rippled laminations. No fossils.
5032.0	0.5	Limestone. Light gray, oolitic-peloidal grainstone containing common fragments of crinoids, bryozoans, brachiopods and mollusks with minor silt. Fine to medium grained, moderately sorted and massive.
5032.5	5.0	Shaly siltstone. Very fine grained, planar to rippled laminations. No fossils.
5037.5	3.5	Shaly siltstone. Very fine grained, abundant shale, planar to rippled laminations. No fossils.
5041.0	9.0	Shale. Dark gray, well sorted containing quartz silt and carbonate lithoclasts. No fossils.
5050.0	3.0	Shaly Siltstone. Light gray to tan, very fine grained, planar to rippled laminations. No fossils.

Core Description
Bennett Petroleum
Lott #19-7 (cont.)
Happy Spraberry Field
Garza County, Texas
Core Interval 4936.0'-5057.0'

Depth (ft.)	Thickness (ft.)	Description
5053.0	4.0	Sandstone. Light gray, fine to medium grained, calcite cemented, massive to rippled laminations. No fossils.
5057.0	------	END OF CORE.

Core Description
Torch Energy
Lott #19-8
Happy Spraberry Field
Garza County, Texas
Core Interval 4916.0'-5036.0'

Depth (ft.)	Thickness (ft.)	Description
4916.0	12.0	Limestone. Light to medium gray, fine grained grainstone composed of ooids and peloids with rare to common undifferentiated skeletal fragments. Massive, well sorted with few shale laminations, large vertical burrow @ 4922', large anhydrite filled vug @4924'. Grain moldic porosity.
4928.0	48.0	No core.
4976.0	3.0	Light to medium gray, fine grained, grainstone composed primarily of ooids and peloids with rare to common undifferentiated skeletal fragments. Well sorted, cross bedded. Grain moldic porosity.
4979.0	2.0	Shaly siltstone. Dark gray to tan, very fine grained, planar and rippled laminations to cross bedded, microfractures. No fossils.
4981.0	7.0	Limestone. Medium to light gray, poorly sorted, coarse grained skeletal rudstone to packstone composed of crinoid, bryozoan and brachiopod fragments with rare to common fragments of tubiphytes, mollusks, foraminifera, ostracods and ooids/peloids with common to rare silt. Coarse brecciated texture with massive growth fabrics and styolites. Vuggy porosity.
4988.0	4.0	Limestone. Light to medium gray, fine grained, grainstone composed of ooids and peloids with common bryozoan and other undifferentiated skeletal fragments. Well sorted and cross bedded. Grain moldic porosity.

Core Description
Torch Energy
Lott #19-8 (cont.)
Happy Spraberry Field
Garza County, Texas
Core Interval 4916.0'-5036.0'

Depth (ft.)	Thickness (ft.)	Description
4992.0	2.0	Limestone. Medium to light gray, poorly sorted, coarse grained skeletal rudstone to packstone composed of crinoid, bryozoan and brachiopod fragments with rare to common fragments of tubiphytes, mollusks, foraminifera, ostracods and ooids/peloids with common to rare silt. Coarse brecciated texture along with massive growth fabrics and styolites. Vuggy porosity.
4994.0	5.5	Floatstone. Dark gray shaly siltstone matrix with light gray skeletal rudstone breccia containing poorly sorted, undifferentiated, well cemented skeletal grains and rare crinoid fragments. Matrix exhibits contorted bedding and lithoclasts.
4999.5	9.5	Shale. Black, carbonaceous, very fine grained, very thinly laminated. No fossils.
5003.0	32.0	Shaly siltstone. Medium gray, very fine grained, planar to rippled laminations with occasional contorted bedding and microfaults. No fossils.
5035.0	1.0	Shale. Black, carbonaceous, very fine grained, very thinly laminated. No fossils.
5036.0	------	END OF CORE.

Core Description
Torch Energy
Lott #19-9
Happy Spraberry Field
Garza County, Texas
Core Interval 4920.0'-4977.5'

Depth (ft.)	Thickness (ft.)	Description
4920.0	8.0	Shaly siltstone. Light gray to tan, very fine grained with lime mud cement, massive with occasional ripple laminations. Few large skeletal fragments.
4928.0	8.5	Shale. Black, carbonaceous, very fine grained, ripple laminated. Rare lithoclasts and no fossils.
4936.5	2.5	Sandstone. Light gray to tan, very well sorted, very fine grained quartz sand containing no clay and minor calcite cement and rare crinoid fragments. Massive to poorly laminated. Intergranular porosity.
4939.0	10.0	Shaly siltstone. Light gray to tan, very fine to fine grained, planar to rippled laminations with occasional contorted bedding and micro-faults. Common skeletal fragments and lithoclasts.
4949.0	16.0	Shaly siltstone. Light gray to tan, very fine to fine grained, coarsening upward beds, laminated to massive soft sediment deformation. Decreasing shale near top of unit, with no fossils.
4965.0	7.5	Shaly siltstone. Dark gray, well sorted, very fine grained quartz silt and shale, exhibiting contorted bedding and lithoclasts.
4972.5	5.0	Shaly siltstone. Light gray to tan, very fine grained, ripple laminated. No fossils.
4977.5	-----	END OF CORE.

Core Description
Torch Energy
Lott #19-9A (Sidetrack)
Happy Spraberry Field
Garza County, Texas
Core Interval 4990.0'-5050.0'

Depth (ft.)	Thickness (ft.)	Description
4990.0	15.0	Shaly siltstone. Dark gray, well sorted, very fine grained quartz silt and shale, exhibiting ripple laminations and rare skeletal fragments.
5005.0	3.0	Mudstone. Brown, very fine grained with interbedded shaly siltstone. High angle planar laminations, anhydrite, no fossils.
5008.0	3.0	Shale. Black, carbonaceous, very fine grained, high angle ripple laminations. Erosional surface at top of unit. No fossils.
5011.0	4.0	Mudstone. Dark gray to brown, fine grained with interbedded shaly siltstone. High angle planar laminations, anhydrite, rare fossils.
5015.0	6.5	Limestone. Light to medium gray, fine grained, packstone, composed of primarily ooids and peloids, with common quartz silt and rare skeletal fragments. Well sorted, high angle cross beds. Minor grain moldic porosity.
5021.5	7.5	Shaly siltstone. Medium gray to tan, very fine grained, high angle cross beds and ripple laminations, calcite cemented with rare fossils.
5029.0	6.5	Shaly siltstone. Dark gray, very fine grained, exhibiting contorted bedding and fluid escape structures. No fossils.

Core Description
Torch Energy
Lott #19-9A (Sidetrack)(cont.)
Happy Spraberry Field
Garza County, Texas
Core Interval 4990.0'-5050.0'

Depth (ft.)	Thickness (ft.)	Description
5035.5	4.5	Shaly siltstone. Dark gray, very fine grained, generally massive with soft sediment deformation. No fossils and few lithoclasts.
5040.0	10.0	Shaly siltstone. Light o medium gray, very fine grained, planar to rippled laminations with contorted bedding and micro-faults. No fossils.
5050.0	------	END OF CORE.

Core Description
Torch Energy
Lott #19-14
Happy Spraberry Field
Garza County, Texas
Core Interval 4910.0'-4947.0'

Depth (ft.)	Thickness (ft.)	Description
4910.0	2.5	Shale. Black, carbonaceous, very fine grained, laminated, microfaults. No fossils.
4912.5	6.0	Mudstone. Dark gray to brown, very fine grained with interbedded shaly siltstone, planar parallel laminations and rare fossils.
4918.5	4.5	Shale. Black, carbonaceous, very fine grained, laminated. No fossils.
4923.0	5.0	Sandstone. Light gray to tan, very well sorted, very fine grained quartz sand containing minor clay and calcite cement. Exhibiting contorted ripple laminations to inclined planar laminations.
4928.0	3.0	Shale. Black, carbonaceous, very fine grained, laminated. No fossils.
4931.0	9.0	Sandstone. Light gray to tan, very well sorted, very fine grained quartz sand containing minor clay and calcite cement and rare skeletal fragments. Ripple laminations with few fractures.
4940.0	1.0	Shale. Black, carbonaceous, very fine grained, laminated. No fossils.
4941.0	6.0	Shaly siltstone. Light gray to tan, very fine grained, massive to planar laminations with abundant soft sediment deformation.
4947.0	------	END OF CORE.

Core Description
Torch Energy
Lott #6-1
Happy Spraberry Field
Garza County, Texas
Core Interval 4926.0'-4984.0'

Depth (ft.)	Thickness (ft.)	Description
4926.0	28.5	Shaly siltstone. Light gray to tan, very fine to fine grained, coarsening upward beds, laminated to massive with no fossils.
4954.5	17.5	Shaly siltstone. Light gray to tan, very fine to fine grained, laminated with interbedded coarse grained skeletal packstone, containing crinoid fragments, bryozoan, brachiopod and other undifferentiated skeletal grains. Skeletal packstone bed present at the top of each coarsening upward cycle.
4972.0	4.0	Shale. Black, carbonaceous, very fine grained, laminated. No fossils.
4976.0	8.0	Shaly siltstone. Medium gray to tan, very fine grained, well sorted, massive with inclined ripple laminations with contorted bedding and micro-faults. Fining upward grain size and increasing upward shale content. No fossils.
4984.0	------	END OF CORE.

Core Description
Bennett Petroleum
Lott #18-1
Happy Spraberry Field
Garza County, Texas
Core Interval 4878.0'-4996.0'

Depth (ft.)	Thickness (ft.)	Description
4878.0	12.0	Limestone. Dark brown to gray, very fine grained shaly mudstone, well sorted, planar parallel laminations. No fossils.
4890.0	46.0	Limestone. Dark brown to dark gray, very fine grained shaly mudstone to Wackestone, ripple to planar laminations, skeletal fragments present, occasional contorted bedding, interbedded skeletal packstone lens.
4936.0	60.0	Shaly siltstone. Tan to dark gray, very fine grained, ripple to planar laminations, lithoclasts, soft sediment deformation, microfaults.
4996.0	------	END OF CORE.

Core Description
Bennett Petroleum
Lott #19-3
Happy Spraberry Field
Garza County, Texas
Core Interval 4865.0'-4977.0'

Depth (ft.)	Thickness (ft.)	Description
4865.0	13.0	Shaly siltstone. Dark tan to dark gray, planar to slightly dipping laminations, calcite cement.
4878.0	2.0	Siltstone. Dark tan, massive, medium grained.
4880.0	10.0	Breccia. Siltstone intraclasts greater than 10 cm, interlaminated siltstone and shale matrix. Highly contorted beds with micro-faults and folds.
4890.0	1.0	Siltstone. Dark tan, medium grained with intraclasts.
4891.0	19.0	Shaly siltstone. Wavy laminations and rare burrows.
4910.0	2.0	Limestone. Oolitic grainstone with leached ooids.
4912.0	2.0	Shaly siltstone. Interlaminated.
4914.0	12.0	Limestone. Oolitic grainstone with leached ooids, rare anhydrite, oil stained, frequent massive beds. Moldic porosity.
4926.0	2.0	Shaly siltstone. Laminated.
4928.0	1.0	Limestone. Oolitic grainstone with leached ooids. Moldic porosity.
4929.0	2.0	Shaly siltstone. Laminated.

Core Description
Bennett Petroleum
Lott #19-3
Happy Spraberry Field
Garza County, Texas
Core Interval 4865.0'-4977.0'

Depth (ft.)	Thickness (ft.)	Description
4931.0	10.0	Shaly siltstone. Planar to ripple laminations. Microfaults and occasional burrows.
4941.0	10.0	Shaly siltstone. Interlaminated with occasional bed dip, rare burrows.
4951.0	4.0	Shaly siltstone. Interlaminated, contorted bedding with frequent microfaults.
4955.0	5.0	Siltstone. Dark tan. Abundant microfossils including mollusks and crinoids. Small clay intraclasts.
4960.0	11.0	Shaly siltstone. Ripple lamination, small clay intraclasts.
4971.0	3.0	Siltstone. Dark tan. Abundant crinoids, bryozoans and mollusks.
4974.0	3.0	Shaly siltstone. Interlaminated, contorted bedding and microfaults.
4977.0	------	END OF CORE.

Core Description
Torch Energy
Lott #19-10
Happy Spraberry Field
Garza County, Texas
Core Interval 4928.0'-5045.0'

Depth (ft.)	Thickness (ft.)	Description
4928.0	1.0	Shaly siltstone. Dark tan to dark gray, interlaminated, occasional clay intraclasts, microfaults.
4929.0	13.0	Limestone. Oolitic grainstone with leached ooids, ripple to planar laminations.
4942.0	2.0	Shaly siltstone. Ripple laminations.
4944.0	1.0	Limestone. Oolitic grainstone with leached ooids.
4945.0	5.0	No core recovery.
4950.0	8.0	Limestone. Oolitic grainstone with leached ooids, planar to ripple laminations.
4958.0	2.0	Shaly siltstone. Contorted bedding.
4960.0	2.0	Limestone. Oolitic grainstone.
4962.0	2.0	Shaly siltstone. Laminated, with microfaults.
4964.0	2.0	Siltstone. Medium grained with mollusks and crinoids.
4966.0	4.0	Shaly siltstone. Interlaminated, ripple to contorted bedding.

Core Description
Torch Energy
Lott #19-10
Happy Spraberry Field
Garza County, Texas
Core Interval 4928.0'-5045.0'

Depth (ft.)	Thickness (ft.)	Description
4970.0	3.0	Limestone. Grainstone with leached ooids. Brecciated with large clasts (greater than 30 cm).
4973.0	13.0	No core recovery.
4986.0	4.0	Shaly siltstone. Occasional ripple laminations with small microfaults.
4990.0	4.0	Siltstone. Brecciated with large carbonate clasts. Matrix has thin, contorted shale laminations.
4994.0	32.0	Shaly siltstone. Interlaminated, contorted bedding with microfaults, calcite cement.
5026.0	19.0	Shaly siltstone. Interlaminated, with occasional ripples. Calcite cement.
5045.0	------	END OF CORE.

APPENDIX B

Lott 19 #2
Happy Spraberry Field
Garza County, Texas
X Location 33.0075664970000
Y Location 101.3569553789990

Z	GR	R_t	D. ϕ	N. ϕ	ϕ	K_{90}	Flow Unit	Electrofacies
4917	22.1	197.6	29.8	30	31.9	19.0	Good	Grainstone
4918	21.5	203.0	29.8	30	30.5	4.6	Int.	Grainstone
4919	21.1	201.8	29.8	30	32.4	34.0	Good	Grainstone
4923	45.3	93.8	6.8	9.3	5.8	0.1	Poor	Grainstone
4924	42.2	87.1	9.4	14.8	7.1	0.1	Poor	Grainstone
4925	24.0	100.0	19.6	22.2	22.4	16.0	Poor	Grainstone
4926	23.7	101.2	23.5	24.8	24.1	39.0	Good	Grainstone
4927	26.7	96.5	23.7	22.7	18.7	15.0	Poor	Grainstone
4928	26.8	97.6	21.7	20.8	18	6.1	Poor	Grainstone
4929	22.4	113.2	25.6	25	32.7	44.0	Good	Grainstone
4930	21.1	128.9	27.8	28.3	28.5	47.0	Good	Grainstone
4931	22.0	121.3	25.8	26.9	19.4	16.0	Poor	Grainstone
4932	22.8	115.2	25.7	25.6	23.2	28.0	Good	Grainstone
4934	22.1	142.1	29.8	29.7	25.1	124.0	Good	Grainstone
4935	22.1	152.4	29.8	30.1	27.1	26.0	Good	Grainstone
4936	22.1	154.5	29.7	30	30.2	23.0	Good	Grainstone
4937	22.1	155.6	29.1	29.7	34.4	16.0	Int.	Grainstone
4938	22.9	143.6	27.2	29.2	27.9	8.8	Int.	Grainstone
4939	25.5	100.4	22.5	24	11.9	2.9	Poor	Grainstone
4940	29.7	77.2	17.9	19.4	22.2	6.2	Poor	Grainstone
4941	29.9	70.1	18.6	19.6	9.4	7.4	Poor	Grainstone
4942	28.5	70.2	21.6	22.8	19.9	15.0	Poor	Grainstone
4943	23.8	85.6	25.9	25.8	21.5	11.0	Poor	Grainstone
4944	20.8	103.6	28.9	29.3	32.4	34.0	Good	Grainstone
4945	22.1	94.6	29.8	29.7	24.3	49.0	Good	Grainstone
4946	21.0	79.2	29.9	29.9	32.4	23.0	Good	Grainstone
4947	22.1	78.0	29.9	29.9	31.8	72.0	Good	Grainstone
4952	23.7	65.6	20	18.9	11.8	0.3	Poor	Grainstone
4955	21.6	84.0	12	20.1	15.4	3.4	Poor	Grainstone
4956	24.6	53.0	11.2	16.4	17	1.8	Poor	SS
4957	30.9	41.2	9.8	14.7	16.2	3.1	Poor	SS

4958	40.9	23.0	10.3	17.8	8.8	0.2	Poor	SS
4959	47.8	18.8	11.7	18.1	13.8	0.3	Poor	SS
4960	52.6	17.4	11.9	17.4	12.7	0.0	Poor	SS
4961	53.3	17.2	12.5	17.7	12.6	0.0	Poor	SS
4962	55.2	18.5	13	19.3	12.6	0.1	Poor	SS
4963	56.5	18.8	12.9	20.4	11.8	0.0	Poor	SS
4964	58.4	18.8	12.8	18.5	11.3	0.0	Poor	SS
4965	64.7	18.5	13.7	16.6	12.7	0.4	Poor	SS
4966	72.5	16.7	14.5	17.8	11.6	0.1	Poor	SS
4967	78.3	16.1	14.8	19.1	14	0.0	Poor	SS
4968	78.6	16.2	14.3	19.2	14.9	0.2	Poor	SS
4969	72.9	17.2	12.7	20.5	13.6	0.1	Poor	SS
4970	67.1	18.8	11.4	21.1	12.5	0.0	Poor	SS
4971	58.6	20.9	10	21	11.9	0.8	Poor	SS
4972	53.8	20.1	10.2	21.2	9.9	0.0	Poor	SS
4973	49.4	19.5	10.2	19.7	12.9	0.4	Poor	SS
4974	49.4	20.5	9.9	19.7	13.3	0.9	Poor	SS
4975	43.4	22.5	8.8	20.8	12.2	0.4	Poor	SS
4976	36.6	27.5	8.1	19.7	11.7	0.6	Poor	SS
4977	35.3	29.2	8.5	19.3	10.6	0.2	Poor	SS
4978	43.7	25.7	9.4	18.5	13.1	1.5	Poor	SS
4979	52.0	21.0	9.7	17.6	12.7	0.8	Poor	SS
4980	55.4	22.6	9.5	17.3	12	0.4	Poor	SS
4981	61.1	23.8	9.5	17.1	10.9	0.2	Poor	SS

Lott #19-3
Happy Spraberry Field
Garza County, Texas
X Location 33.0033564599999000
Y Location 101.3570927529990000

Z	GR	R_t	D. ϕ	N. ϕ	ϕ	K_{90}	Flow Unit	Electrofacies
4888	41.3	10.4	10.1	10.7	9.3	0.0	Poor	SS
4889	31.0	11.5	7.6	8.5	7.4	0.0	Poor	SS
4890	24.2	12.0	8.6	8.7	9.0	0.0	Poor	SS
4891	23.8	12.3	10.7	11.0	10.8	0.5	Poor	SS
4892	26.3	11.0	11.7	11.5	6.3	0.2	Poor	SS
4893	33.5	10.4	13.1	11.7	6.4	0.1	Poor	SS
4894	34.9	9.9	13.6	12.5	7.9	0.7	Poor	SS
4895	34.5	9.9	13.8	12.7	5.7	0.2	Poor	SS
4896	26.4	10.5	12.9	12.8	12.3	1.0	Poor	SS
4897	17.8	11.0	12.7	11.7	9.2	0.7	Poor	SS
4898	20.9	11.7	12.9	12.2	9.1	0.6	Poor	SS
4899	27.4	11.7	13.3	12.3	12.2	0.6	Poor	SS
4900	31.0	11.7	14.1	12.5	5.9	5.0	Poor	SS
4901	31.5	11.7	14.9	13.3	11.9	0.9	Poor	SS
4902	26.3	11.7	16.0	13.6	8.6	0.8	Poor	SS
4903	23.7	12.5	14.7	12.0	14.2	2.0	Poor	SS
4904	20.4	13.5	12.6	11.8	10.5	2.3	Poor	SS
4905	22.5	15.1	11.6	12.5	7.2	0.2	Poor	SS
4906	34.5	17.5	12.6	15.3	4.8	0.0	Poor	SS
4907	31.7	26.1	19.1	19.1	9.9	14.0	Poor	SS
4908	23.7	38.5	22.8	22.0	26.3	47.0	Good	Grainstone
4909	20.9	43.2	24.1	23.1	21.7	20.0	Int.	Grainstone
4910	22.0	37.3	18.6	20.7	25.8	14.0	Int.	Grainstone
4911	24.9	29.0	15.1	13.0	23.4	16.0	Int.	Grainstone
4912	27.8	22.6	9.8	11.7	6.9	0.1	Poor	Grainstone
4913	30.1	25.1	13.0	14.6	6.5	0.0	Poor	Grainstone
4914	23.1	29.6	19.4	19.9	14.2	3.9	Poor	Grainstone
4915	19.6	38.2	24.5	22.0	23.9	12.0	Int.	Grainstone
4916	24.2	37.9	23.5	22.3	23.4	17.0	Good	Grainstone
4917	26.2	34.7	19.8	21.6	13.1	6.0	Poor	Grainstone
4918	20.9	32.6	19.7	21.4	15.1	1.9	Poor	Grainstone

4919	21.1	31.6	18.0	20.7	18.4	15.0	Poor	Grainstone
4920	22.7	33.0	17.1	19.5	20.2	12.0	Poor	Grainstone
4921	24.0	37.1	19.2	20.6	16.5	12.0	Poor	Grainstone
4922	24.6	40.9	23.8	24.3	16.7	8.8	Poor	Grainstone
4923	21.4	41.9	25.4	24.6	24.2	19.0	Good	Grainstone
4924	19.4	28.3	20.5	21.9	26.2	22.0	Good	Grainstone
4925	20.0	22.1	14.6	16.0	21.4	23.0	Good	Grainstone
4926	25.8	17.1	10.8	12.8	13.7	5.5	Poor	SS
4927	37.6	14.1	11.6	13.7	6.5	0.4	Poor	SS
4928	34.9	11.9	13.1	15.7	6.6	0.1	Poor	SS
4929	34.8	9.9	12.6	16.3	14.1	5.0	Poor	SS
4930	52.8	9.2	12.7	15.8	9.2	1.8	Poor	SS
4931	46.8	9.0	12.7	14.6	13.2	2.5	Poor	SS
4932	34.6	9.0	9.6	12.9	8.8	0.3	Poor	SS
4933	31.5	8.3	9.4	12.9	6.2	0.1	Poor	SS
4934	28.8	7.6	10.1	14.4	9.9	0.2	Poor	SS
4935	37.9	6.0	12.4	17.3	11.0	0.3	Poor	SS
4936	41.2	5.5	13.5	17.1	13.4	1.0	Poor	SS
4937	37.1	6.0	14.3	16.1	13.5	1.7	Poor	SS
4938	38.1	8.5	15.3	15.6	9.4	0.1	Poor	SS
4939	30.1	9.3	13.4	14.0	20.0	1.3	Poor	SS
4940	31.8	9.2	10.1	12.8	11.8	0.7	Poor	SS
4941	47.1	8.3	10.3	14.1	4.9	0.0	Poor	SS
4950	74.8	6.1	11.5	20.0	6.5	7.1	Poor	SS
4952	61.7	5.4	10.9	19.6	11.5	0.0	Poor	SS
4954	44.1	5.7	9.2	17.8	11.7	0.2	Poor	SS
4956	28.2	7.1	10.7	16.5	13.5	2.1	Poor	SS
4958	20.6	10.4	8.0	16.0	11.1	0.9	Poor	SS
4960	29.8	8.5	7.8	16.9	11.5	1.8	Poor	SS
4962	32.9	5.9	13.0	18.4	12.9	1.9	Poor	SS
4969	61.6	4.3	10.1	17.1	9.6	0.0	Poor	SS
4971	62.1	7.5	9.9	16.9	11.9	0.6	Poor	SS
4973	25.7	8.3	9.8	14.4	9.5	0.3	Poor	SS
4975	31.7	5.4	12.1	14.9	13.1	2.1	Poor	SS

Lott 19 #4
Happy Spraberry Field
Garza County, Texas
X Location 33.0034125350000000
Y Location 101.3614070400000000

Z	GR	R_t	D. ϕ	N. ϕ	ϕ	K_{90}	Flow Unit	Electrofacies
4910	18.7	168.2	17.4	17.2	17.1	0.3	Poor	Grainstone
4911	19.4	166.2	15.5	15.8	16.4	4.5	Poor	Grainstone
4912	19.0	158.2	23.7	18.1	26.7	38.0	Good	Grainstone
4913	19.9	123.7	27.0	21.2	25.7	12.0	Int.	Grainstone
4914	21.2	83.3	22.9	17.4	12.7	6.7	Poor	Grainstone
4915	23.6	52.1	18.3	13.0	14.9	4.1	Poor	Grainstone
4916	24.7	52.9	12.6	13.0	10.6	1.1	Poor	Grainstone
4917	24.7	66.2	16.2	16.6	24.2	37.0	Poor	Grainstone
4918	21.7	150.7	24.1	22.8	28.4	9.3	Int.	Grainstone
4919	16.7	156.3	26.9	23.7	22.1	3.8	Poor	Grainstone
4920	16.2	160.9	26.7	23.8	22.0	2.3	Poor	Grainstone
4924	15.6	153.6	8.2	24.5	25.5	3.4	Int.	Grainstone
4925	16.4	144.1	22.6	24.8	27.7	3.2	Int.	Grainstone
4926	17.7	137.2	26.1	25.2	28.5	2.9	Int.	Grainstone
4927	16.5	135.2	26.3	24.5	29.8	4.1	Int.	Grainstone
4928	16.0	133.3	21.9	22.9	21.4	21.0	Int.	Grainstone
4929	14.2	131.2	16.3	22.4	21.8	11.0	Poor	Grainstone
4938	21.5	100.3	22.1	26.4	22.1	4.2	Poor	Grainstone
4939	21.9	94.4	25.7	27.2	27.9	12.0	Int.	Grainstone
4940	22.0	88.2	24.5	25.0	16.6	0.2	Poor	Grainstone
4943	19.4	63.2	10.3	22.5	17.2	4.8	Poor	Grainstone
4944	20.8	50.9	6.8	21.2	14.7	7.3	Poor	Grainstone
4949	18.0	39.2	8.3	22.5	9.5	0.1	Poor	Grainstone
4959	22.1	21.7	7.4	21.0	13.3	3.2	Poor	Grainstone
4961	25.1	8.7	13.7	15.6	16.6	4.8	Poor	Rudstone
4962	29.9	7.3	13.0	13.9	11.0	18.0	Poor	Rudstone

Lott 19 #5
Happy Spraberry Field
Garza County, Texas
X Location 32.9997824390000000
Y Location 101.3614689309990000

Z	GR	R_t	D. ϕ	N. ϕ	ϕ	K_{90}	Flow Unit	Electrofacies
4926	32.8	50.7	10.8	12.2	10.9	1.0	Poor	Grainstone
4927	31.4	61.4	11.7	12.0	7.5	1.0	Poor	Grainstone
4928	28.7	73.9	10.2	11.4	7.9	0.1	Poor	Grainstone
4929	43.0	62.6	8.1	9.8	3.5	0.2	Poor	Grainstone
4930	65.9	64.5	7.8	10.3	6.4	0.1	Poor	Grainstone
4931	67.4	70.8	7.3	9.4	4.2	0.1	Poor	Grainstone
4932	54.3	77.1	5.9	7.8	3.9	0.3	Poor	Grainstone
4933	46.2	74.5	6.1	7.6	4.3	0.2	Poor	Grainstone
4934	47.7	69.2	6.8	8.6	4.4	0.0	Poor	Grainstone
4935	53.1	75.7	7.7	10.1	5.3	0.1	Poor	Grainstone
4936	36.4	157.2	12.3	12.7	9.6	0.1	Poor	Grainstone
4937	25.9	201.7	20.9	20.9	22.7	61.8	Int.	Grainstone
4938	20.0	261.0	27.6	28.8	32.4	34.9	Good	Grainstone
4939	20.4	292.9	28.0	29.1	5.9	0.8	Poor	Grainstone
4940	20.0	296.9	24.4	29.0	23.1	18.3	Good	Grainstone
4941	17.2	292.9	25.2	28.9	23.2	31.3	Good	Grainstone
4942	16.2	270.3	29.4	29.0	26.4	23.9	Good	Grainstone
4943	18.9	211.2	29.5	28.3	25.9	42.6	Good	Grainstone
4944	21.1	116.6	25.9	24.2	21.7	18.7	Int.	Grainstone
4945	35.5	91.6	10.1	16.1	5.6	1.3	Poor	Grainstone
4946	36.6	78.5	8.2	12.2	5.4	0.2	Poor	Grainstone
4947	25.5	79.1	10.8	13.4	11.6	1.9	Poor	Grainstone
4948	22.4	90.0	18.2	18.1	18.3	37.2	Int.	Grainstone
4949	21.1	142.8	25.4	24.4	25.1	40.8	Good	Grainstone
4950	18.7	186.1	29.9	30.1	25.1	17.5	Good	Grainstone
4951	20.3	185.7	30.0	30.0	30.9	23.1	Good	Grainstone
4952	24.1	174.4	28.9	30.0	18.7	25.3	Int.	Grainstone
4953	26.2	165.6	27.4	29.9	22.9	43.6	Int.	Grainstone
4954	21.6	164.1	26.4	29.8	22.9	30.1	Int.	Grainstone
4955	20.2	155.1	25.3	29.7	21.8	82.8	Int.	Grainstone
4956	21.8	148.9	25.1	28.7	14.5	29.1	Poor	Grainstone
4957	23.6	149.9	25.8	28.8	25.8	50.2	Good	Grainstone

4958	22.6	165.5	26.8	29.8	31.3	39.1	Good	Grainstone
4964	37.4	51.7	11.8	13.4	19.2	0.1	Poor	Grainstone
4965	40.5	51.9	8.2	13.5	10.2	0.1	Poor	Grainstone
4966	36.3	75.9	11.7	15.8	17.5	15.3	Poor	Grainstone
4967	24.2	104.0	19.9	21.3	17.1	20.3	Int.	Grainstone
4968	21.3	109.5	20.4	22.6	23.3	12.3	Int.	Grainstone
4969	20.9	117.3	20.5	23.3	18.8	1.0	Poor	Grainstone
4970	21.9	108.5	19.5	22.5	13.9	0.1	Poor	Grainstone
4971	28.9	80.1	16.6	20.0	15.7	20.7	Poor	Grainstone
4972	30.7	35.0	13.5	16.5	11.1	0.3	Poor	Grainstone

Lott 19 #6
Happy Spraberry Field
Garza County, Texas
X Location 32.9997371370000000
Y Location 101.3574875190000000

Z	GR	R_t	D. ϕ	N. ϕ	ϕ	K_{90}	Flow Unit	Electrofacies
4940	29.1	12.1	8.6	10.2	6.7	0.3	Poor	Grainstone
4941	31.2	10.7	9.0	10.1	7.9	0.2	Poor	Grainstone
4942	33.5	9.7	9.7	10.6	4.9	0.4	Poor	Grainstone
4943	33.2	8.3	11.1	13.1	8.3	0.4	Poor	Grainstone
4944	29.0	6.6	12.9	14.6	10.5	1.9	Poor	Grainstone
4945	25.5	5.7	14.1	17.1	12.3	0.2	Poor	Grainstone
4946	20.9	4.8	16.8	20.8	16.3	1.4	Poor	Grainstone
4947	20.3	4.0	19.0	22.6	17.2	8.4	Poor	Grainstone
4948	20.8	3.4	21.0	23.6	21.2	11.6	Poor	Grainstone
4949	18.1	3.3	22.1	23.8	15.8	2.5	Poor	Grainstone
4950	15.4	3.3	21.8	25.5	18.9	14.4	Poor	Grainstone
4951	15.4	3.4	22.3	25.1	23.5	7.6	Int.	Grainstone
4952	16.0	3.6	23.2	24.6	22.4	8.8	Poor	Grainstone
4953	16.3	3.7	23.9	24.5	23.1	7.5	Int.	Grainstone
4954	15.6	3.7	24.5	25.9	10.0	0.1	Poor	Grainstone
4956	18.4	3.7	23.0	25.6	23.7	9.4	Int.	Grainstone
4957	17.6	3.7	21.8	25.4	23.5	4.0	Int.	Grainstone
4958	17.6	3.7	22.6	27.4	19.3	3.2	Poor	Grainstone
4959	15.8	4.0	26.0	28.1	23.5	2.9	Int.	Grainstone
4960	14.0	4.2	28.0	29.6	24.9	4.8	Int.	Grainstone
4961	14.1	4.5	27.7	28.8	22.7	3.8	Poor	Grainstone
4962	15.4	4.6	27.5	29.1	21.4	2.1	Poor	Grainstone
4963	15.4	4.6	27.3	27.7	21.3	5.8	Poor	Grainstone
4964	16.7	5.0	25.6	25.7	15.3	1.5	Poor	Grainstone
4965	18.1	5.4	23.7	25.2	19.6	3.4	Poor	Grainstone
4966	18.1	5.6	21.9	25.1	20.0	4.1	Poor	Grainstone
4967	18.1	4.8	21.2	24.0	17.3	4.5	Poor	Grainstone
4968	19.1	4.9	20.9	22.3	14.5	1.4	Poor	Grainstone
4969	19.7	8.9	20.1	21.7	7.3	0.2	Poor	Grainstone
4970	23.4	11.1	18.5	20.5	5.9	0.2	Poor	Grainstone
4971	27.3	11.7	14.3	17.7	5.6	0.2	Poor	Grainstone

Lott 19 #8
Happy Spraberry Field
Garza County, Texas
X Location 33.005244000000000000
Y Location 101.363365999999000000

Z	GR	R_t	D. ϕ	N. ϕ	ϕ	K_{90}	Flow Unit	Electrofacies
4917	15.8	30.5	22.5	18.2	24.6	25.6	Good	Grainstone
4918	20.3	25.2	16.9	14.4	21.2	21.8	Int.	Grainstone
4919	25.5	22.1	16.0	13.9	12.2	6.1	Poor	Grainstone
4920	24.8	20.5	16.9	14.8	11.8	6.9	Poor	Grainstone
4921	21.1	22.1	18.0	16.2	13.5	2.1	Poor	Grainstone
4922	18.8	25.1	18.9	16.5	10.9	1.0	Poor	Grainstone
4923	18.2	28.7	19.1	16.9	14.9	8.3	Poor	Grainstone
4924	20.1	32.3	20.0	16.9	16.8	13.0	Poor	Grainstone
4925	21.3	39.9	20.7	17.4	14.6	6.1	Poor	Grainstone
4926	20.9	52.8	22.8	19.8	14.8	5.2	Poor	Grainstone
4927	18.6	69.8	27.2	23.1	13.6	6.8	Poor	Grainstone
4928	16.4	77.8	28.1	24.8	11.9	0.2	Poor	Grainstone
4977	23.4	17.5	16.3	18.6	15.5	32.8	Poor	Grainstone
4978	27.9	14.8	17.5	18.3	16.4	14.9	Poor	SS
4979	36.7	10.1	14.9	15.0	14.0	5.4	Poor	SS
4980	55.1	9.3	10.7	12.8	10.0	0.2	Poor	SS
4981	50.0	8.1	10.1	13.3	10.2	0.3	Poor	SS
4982	38.1	7.5	9.2	14.3	10.8	3.0	Poor	Rudstone
4983	36.1	7.1	10.4	15.2	13.1	1.7	Poor	Rudstone
4984	32.6	7.1	13.3	16.4	12.9	1.5	Poor	Rudstone
4985	27.7	6.9	15.5	18.4	19.0	6.8	Poor	Rudstone
4986	26.1	6.6	20.0	19.8	20.4	16.5	Int.	Rudstone
4987	24.3	6.5	20.7	20.8	22.4	21.5	Int.	Rudstone
4988	23.8	6.5	21.4	21.8	20.4	20.7	Int.	Rudstone
4989	23.4	6.6	22.6	22.8	24.6	21.0	Good	Rudstone
4990	31.2	6.8	24.1	23.9	26.1	37.8	Good	Rudstone
4991	30.1	6.9	25.6	24.8	26.1	17.2	Good	Rudstone
4992	28.2	6.7	24.8	24.5	26.6	51.3	Good	Rudstone
4993	30.7	6.4	22.9	23.1	21.3	31.0	Int.	Rudstone
4995	50.6	5.8	14.0	16.4	10.9	0.5	Poor	Floatstone
4996	58.5	5.1	10.8	16.6	9.8	4.1	Poor	Floatstone
4997	55.3	4.5	10.6	16.1	9.4	0.1	Poor	Floatstone

4998	55.3	4.1	10.8	15.2	11.5	0.4	Poor	Floatstone

Lott 19 #9 Sidetrack
Happy Spraberry Field
Garza County, Texas
X Location 33.008594156999900000
Y Location 101.362817282000000000

Z	GR	R_t	D. ϕ	N. ϕ	ϕ	K_{90}	Flow Unit	Electrofacies
4998	70.0	8.0	x	20.6	8.1	1.4	Poor	SS
5004	80.0	3.5	x	19.9	12.5	0.3	Poor	SS
5005	65.0	4.2	x	19.1	5.9	0.2	Poor	Grainstone
5006	40.0	5.6	x	19.1	15.8	5.4	Poor	Grainstone
5007	31.0	8.5	x	19.8	3.2	0.2	Poor	Grainstone
5008	50.0	8.6	x	20.1	9.8	0.3	Poor	Grainstone
5009	75.0	8.3	x	19.4	7.3	0.2	Poor	SS
5010	87.0	8.6	x	18.8	9.0	0.1	Poor	SS
5011	80.0	10.1	x	18.8	4.1	0.1	Poor	SS
5012	60.0	11.0	x	19.4	9.2	0.6	Poor	SS
5013	52.0	8.1	x	19.9	14.2	11.0	Poor	SS
5014	65.0	7.7	x	20.7	11.7	6.7	Poor	SS
5015	58.0	7.7	x	22.4	11.8	10.1	Poor	SS
5016	40.0	9.3	x	23.3	15.4	11.5	Poor	Grainstone
5017	30.0	11.9	x	23.5	11.2	4.8	Poor	Grainstone
5018	30.0	14.2	x	22.6	11.3	2.7	Poor	Grainstone
5019	30.0	14.3	x	23.2	15.2	0.8	Poor	Grainstone
5020	30.0	13.8	x	24.9	12.8	8.6	Poor	Grainstone
5021	30.0	13.3	x	25.0	11.0	4.6	Poor	Grainstone
5022	34.0	10.6	x	22.0	16.6	34.1	Int.	Grainstone
5023	38.0	8.8	x	16.0	9.7	6.9	Poor	Grainstone
5024	36.0	7.8	x	12.3	11.8	18.5	Poor	Grainstone
5025	35.0	7.1	x	11.1	15.1	30.4	Poor	Grainstone
5026	44.0	6.4	x	11.7	12.4	6.7	Poor	Grainstone
5027	45.0	5.9	x	12.3	10.7	7.2	Poor	Grainstone
5028	50.0	5.8	x	13.3	12.7	2.0	Poor	Grainstone
5029	70.0	5.4	x	13.0	8.7	0.0	Poor	Grainstone

Lott 19 #10
Happy Spraberry Field
Garza County, Texas
X Location 32.9978898240000000
Y Location 101.3651483879990000

Z	GR	R_t	D. ϕ	N. ϕ	ϕ	K_{90}	Flow Unit	Electrofacies
4928	14.9	46.4	16.9	17.7	17.3	20.4	Int.	Grainstone
4929	18.5	43.0	19.2	20.8	15.0	3.2	Poor	Grainstone
4930	20.3	39.1	19.6	20.3	15.5	16.2	Poor	Grainstone
4931	23.0	36.6	16.0	17.9	17.8	12.8	Poor	Grainstone
4932	30.3	39.2	13.5	17.2	15.6	10.2	Poor	Grainstone
4933	30.3	44.2	15.4	18.8	10.8	0.5	Poor	Grainstone
4934	21.6	52.7	18.9	21.5	20.0	10.2	Poor	Grainstone
4935	17.2	61.2	20.1	22.0	38.3	67.6	Good	Grainstone
4936	16.1	76.0	19.0	21.0	10.4	3.8	Poor	Grainstone
4937	15.8	94.3	16.9	20.7	15.2	13.7	Poor	Grainstone
4938	15.4	102.4	22.2	22.2	18.7	2.2	Poor	Grainstone
4939	16.4	103.6	27.5	25.8	28.5	43.5	Good	Grainstone
4940	17.6	106.5	29.0	26.0	20.0	18.8	Int.	Grainstone
4941	19.5	112.3	26.7	23.3	5.9	0.5	Poor	Grainstone
4942	17.4	113.8	25.3	23.2	7.9	0.1	Poor	Grainstone
4943	14.9	110.8	27.7	25.9	11.5	0.9	Poor	Grainstone
4944	14.2	83.5	29.9	28.6	18.4	1.7	Poor	Grainstone
4950	26.3	28.8	14.6	17.1	21.6	4.2	Poor	Grainstone
4951	24.8	37.3	21.3	20.8	22.6	15.8	Poor	Grainstone
4952	18.9	48.7	24.7	24.5	31.6	70.6	Good	Grainstone
4953	16.0	59.4	29.4	26.9	25.9	35.0	Good	Grainstone
4954	14.9	64.1	30.8	27.8	25.7	1.4	Int.	Grainstone
4955	14.0	66.3	31.6	28.8	24.5	27.3	Good	Grainstone
4956	14.9	64.3	31.6	29.5	29.1	2.7	Int.	Grainstone
4957	14.9	58.9	31.7	30.1	27.9	3.1	Int.	Grainstone
4958	13.5	54.4	29.2	30.1	11.3	0.5	Poor	Grainstone
4960	16.9	48.1	22.1	30.1	17.5	6.5	Poor	Grainstone
4961	16.5	44.5	26.6	30.0	11.8	3.7	Poor	Grainstone
4963	18.9	30.4	28.4	30.0	9.6	0.7	Poor	Rudstone
4964	21.3	20.5	25.1	27.3	8.5	0.6	Poor	Rudstone
4965	21.3	12.2	11.8	24.3	5.3	0.3	Poor	Rudstone
4966	33.5	9.2	8.5	20.2	10.0	0.5	Poor	Rudstone

4967	43.0	7.5	9.6	17.5	12.4	0.7	Poor	Rudstone
4968	42.4	5.8	11.1	17.0	11.9	0.5	Poor	Rudstone
4969	35.9	5.1	14.5	16.3	15.2	1.5	Poor	Rudstone
4970	30.1	4.4	14.1	15.3	7.6	0.2	Poor	Rudstone
4971	33.0	3.8	10.2	13.7	5.1	0.2	Poor	Rudstone
4972	39.8	3.3	8.8	15.3	8.0	0.2	Poor	Rudstone

Lott 19 #11
Happy Spraberry Field
Garza County, Texas
X Location 33.0052000229999000
Y Location 101.3592194259990000

Z	GR	R_t	D. ϕ	N. ϕ	ϕ	K_{90}	Flow Unit	Electrofacies
4873	22.1	191.4	20.2	21.1	19.0	3.7	Poor	Grainstone
4874	22.1	165.4	19.8	20.1	26.0	12.7	Int.	Grainstone
4875	21.4	140.5	19.8	20.4	25.5	6.6	Int.	Grainstone
4876	19.1	126.8	19.8	20.9	20.2	2.6	Poor	Grainstone
4877	18.4	137.3	19.1	18.7	23.4	15.3	Int.	Grainstone
4878	17.9	150.6	17.9	17.8	21.4	13.8	Poor	Grainstone
4879	19.3	164.8	21.7	21.9	17.6	9.7	Poor	Grainstone
4880	21.8	199.8	24.8	24.7	12.6	6.0	Poor	Grainstone
4881	20.9	240.4	28.2	26.8	21.7	32.1	Int.	Grainstone
4882	16.9	374.0	29.9	28.6	17.0	44.1	Int.	Grainstone
4883	16.7	421.1	29.8	29.5	27.4	50.6	Good	Grainstone
4886	18.9	487.2	27.8	27.7	28.6	16.1	Good	Grainstone
4887	18.9	558.0	30.4	30.0	25.7	14.6	Int.	Grainstone
4888	14.6	632.8	31.2	29.9	32.0	8.0	Int.	Grainstone
4889	14.9	624.5	31.0	29.9	27.7	4.3	Int.	Grainstone
4890	17.9	593.3	28.7	26.7	33.9	5.2	Int.	Grainstone
4891	17.3	485.8	28.1	27.5	33.3	5.0	Int.	Grainstone
4892	17.0	590.4	29.5	29.6	36.4	44.7	Good	Grainstone
4893	16.6	684.5	29.9	28.9	20.8	1.5	Poor	Grainstone
4894	15.4	692.6	29.0	26.2	30.6	11.2	Int.	Grainstone
4895	19.5	649.0	26.9	26.4	31.1	9.1	Int.	Grainstone
4896	21.0	539.7	28.8	29.3	21.2	35.2	Int.	Grainstone
4897	21.2	269.4	25.9	26.5	18.4	21.2	Int.	Grainstone
4898	18.4	179.8	24.1	24.9	30.0	17.0	Good	Grainstone
4899	18.4	135.3	27.2	26.5	29.6	18.1	Good	Grainstone
4900	22.1	122.8	29.5	29.3	15.9	6.0	Poor	Grainstone
4901	26.1	110.3	27.1	23.7	15.0	13.4	Poor	Grainstone
4902	27.8	101.7	19.0	19.1	33.2	31.0	Good	Grainstone
4903	24.3	100.4	21.6	22.1	33.4	25.1	Good	Grainstone
4904	21.6	109.2	26.5	25.8	19.6	7.7	Poor	Grainstone
4905	22.3	135.1	27.2	25.9	29.9	31.4	Good	Grainstone
4906	21.5	161.0	23.9	25.0	29.2	26.8	Good	Grainstone

4907	19.1	232.6	25.3	25.4	34.3	39.9	Good	Grainstone
4908	17.6	273.0	27.7	28.1	33.0	31.0	Good	Grainstone
4909	17.4	344.9	29.9	28.8	25.4	49.1	Good	Grainstone
4910	21.1	313.4	29.9	28.9	30.3	64.7	Good	Grainstone
4911	19.8	281.8	27.2	28.1	19.1	33.9	Int.	Grainstone
4912	19.5	250.3	27.3	28.5	16.6	23.0	Int.	Grainstone
4913	22.4	219.6	26.2	28.2	24.5	29.2	Good	Grainstone
4914	20.5	194.1	21.7	20.9	30.2	4.0	Int.	Grainstone
4915	17.0	168.6	22.3	22.3	19.0	6.0	Poor	Grainstone
4916	19.9	143.1	28.5	27.5	20.7	7.3	Poor	Grainstone
4917	22.3	118.1	29.0	28.9	18.3	6.6	Poor	Grainstone
4918	19.5	94.9	23.9	25.4	23.5	9.7	Int.	Grainstone
4919	19.1	75.0	18.0	21.6	18.8	5.5	Poor	Grainstone
4920	18.9	76.5	18.3	22.2	24.4	3.9	Int.	Grainstone
4921	19.5	78.1	18.5	23.7	30.4	14.4	Int.	Grainstone
4922	19.5	78.7	18.0	24.2	28.5	22.6	Good	Grainstone
4923	18.9	78.7	19.0	24.8	10.4	0.1	Poor	Grainstone
4924	18.9	71.3	20.0	25.5	5.6	0.2	Poor	Grainstone
4925	18.9	59.1	21.3	27.0	6.9	0.9	Poor	Grainstone
4926	20.4	45.7	20.7	27.9	6.1	0.1	Poor	Grainstone
4941	22.8	6.8	12.5	18.5	11.7	1.1	Poor	Rudstone
4942	24.1	6.8	15.5	18.8	16.6	5.0	Poor	Rudstone
4943	23.7	6.9	16.1	18.6	16.5	3.6	Poor	Rudstone
4944	18.4	7.3	13.2	16.7	15.3	5.2	Poor	Rudstone
4945	19.1	7.6	10.1	14.8	12.4	5.3	Poor	Rudstone
4946	19.8	8.2	10.6	16.5	11.5	3.9	Poor	Rudstone
4947	19.5	9.8	10.8	17.6	14.5	4.1	Poor	Rudstone
4948	24.7	10.6	11.2	18.7	16.6	8.4	Poor	Rudstone
4949	28.8	10.7	13.4	20.0	14.3	3.1	Poor	Rudstone
4950	26.6	10.7	17.5	22.0	17.9	6.2	Poor	Rudstone
4951	23.9	10.8	20.9	23.8	20.5	27.8	Int.	Rudstone
4952	21.4	11.2	22.4	23.0	22.9	26.2	Int.	Rudstone
4953	20.3	11.7	20.5	22.2	18.8	15.9	Poor	Rudstone
4954	20.3	12.1	18.4	22.6	18.5	19.6	Int.	Rudstone
4955	19.2	12.4	20.2	24.4	21.5	19.9	Int.	Rudstone
4956	17.4	14.1	16.2	24.3	20.3	33.3	Int.	Rudstone
4957	20.0	17.8	10.8	18.4	17.6	20.5	Int.	Rudstone
4974	25.3	6.9	4.9	13.7	13.6	1.1	Poor	Rudstone

4975	40.6	6.4	6.6	13.8	11.1	0.8	Poor	Rudstone
4976	58.9	6.0	8.6	15.7	14.7	0.4	Poor	SS
4977	59.6	5.6	9.0	18.5	12.3	1.3	Poor	SS
4978	70.7	5.4	9.4	18.3	7.7	0.3	Poor	SS

Lott Trust #1
Happy Spraberry Field
Garza County, Texas
X Location 32.9979909719999000
Y Location 101.3694612000000000

Z	GR	R_t	D. ϕ	N. ϕ	ϕ	K_{90}	Flow Unit	Electrofacies
4948	23.1	8.8	18.0	19.6	10.3	1.3	Poor	Rudstone
4949	26.4	8.8	20.6	19.5	9.4	4.2	Poor	Rudstone
4950	24.9	7.8	17.8	18.0	13.5	3.2	Poor	Rudstone
4951	22.8	7.5	14.6	17.0	17.6	13.2	Poor	Rudstone
4952	23.1	8.2	13.1	16.3	14.0	2.5	Poor	Rudstone
4953	24.5	8.2	14.1	16.2	13.4	4.7	Poor	Rudstone
4954	24.1	7.9	14.6	16.5	13.5	2.3	Poor	Rudstone
4955	22.8	7.8	14.9	17.1	9.9	0.8	Poor	Rudstone
4956	22.8	6.7	14.7	17.4	11.6	3.1	Poor	Rudstone
4957	23.8	7.3	14.1	17.2	11.6	4.0	Poor	Rudstone
4958	23.8	7.4	14.9	17.2	11.2	0.9	Poor	Rudstone
4959	27.1	6.5	16.8	17.1	13.3	3.9	Poor	Rudstone
4960	28.6	6.0	15.7	15.9	17.6	4.3	Poor	Rudstone
4961	32.3	5.6	15.7	15.6	14.8	7.0	Poor	Rudstone
4962	38.4	5.3	15.0	14.0	10.0	0.4	Poor	Rudstone
4963	38.9	5.3	11.5	12.1	12.6	0.7	Poor	Rudstone
4964	34.9	6.4	10.6	11.8	10.9	0.5	Poor	Rudstone
4965	32.5	6.9	11.3	12.5	12.5	0.7	Poor	Rudstone
4966	34.3	7.3	11.2	13.3	5.8	0.2	Poor	Rudstone
4967	34.7	7.8	12.4	14.0	9.2	0.4	Poor	Rudstone
4968	34.3	7.8	14.4	14.8	11.6	0.5	Poor	Rudstone
4969	36.6	7.2	15.4	15.6	13.2	0.6	Poor	Rudstone
4970	39.7	6.0	14.7	14.6	14.9	0.6	Poor	Rudstone
4971	39.2	5.5	13.2	13.6	12.2	0.2	Poor	Rudstone
4981	49.1	3.7	15.3	17.8	8.5	0.4	Poor	SS
4982	57.1	2.6	15.4	17.9	7.8	0.8	Poor	SS
4983	56.6	2.7	14.2	17.6	11.4	0.4	Poor	SS
4984	55.6	3.2	13.0	17.9	10.3	0.3	Poor	SS
4985	56.0	3.3	13.2	18.5	10.3	0.2	Poor	SS
4986	59.8	3.1	14.3	19.1	10.4	0.2	Poor	SS
4987	60.7	2.9	14.3	19.1	11.6	0.1	Poor	SS
4988	57.9	2.9	13.3	18.5	17.4	0.2	Poor	SS

4989	56.4	3.5	12.4	18.3	11.3	0.1	Poor	SS
4990	55.8	3.4	12.6	18.2	8.3	0.1	Poor	SS
4991	59.6	3.1	12.9	18.1	12.1	0.7	Poor	SS
4992	61.0	3.2	13.2	17.6	11.3	0.1	Poor	SS
4993	58.5	3.7	13.4	17.9	10.0	0.1	Poor	SS
4994	56.6	3.6	14.5	19.1	10.8	0.1	Poor	SS
4995	57.9	3.1	17.5	20.4	9.3	0.1	Poor	SS
4996	60.0	2.8	18.0	21.2	14.9	0.3	Poor	SS
5002	53.5	2.5	17.4	20.0	14.2	0.3	Poor	SS
5003	48.8	2.8	17.9	20.1	13.5	0.6	Poor	SS
5004	47.2	2.7	17.3	19.7	14.5	1.8	Poor	SS
5005	49.7	2.7	15.9	19.3	13.0	7.2	Poor	SS
5006	49.8	2.7	15.1	18.8	13.8	11.4	Poor	SS
5007	47.4	2.8	13.4	16.9	12.0	1.2	Poor	SS
5008	47.5	3.1	12.5	16.0	12.7	1.0	Poor	SS

APPENDIX C

Electrofacies Model 1

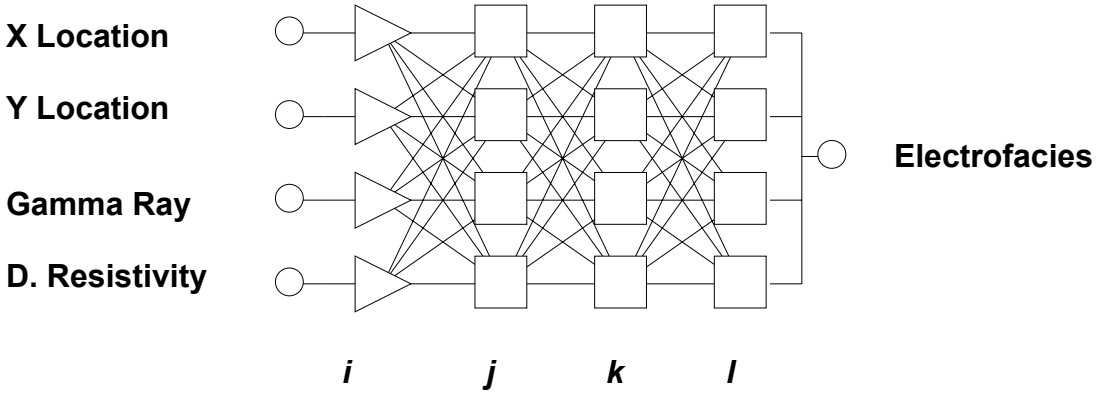

The above neural network consists of four layers: one input layer, *i*. with 4 neurons, two hidden layers, *j* and *k*, with 4 neurons each, and one output layer, *l*, with four neurons (MLP 4:4-4-4-4:1). The starting algorithm was back propagation (50 iterative cycles) followed by conjugate gradient descent (156 iterative cycles). A table of weights and threshold values is found below. A logistic activation function was used in all hidden layers and the output layer.

Hidden Layer 1 – Electrofacies Model 1 W_{ij}				
i/j	1	2	3	4
X	-7.776554	-1.413037	3.713176	-0.20100
Y	11.65996	-1.463521	1.257090	1.742806
Gr	-1.205627	7.155684	-2.590508	2.367146
Rt	8.103943	11.07065	6.483290	-19.56152
Threshold	-3.764091	0.3730844	2.922091	0.2626152

Activation Function = Logistic

Hidden Layer 2 – Electrofacies Model 1 W_{jk}				
j/k	1	2	3	4
HL1#1	8.259349	3.879791	5.204394	-11.96366
HL1#2	5.430399	6.418514	-9.723235	5.625044
HL1#3	1.495675	5.20845	2.359304	-6.163036
HL1#4	-11.91882	-12.90442	4.640538	7.807119
Threshold	2.7715	0.5566229	1.456605	-0.5976

Activation Function = Logistic

Output Layer – Electrofacies Model 1 W_{kl}				
k/l	1	2	3	4
HL2#1	9.047725	-11.7587	-6.909245	-0.7899
HL2#2	9.961746	-1.434467	-9.649143	-2.130274
HL2#3	-6.287905	-5.488908	8.682433	-1.69299
HL2#4	-8.421186	12.06136	-6.011934	-1.478924
Threshold	5.349547	0.3249486	-1.697829	2.342264

Activation Function = Logistic

Electrofacies Model 2

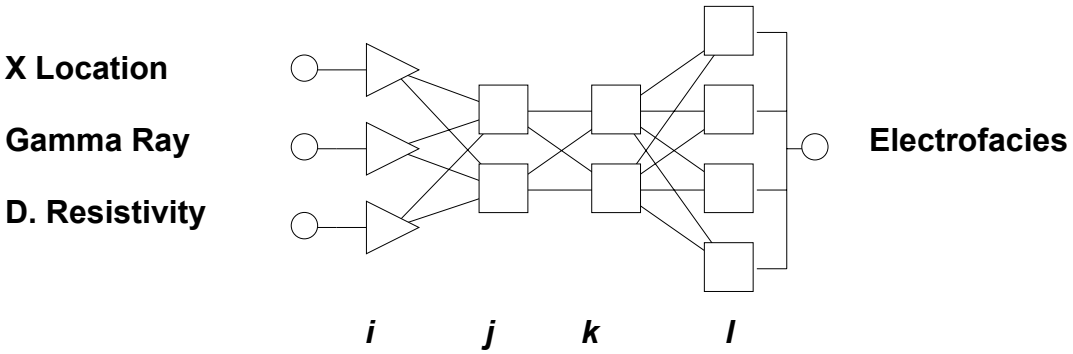

The above neural network consists of four layers: one input layer, *i*. with 3 neurons, two hidden layers, *j* and *k*, with 2 neurons each, and one output layer, *l*, with four neurons (MLP 3:3-2-2-4:1). The starting algorithm was back propagation (50 iterative cycles) followed by conjugate gradient descent (132 iterative cycles). A table of weights and threshold values is found below. A logistic activation function was used in all hidden layers and the output layer.

Hidden Layer 1 – Electrofacies Model 2		
W_{ij}		
i/j	1	2
X	2.446486	-17.32242
Gr	3.25401	-8.028369
Rt	-20.60128	-7.623234
Threshold	0.724107	-1.710314

Activation Function = Logistic

Hidden Layer 2 – Electrofacies Model 2		
W_{jk}		
j/k	1	2
HL1#1	-16.74222	8.488067
HL1#2	-10.54984	-6.062494
Threshold	-9.869502	4.949968

Activation Function = Logistic

Output Layer – Electrofacies Model 2				
W_{kl}				
k/l	1	2	3	4
HL2#1	16.78067	-3.471805	-15.81959	-1.286445
HL2#2	-0.7521	4.626301	-8.580968	0.3047274
Threshold	4.167455	2.911903	-6.735344	3.919468

Activation Function = Logistic

Reservoir Quality Classification Model 1

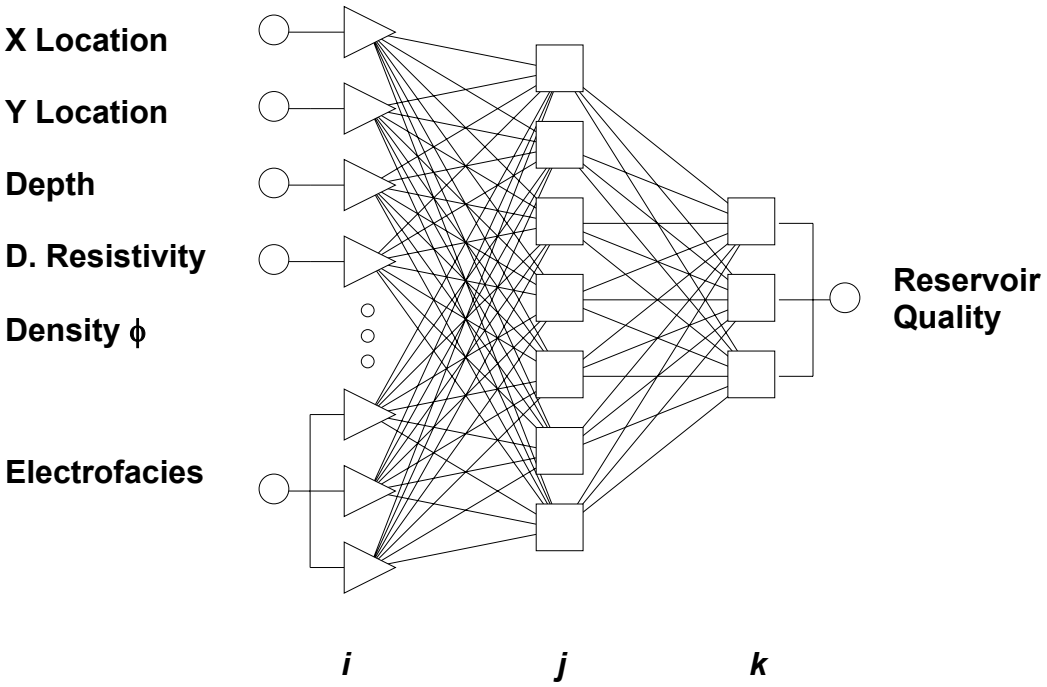

The above neural network consists of three layers: one input layer, *i*. with 6 inputs and 9 neurons, one hidden layer, *j*, with 7 neurons, and one output layer, *k*, with 3 neurons (MLP 6:9-7-3:1). The starting algorithm was back propagation (50 iterative cycles) followed by conjugate gradient descent (25 iterative cycles). A table of weights and threshold values is found below. A logistic activation function was used in the hidden layer and the output layer.

Hidden Layer 1 – RQC Model 1							
W_{ij}							
i/j	1	2	3	4	5	6	7
X	-4.9067	2.62031	-1.3751	8.91632	-1.0460	1.09005	1.32106
Y	0.87824	-0.7072	1.1040	0.46527	1.56900	0.07464	-3.6721
Z	0.52510	1.11263	-1.7140	-1.9688	1.11971	-0.1445	1.49932
Rt	0.40394	-5.2422	-6.4582	2.92945	-2.3525	0.51251	4.70518
Density	-0.2327	-0.7844	0.12570	1.44190	-7.5468	0.80654	-8.5677
Grain	-0.9885	-0.7663	1.0060	1.93134	-0.7665	0.31019	-1.1329
SS	0.21890	2.01507	1.57824	-0.2077	2.47966	0.36636	1.61816
Rud	1.29260	-4.3062	-1.9568	-2.4101	-0.6373	-0.8968	0.47200
Float	0.02571	0.3093	0.20489	-0.0073	0.07558	0.02736	0.19092
Threshold	0.18183	1.52071	-1.4981	0.44885	-2.4277	0.06194	-3.3042

Activation Function = Logistic

Hidden Layer 2 – RQC Model 1			
W_{jk}			
j/k	1	2	3
HL1#1	0.9372031	-2.057497	3.705125
HL1#2	1.557017	-5.446056	5.460113
HL1#3	-4.774033	0.893047	3.195236
HL1#4	3.087045	3.979578	-4.933621
HL1$5	-1.637171	-5.54965	2.672416
HL1#6	0.02385	-2.288395	0.9577939
HL1#7	-7.674235	0.452667	4.885047
Threshold	0.952503	2.120341	0.008799

Activation Function = Logistic

Reservoir Quality Classification Model 2

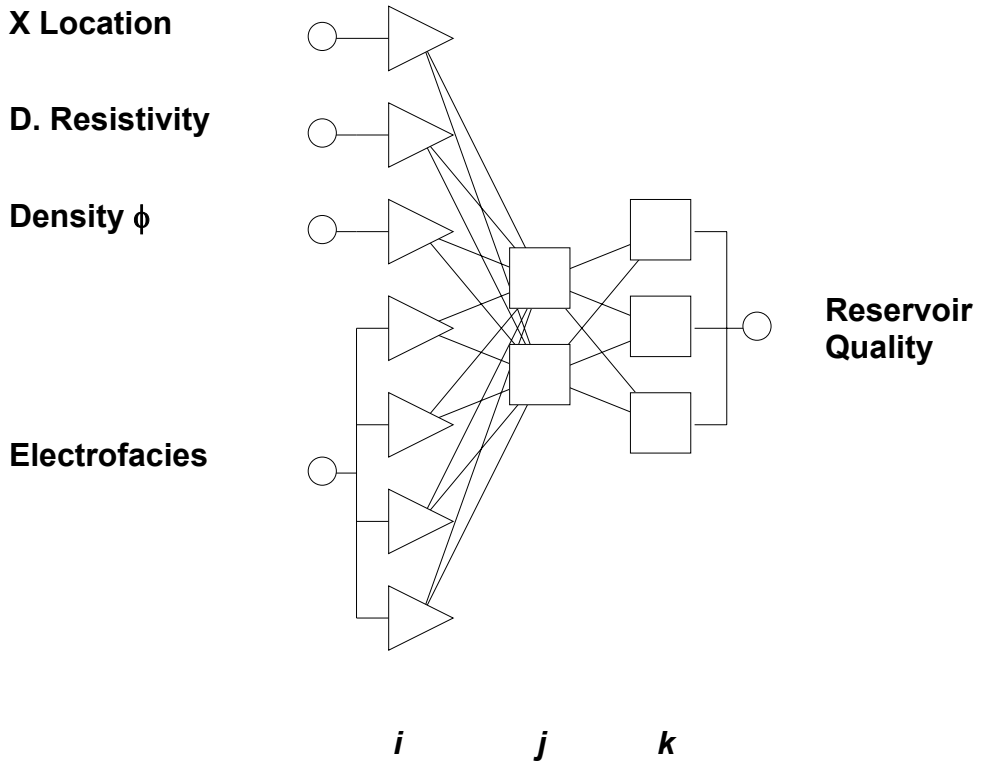

The above neural network consists of three layers: one input layer, *i*. with 4 inputs and 7 neurons, one hidden layer, *j,* with 2 neurons each, and one output layer, *l*, with 3 neurons (MLP 4:7-2-3:1). The starting algorithm was back propagation (50 iterative cycles) followed by conjugate gradient descent (25 iterative cycles). A table of weights and threshold values is found below. A logistic activation function was used in the hidden layer and the output layer.

Hidden Layer 1 – RQC Model 2		
W_{ij}		
i/j	1	2
X	0.7545402	-0.4672
Rt	1.635781	-5.765697
Density	2.070093	-7.65679
Grain	-0.4423	0.3796996
SS	-0.7999	2.643054
Rud	0.6074992	0.05798
Float	0.216151	0.6095667
Threshold	1.830855	-3.036244

Activation Function = Logistic

Hidden Layer 2 – RQC Model 2			
W_{jk}			
j/k	1	2	3
HL1#1	2.314973	-0.1374	-2.641681
HL1#2	-7.284181	-3.502543	7.210451
Threshold	1.724803	0.4533026	-0.207724

Activation Function = Logistic

VITA

NAME:	Matthew David Gentry
PERMANENT ADDRESS:	533 Patterson Road Kings Mountain, North Carolina
EDUCATION:	Texas A&M University College Station, Texas M.S. Geology, August 2003
	Mississippi State University Starkville, Mississippi B.S. Geoscience, August 1998
	University of Hawaii Hilo, Hawaii
	University of North Carolina Chapel Hill, North Carolina
PROFESSIONAL EXPERIENCE:	Shell Exploration and Production Company Offshore Gulf of Mexico Exploration New Orleans, Louisiana
	Amerada Hess Western Gulf of Mexico Exploration Houston, Texas
	Paramount Petroleum Mississippi & Alabama Exploration & Development Jackson, Mississippi
PROFESSIONAL MEMBERSHIP:	American Association of Petroleum Geologists Mississippi Geological Society Houston Geological Society